MALAYSIAN Journal of Catalysis

Vol. 9, No. 1, 2025 eISSN 0128-2581

Topics of journal (but are not limited to):

1. Catalytic Mechanisms
1-1. Spectroscopic and Visualizing Characterizations
1-2. Surface Chemistry, Reaction Kinetics and Mechanisms
1-3. Molecular Simulation and Theoretical Modeling
1-4. New Concepts for Catalysis

2. Catalytic Materials
2-1. Nanostructured Catalytic Materials
2-2. Micro- and Meso-Porous Catalytic Materials
2-3. Hybrid materials for catalysis

2-4. Novel Design and Synthetic Approaches

3. Catalysis for Energy
3-1. Efficient Utilization of Fossil Sources
3-2. Clean Energy Conversion: Electrocatalysis
3-3. Biomass Conversion
3-4. Photocatalysis for Hydrogen Production

4. Environmental Catalysis
4-1. Automotive Exhaust Cleanup
4-2. Water Pollution Control
4-3. Air Pollution Control
4-4. Updating and Utilization of Wastes

5. Catalysis for Chemical Synthesis
5-1. Green Synthesis
5-2. Petrochemicals
5-3. Fine Chemicals and Pharmaceuticals
5-4. Selective Oxidation & Hydrogenation

6. Cross-Disciplinary
6-1. Integration of Heterogeneous and Homogeneous
6-2. Organic and Biomimetic Catalysis
6-3. Industrial Catalysis
6-4. Other Surface Active Site Phenomena
6-5. Adsorption-Desorption Phenomena
6-6. Active sites Studies
6-7. Others

Faculty of Chemical and Energy Engineering
Universiti Teknologi Malaysia
http:/mjcat.utm.my/

Malaysian Journal of Catalysis
http://mjcat.utm.my/
MJCat Research Article

Biomass-based Sorbents for Oil spill Clean-up: A review

Taofiqat Omotayo Abu[2], Abdulkadir Ahmed Zubairu[1*], Ochoche Victor Achepa[1], Gbadamosi Kudirat Olansile[1], Tunmise Latifat Adewoye[1], Hambali Umar Hambali[1*]

[1]*Department of Chemical Engineering, Faculty of Engineering and Technology University of Ilorin, P. M. B. 1515, Ilorin, Nigeria*
[2]*Department of Industrial Chemistry, University of IIorin, P. M. B. 1515, IIorin, Nigeria.*

**Corresponding Authors: hambaliuh313@gmail.com; zubyrabk@gmail.com*

Article history:
Received 11 November 2024
Accepted 01 January 2025

ABSTRACT

The pervasive environmental and health impacts of oil spills, stemming from the extraction, transportation, and handling of crude oil, highlight an urgent need for sustainable remediation techniques. Traditional cleanup methods such as oil skimming, combustion, and synthetic sorbents are often limited by high costs, non-biodegradability, and potential environmental risks. As oil spills continue to rise with global oil consumption, sustainable, eco-friendly alternatives are essential. This review evaluates biomass-based sorbents, particularly agricultural fibres, as promising substitutes for synthetic materials. These natural sorbents exhibit high oil sorption capacities, are biodegradable, and possess hydrophobic properties that enable effective oil retention while repelling water. Their low cost, availability, and potential for reuse through carbonization also position them as economically viable and environmentally responsible solutions. Carbonized biomass sorbents produce biochar, a porous material applicable in wastewater treatment and soil conditioning, contributing to resource circularity and aligning with sustainability goals. Through an analysis of recent advancements, sorption efficiencies, and environmental impacts, this review assesses biomass-based sorbents' potential to reduce environmental degradation and enhance waste management, underscoring their role in supporting a circular economy approach for oil spill cleanup.

Keywords: *Biomass-based sorbents, Oil spill remediation, Carbonized biomass*

| eISSN 0128-2581 |

1. INTRODUCTION

Crude oil has been the backbone of industrial economies and the primary energy source since the mid-20th century, with products that fuel industries, transportation, and households worldwide. Despite its essential role, oil extraction, transportation, and handling have raised significant environmental concerns due to oil spills. Oil spills release petroleum hydrocarbons into marine or terrestrial environments, often causing extensive harm. In marine ecosystems, for example, oil affects aquatic wildlife, impairing functions such as respiration and insulation, while its toxicity leads to developmental abnormalities, reduced growth rates, and compromised reproductive success in organisms exposed to contaminated water [1-2]. Field studies indicate that oil contamination in water can disrupt entire ecosystems by altering food webs, depleting oxygen levels, and reducing biodiversity [3]. These persistent pollutants can remain in sediments and biota for years, demonstrating the long-term ecological impacts of oil spills [4-5].

On land, oil spills degrade soil quality, affecting both flora and fauna and limiting the land's agricultural potential. In many cases, spills stem from activities like crude oil mining, transportation, and sabotage, which collectively contribute to widespread environmental damage. The negative effects of oil contamination are not restricted to the environment; human health is also at risk, particularly through exposure to polluted water or seafood in oil spill zones. Studies have shown an increase in respiratory issues, skin irritations, and even cancer in populations residing near oil spill sites [6]. The adverse effects of oil spills on human health and biodiversity, combined with the difficulty of removing oil residues, underscore the need for efficient, cost-effective, and sustainable remediation techniques.

Traditional oil spill clean-up methods, including oil skimming, combustion, and synthetic sorbents, are limited in terms of cost, effectiveness, and environmental impact. Synthetic materials like polypropylene are widely used due to their significant oil adsorption capacity, but they are costly and non-biodegradable, contributing to further environmental degradation [7-8]. As oil spills become increasingly common with the rise in global oil consumption, there is a pressing demand for sustainable alternatives that not only remediate affected areas but also minimize secondary environmental impacts. Natural biomass-based sorbents, such as agricultural fibres, are

emerging as eco-friendly alternatives, combining high oil sorption capabilities with biodegradability and low cost [9]. The sustainable sorbent materials possess high oil sorption capacity, absorbing high amounts of crude oil per gram of fibre, and effectively retaining oil while repelling water due to hydrophobic properties [10-12]. Beyond oil sorption ability, sorbent materials are readily available and cost-effective, with the potential for reusability through carbonization, making them attractive options for large-scale application in oil spill remediation [13-14].

Carbonizing sorbent materials produces biochar, a material known for its high porosity and surface area, which can also serve as an adsorbent in wastewater treatment applications [15-17]. This approach enhances resource circularity by allowing the reuse of sorbent materials, reducing waste, and offering potential benefits for soil conditioning and carbon sequestration. The process also aligns with environmental sustainability and economic feasibility by converting waste into biochar. Such practices not only address environmental remediation but also adhere to resource conservation principles [18-19].

This review aims to evaluate the effectiveness of biomass-based sorbents in oil spill remediation. By analyzing recent advancements, sorption capacities, and the environmental impact of these natural fibres, this review seeks to establish the viability of biomass-based sorbents as sustainable alternatives to conventional synthetic materials. Specifically, the review addresses critical research questions, such as how biomass sorbents compare to synthetic sorbents in terms of sorption efficiency, environmental impact, and cost-effectiveness, and what role chemical or physical modifications play in enhancing their performance. It also investigates the long-term feasibility of integrating biomass sorbents into large-scale oil spill cleanup operations. Furthermore, this review contributes to the existing literature by identifying and addressing key gaps, such as the lack of extensive field trials and limited understanding of the environmental fate of biomass sorbents under marine conditions. Through insights into carbonization processes and the potential reuse of these sorbents, the review underscores the importance of natural materials in reducing environmental degradation, addressing waste management challenges, and supporting a circular economy approach in oil spill cleanup efforts.

2. NATURE OF OIL

Oil is a complex mixture of hydrocarbons, which are organic compounds made up of hydrogen and carbon atoms. Its nature varies depending on its source, which can include crude oil, refined petroleum products, or natural oils from plants and animals. Crude oil, the most common form, consists of various hydrocarbon molecules such as alkanes, cycloalkanes, and aromatic hydrocarbons. These molecules differ in size, structure, and properties, influencing characteristics like viscosity, density, volatility, and flammability. Additionally, oil can contain impurities such as sulfur, nitrogen, and heavy metals, which impact its environmental and health effects. Understanding these properties is crucial for managing oil effectively and mitigating the impacts of spills and pollution.

Oil plays a crucial role in various aspects of modern life, serving both practical and industrial purposes: Oil is a major source of energy, primarily used in transportation (as gasoline, diesel, and jet fuel) and electricity generation (through combustion in power plants). It serves as a feedstock for the production of numerous industrial products, including plastics, lubricants, solvents, asphalt, and synthetic fibres. Oil is used for heating homes and buildings, as well as in cooking and food preparation (e.g., vegetable oil, olive oil). Oil fuels the global transportation sector, powering cars, trucks, ships, aeroplanes, and trains, enabling the movement of people and goods across the world. It also serves as a raw material for the chemical industry, contributing to the production of fertilizers, pesticides, pharmaceuticals, cosmetics, and a wide range of other chemical products. The oil industry contributes significantly to national and global economies, providing employment, revenue, and investment opportunities. Oil-based products such as asphalt and bitumen are essential for building roads, highways, and infrastructure projects. Some medical products and pharmaceuticals are derived from oil-based compounds, including certain medications and medical devices.

While oil serves as a vital resource in numerous aspects of our daily lives, it's essential to acknowledge the significant environmental and economic repercussions associated with oil spillage. Despite its usefulness, the release of oil into our oceans, rivers, and land can have devastating consequences on ecosystems, wildlife, and communities.

3. OIL SPILLS

Oil spillage, defined as the release of liquid petroleum hydrocarbons into the environment due to human activity, presents significant ecological and health threats globally [20]. These releases are predominantly associated with crude oil mining and transport, including pipeline ruptures, tanker accidents, and spills at offshore drilling platforms or storage facilities. Oil spills occur not only in the production phase but also in various other stages, such as transportation, storage, and end-use scenarios, such as leaks at automobile workshops or PMS (premium motor spirit) outlets. These incidents highlight the ubiquity and complexity of oil-related pollution sources, complicating efforts to mitigate their effects on the environment and human health, Figure 1 shows the fate of oil spills in the marine environment.

The environmental consequences of oil spills are severe, as oil’s destructive characteristics lead to substantial ecosystem damage once it contaminates an area [21]. When oil comes in contact with soils, floors, or water bodies, its removal is notoriously difficult, often leaving persistent contamination that can extend far beyond the initial spill location [22]. Oil spill incidents are particularly impactful in

aquatic environments; when spilled in water bodies, oil rapidly spreads across the surface, forming slicks or reaching shorelines, where it poses a direct threat to marine and coastal ecosystems. The rapid spread of oil on water prevents effective containment and clean-up, amplifying the likelihood of prolonged ecological harm, particularly to coastal marshes. These marshes are vulnerable because they are low-energy and anoxic environments, conditions that slow oil dispersal and decomposition, allowing them to persist within soils for decades [23].

While the most visible and dramatic oil spill incidents occur in marine settings due to tanker or platform accidents, it is crucial to understand that these large-scale incidents represent less than 10% of total petroleum hydrocarbon discharges globally. Instead, up to 90% of hydrocarbons enter the environment through low-level, routine releases, including operational discharges and maintenance leaks [24]. This routine contamination underscores a steady influx of oil pollutants, with an estimated two million tonnes of oil released into marine environments annually. Notably, only about 18% of this oil pollution comes from refinery processes, offshore operations, and tanker activity, highlighting the pervasive nature of smaller, ongoing sources that contribute significantly to long-term environmental degradation.

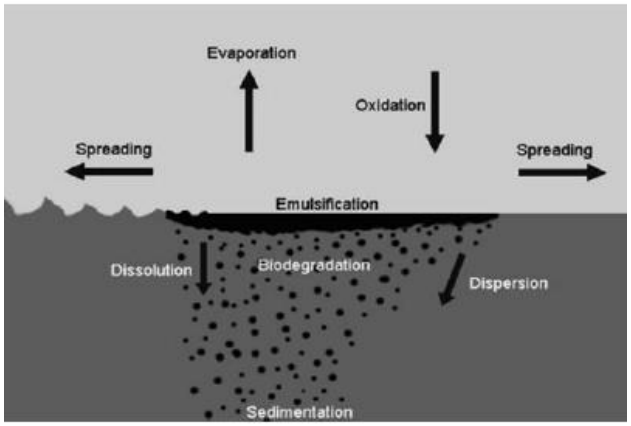

Figure 1. An illustration of the fate of oil spills in the marine environment [25]

In Nigeria, Africa's largest oil producer, oil spillage is both frequent and devastating due to pipeline vandalism, oil theft, and insufficient maintenance [26]. These spills pollute the air, soil, and water, where the volatile components of crude oil may evaporate or permeate into groundwater and surface water. This widespread pollution extends beyond environmental concerns, posing substantial health risks to communities through various exposure routes, including direct dermal contact with contaminated soil and water, ingestion of polluted food sources like crops and fish, or inhalation of vaporized toxins and particulate matter from fires [27]. Oil spills frequently result in fires, which release respirable particulate matter (PM) into the air, intensifying health hazards for nearby populations. Furthermore, these onshore spills disrupt critical livelihood resources by degrading agricultural land and fishing grounds, leading to indirect health and socioeconomic impacts, particularly in the Niger Delta region. While multiple studies document extensive soil and water contamination in this region, research has yet to provide causal evidence directly linking onshore spills to specific human health outcomes [28].

This extensive contamination in oil-producing regions like Nigeria's Niger Delta [29] illustrates the multifaceted nature of oil spills, encompassing both immediate environmental destruction and longer-term health and livelihood implications. Given the difficulty of effectively cleaning oil spills from affected ecosystems and the persistence of oil residues in anoxic soils and low-energy aquatic environments, it is evident that oil spillages present enduring environmental and public health challenges that require concerted global attention and action. Table 1 shows some past oil spill incidents in the world, their cost implications, and the most suitable technique used for remediation.

4. OIL SPILL CLEAN-UP

Oil spills present a formidable global challenge, creating extensive environmental damage and impacting ecosystems and human livelihoods. Clean-up efforts following spills are essential to mitigate their severe consequences on wildlife, local economies, and marine and terrestrial habitats. Effective oil spill remediation involves diverse strategies that vary widely in cost, environmental impact, and efficiency, with ongoing research aiming to optimize these approaches to address the limitations of existing methods [12].

Current remediation technologies include in situ burning, mechanical methods, chemical dispersants, and synthetic sorbents. In situ burning involves igniting spilled oil, ideally on the surface of the water, to quickly remove large volumes; however, it poses health risks and potential air pollution [30]. Mechanical tools, such as skimmers, leverage the adhesive nature of oil to physically separate it from the water surfaces. Skimmers vary by design, belt, brush, mop, and floating suction, all engineered to optimize oil recovery in different conditions. Nevertheless, their high operational costs and inefficiency at trace-level removal make them less ideal for large-scale or ongoing spills, especially in economically challenged regions [8]. The broad classifications of oil spill remediation are illustrated in Figure 2.

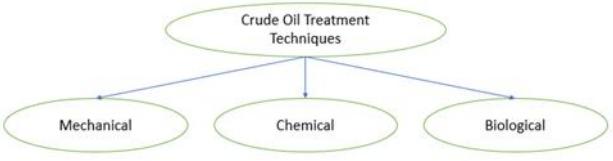

Figure 2. Broad classification of oil spill remediation

Table 1. Major oil spill incidents, their cost implication and remediation methods [30]

Incidence	Amount spilled	Length of affected areas	Cost implication	Environmental effect	Cleanup technique(s)
1967, Torrey Canyon off the English Channel	120,000 tons of crude oil	100 miles of coastlines	-	An estimated 25,000 birds died.	-Natural weathering. Dispersants were also used. Bombs were used to ignite a fire for in-situ combustion of remaining oil before it spread. Straws and gorse were used on many of the sandy beaches to soak oil. Floating booms were unsuccessful
1970, Liberian Registered Tanker at Chedabucto Bay, Nova Scotia	16,000 tons	190 miles of coastline	-	-	Skimmers successfully in sheltered waters. Dispersants could not penetrate thick layers of oil that formed as a result of low temperatures and wind. Sorbents such as peat moss proved to be a good sorbent; straw was used on some beaches. In-situ burning is used successfully on beaches and in solid slicks. Microbial degradation. On the shore, oil was removed mechanically and manually. Pressure-washing with hot water. Beaches sprayed with artificial fertilizers and bacterial cultures. Rubber powder and chalk-sinking agents were also not very successful.
2010, BP Gulf of Mexico	About 4.9 million barrels (208.5 million gallons)	Over 790 km of shorelines	$5.4 billion possible fines and $21 billion (if gross negligence) $20 billion for compensation and clean up (Welch and Joyner, 2010)	997 birds dead; 400 sea turtles dead; 47 Mammals including Dolphins dead	50% of the oil dispersed naturally; some oil was removed mechanically at sea; and some was dispersed with chemical dispersants; Booms and Skimmers; Dispersants; and Controlled burning.
1996, Sea Empress	Over 70,000 tonnes	100 km of coastline	$60 million of which $37 million was used for clean up	2200 birds killed. Seaweeds and, shellfishes were affected	50% of the oil dispersed naturally; some oil was removed mechanically at sea; and some was dispersed with chemical dispersants; Booms and Skimmers; Dispersants; and Controlled burning.
1990, the Gulf War in which 650 oil wells in Kuwait were set ablaze	1 million tonnes	-	-	20,000 sea birds were killed.	-

Chemical dispersants are another approach that has been extensively applied, particularly in cases of large offshore spills. Dispersants break down oil into smaller droplets, promoting natural biodegradation processes, yet they have been criticized for potential toxicity to marine life and limitations in certain environments [30]. Synthetic sorbents, often polymers, can be highly effective in absorbing oil; however, they tend to be costly and less biodegradable, posing challenges for eco-friendly disposal.

Despite these established methods, there are limitations in cost-effectiveness, efficiency, and environmental sustainability. Each approach comes with trade-offs, and there is a continuous need for novel solutions that balance economic feasibility and environmental safety. Some studies suggest that natural sorbents, including biomass-derived materials, show potential for being both low-cost and eco-friendly. However, further research and development are needed to verify their large-scale applicability and effectiveness, particularly in challenging field conditions [12], [30].

The impact on local communities and the environment is severe in countries like Nigeria, where oil spills are frequent due to pipeline vandalism, theft, and maintenance issues. Nigeria's Niger Delta region, an area rich in biodiversity, has endured decades of oil spills, leading to contaminated water sources, degraded farmlands, and compromised health among the local population. Conventional remediation methods face financial, logistical, and infrastructural hurdles, as the high costs associated with advanced technologies are often prohibitive [31]. Furthermore, environmental and socioeconomic conditions in regions like the Niger Delta necessitate affordable and adaptable solutions that can be implemented locally [29].

The search for more accessible oil spill cleanup solutions is critical in regions facing high spill frequency and limited resources. By exploring a wider range of cleanup options, including both established and experimental approaches, Nigeria and other similarly affected regions can work towards sustainable cleanup practices that align with local needs and resource availability. Evaluating each method's performance in real-world conditions, particularly those that are more cost-effective and sustainable, will be key in mitigating the ongoing impact of oil spills and fostering resilience against future incidents. In another study [32], treatment methods for oil spillage were classified into three major classes namely: biological treatment such as microbial remediation and enzymatic treatment; chemical treatment such as chemical coagulation and dispersion; and physical or mechanical treatment such as skimming, oil booms and adsorption. Figure 2 highlights these methods.

5. METHODS OF OIL CLEAN-UP

In most cases, two or more methods are combined to achieve an effective cleanup. Treating oil spills typically involves extensive methods, including Mechanical containment, chemical dispersions, in-situ burning and bioremediation. The methods and their examples as shown in Table 2.

5.1 Mechanical containment and recovery

It involves the use of booms spread over the surface of seas, estuaries and coastal waters to prevent the spread of oil slicks or to direct their movements [33]. This is among the primary methods used to address oil spills. This involves the use of booms to contain the oil and skimmers to remove it from the water's surface. Examples of mechanical containment and recovery methods for oil spill treatment include:

Boom Deployment: Booms are deployed to contain the spread of oil, while skimmers and vacuum trucks are employed to remove the oil from the water's surface. Mechanical methods are particularly effective in calm waters and can help prevent the oil from spreading further. Booms are floating barriers deployed around the perimeter of an oil spill to contain the oil and prevent its spread. Various types of booms, such as sorbent booms and inflatable booms, can be used depending on the specific conditions of the spill. Studies have shown that booms effectively contain oil, preventing it from spreading to sensitive areas and facilitating its recovery [34].

Table 2. Methods of Oil Spill Clean-up and their examples.

Mechanical containment	Chemical dispersions	In-situ burning	Bioremediation
Boom Deployment	Dispersant Application	Controlled Ignition	Biostimulation
Skimming	Remote Application Systems	Fire-Resistant Booms	Bioaugmentation
Sorbent Materials	Controlled Release	Ignition Techniques	Landfarming
Vacuum Trucks	-	--	Bioventing
Manual Cleanup	-	-	-

Skimming: Skimmers are specialized vessels or equipment that remove oil from the water's surface. These devices use various mechanisms, such as suction or absorption, to collect the oil, which is then transferred to storage tanks for disposal or recycling. Skimmers are highly effective in calm water conditions and have been widely used in oil spill response operations [35].

Sorbent Materials: Sorbents are particularly useful for small-scale spills or in situations where access is limited for larger vessels [36]. Sorbent materials, such as pads, booms, and loose materials like peat moss or hay, are used to absorb or adsorb oil from the water's surface. These materials act like sponges, capturing the oil and allowing for its removal from the environment. The effectiveness of various sorbents in recovering oil from water surfaces depends on their capacity to transform the oil from a liquid phase into a semi-solid or solid phase [25], [37].

Vacuum Trucks: Vacuum trucks equipped with suction hoses are used to remove oil from the water's surface, particularly in areas where access is limited for larger vessels. Vacuum trucks provide an efficient means of collecting oil and can be deployed quickly in response to spill incidents [38]. These trucks can efficiently collect oil and transport it to designated disposal facilities.

Manual Cleanup: In some cases, manual labour is employed to manually remove oil from shorelines or sensitive habitats. Workers may use shovels, rakes, and other tools to collect oil-contaminated debris, which is then disposed of properly.

5.2 Chemical dispersion

Chemical dispersion involves the application of dispersants to break up the oil into smaller droplets, enhancing microbial degradation. Dispersants contain surfactants that reduce the surface tension of the oil, facilitating its dispersion into the water column. However, the use of dispersants remains controversial due to potential environmental impacts and toxicity to marine life [39]. Chemical dispersants are applied to break up the oil into smaller droplets, enhancing microbial degradation. Examples of chemical dispersion methods in oil spill treatment include:

Dispersant Application: Chemical dispersants, such as Corexit, are applied directly to the oil spill either by spraying from aircraft or vessels or by injecting the dispersant underwater at the source of the spill. These dispersants contain surfactants that reduce the surface tension of the oil, breaking it into smaller droplets that can disperse throughout the water column. Dispersant application can significantly reduce the surface area coverage of oil slicks and enhance the rate of biodegradation [40].

Remote Application Systems: These systems allow for precise and targeted application of dispersants, minimizing environmental impacts. Remote-controlled or autonomous vehicles equipped with dispersant spraying systems are used to apply dispersants to oil spills in hard-to-reach or sensitive areas, such as near shorelines or in rough seas.

Controlled Release: Dispersants can also be released continuously or intermittently from vessels or platforms near the source of the spill, allowing for controlled dispersion of the oil over a larger area. This method helps to prevent the formation of large oil slicks and facilitates the dilution of the oil in the water column.

5.3 In-situ burning

Controlled burning of the oil on the water's surface, can be effective under certain conditions. It is another method used to address oil spills, particularly in situations where mechanical recovery is not feasible. Controlled burning of the oil on the water's surface can effectively reduce the volume of oil and minimize its impact on the environment. However, this method requires careful planning and consideration of air quality impacts. Examples of in-situ burning methods in oil spill treatment include:

Controlled Ignition: In-situ burning involves the controlled ignition of oil slicks on the water's surface, typically using specialized equipment such as fire-resistant booms or fire-resistant igniters towed behind vessels. The burning process consumes the oil, reducing its volume and minimizing its environmental impact. Controlled ignition effectively reduces the volume of oil and minimizes environmental damage, particularly in offshore environments.

Fire-Resistant Booms: Fire-resistant booms play a critical role in ensuring the safety and effectiveness of in-situ burning operations [41]. Fire-resistant booms are deployed to contain the oil slick and facilitate controlled burning. These booms are designed to withstand high temperatures and prevent the fire from spreading beyond the desired area.

Ignition Techniques: Various ignition techniques, such as aerial ignition using helicopters or fixed-wing aircraft, can be employed to ignite the oil slick safely and efficiently. Ignition timing and placement are critical factors in ensuring the success of in-situ burning operations. In-situ burning is typically used in situations where mechanical recovery or other methods are not feasible, such as in remote or inaccessible locations or rough sea conditions.

5.4 Bioremediation

Bioremediation involves the stimulation of naturally occurring microorganisms to degrade the oil, either through the addition of nutrients or the manipulation of environmental conditions. Microorganisms such as bacteria and fungi play a crucial role in breaking down hydrocarbons present in oil, ultimately reducing their toxicity and environmental impact (Premnath et al., 2021). Examples of bioremediation methods in oil spill treatment include:

Biostimulation: Biostimulation involves the addition of nutrients, such as nitrogen and phosphorus, to the environment to stimulate the growth of indigenous microorganisms capable of degrading oil. These nutrients enhance the metabolic activity of microorganisms, accelerating the biodegradation process.

Bioaugmentation: Bio-augmentation involves the introduction of specialized microbial cultures or enzymes to the oil-contaminated environment to enhance the biodegradation of oil. These introduced microorganisms or enzymes may have specific capabilities to degrade hydrocarbons efficiently.

Landfarming: Land farming, also known as bio-piling, involves the spreading of contaminated soil or sediment in a controlled environment and stimulating the growth of indigenous microorganisms to degrade the oil. This method is often used for onshore oil spill remediation. Studies have shown that land farming promotes the degradation of various hydrocarbons by indigenous microbial communities [26].

Bioventing: Bioventing is a technique used to enhance the aerobic biodegradation of oil vapours in the soil by supplying oxygen to Indigenous microorganisms. This method is particularly effective for treating subsurface oil contamination. Research has demonstrated the effectiveness of bio-venting in treating subsurface oil contamination at spill sites and petroleum storage facilities [42]. Bioremediation methods harness the natural abilities of microorganisms to degrade oil and can be applied in both marine and terrestrial environments to mitigate the environmental impact of oil spills.

5.5 Factors Affecting Methods of Oil Spill

Oil spills pose significant environmental threats, demanding effective mitigation strategies. Various factors influence the selection and efficacy of treatment methods, ranging from the type of oil spilled to environmental conditions and

technological capabilities. Concurrently, the exploration of alternative sorbent materials, such as ginger fibre, introduces another dimension to oil spill remediation efforts, with considerations extending from suction capacity determination to reutilization potential. Factors Influencing Oil Spill Treatment Methods:

Oil Type: Different types of oil possess distinct physical and chemical properties, impacting their behaviour in aquatic environments and responses to treatment methods. For instance, heavy oils tend to linger longer, requiring specialized approaches for containment and removal [34].

Environmental Conditions: Factors like temperature, water currents, and weather conditions significantly affect oil spill behaviour and treatment effectiveness. Cold temperatures can increase oil viscosity, complicating cleanup efforts, while strong currents may disperse oil over larger areas, necessitating rapid response strategies [40].

Proximity to Sensitive Ecosystems: Oil spills occurring near sensitive ecosystems, such as coral reefs or mangrove forests, present unique challenges due to the heightened risk of ecological damage. Treatment methods must prioritize minimizing environmental impact while effectively containing and removing spilled oil [43].

Resource Availability and Technology: The availability of resources, including equipment, manpower, and funding, influences the choice and implementation of oil spill treatment methods. Advanced technologies, such as unmanned aerial vehicles (UAVs) and satellite monitoring, enhance response capabilities but may not be readily accessible in all regions [38].

6. SORBENT MATERIALS FOR OIL CLEAN-UP

6.1 Mechanism of sorption

Sorption is a common term used for both absorption and adsorption processes [44]. Mechanism of Sorption for Oil Spill Cleanup, the process by which substances are adsorbed or absorbed onto a surface, plays a crucial role in oil spill cleanup. Understanding the mechanisms of sorption is essential for developing effective strategies to remove oil from contaminated environments and mitigate environmental damage.

Adsorption Mechanism: Adsorption refers to the adherence of oil molecules onto the surface of a sorbent material as illustrated in Figure 3. This process occurs due to the attractive forces between the oil molecules and the surface of the sorbent material [45]. The surface of the sorbent material plays a critical role in adsorption, as it provides sites for oil molecules to adhere. Materials with a high surface area and specific surface chemistry are more effective in adsorbing oil molecules [46]. Hydrophobic materials are particularly effective in adsorbing oil molecules due to their strong affinity for non-polar substances. The hydrophobic nature of the sorbent material promotes the adsorption of oil while repelling water [47]. Adsorption is a rapid process, as oil molecules can quickly adhere to the surface of the sorbent material upon contact. However, the capacity of the sorbent material to adsorb oil may become saturated over time, limiting its effectiveness [7].

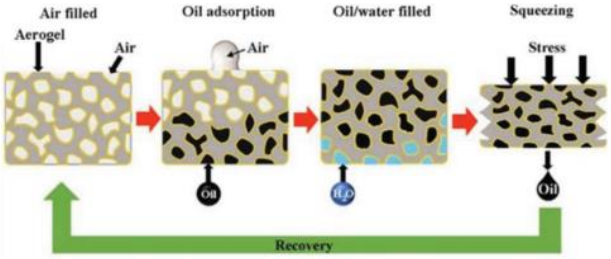

Figure 3. Adsorption mechanism of oil to fill pore space of graphene structures [48]

Absorption Mechanism: Absorption involves the penetration of oil molecules into the pores or structure of the sorbent material (Figure 4). Unlike adsorption, which occurs on the surface of the material, absorption occurs within the bulk of the material [49]. The pore structure of the sorbent material significantly influences its absorption capacity. Materials with well-defined pores provide ample space for oil molecules to infiltrate, increasing the overall absorption capacity [50]. Absorption is a slower process compared to adsorption, as it involves the diffusion of oil molecules into the interior of the sorbent material. However, absorption can result in higher oil retention capacity, as oil molecules are securely trapped within the structure of the material [51].

Surface Interaction: The surface interaction mechanism is a fundamental aspect of the sorption process for oil spill cleanup, influencing the adhesion and retention of oil molecules onto the sorbent material's surface. Understanding this mechanism is crucial for optimizing sorbent materials and enhancing their effectiveness in mitigating the environmental impact of oil spills. The effectiveness of sorption depends on the interaction between the oil molecules and the surface of the sorbent material. Hydrophobic materials exhibit a strong affinity for non-polar oil molecules, facilitating their adhesion and retention [14]. Surface chemistry plays a critical role in determining the sorption capacity and selectivity of the sorbent material. Functional groups present on the surface of the material may interact with specific components of the oil, influencing adsorption kinetics and sorption [52]. The surface roughness and topography of the sorbent material also influence surface interactions. Materials with a rough surface texture may provide more sites for oil molecules to adhere to, enhancing sorption performance [53]. Furthermore, electrostatic interactions between the oil molecules and the surface of the sorbent material may contribute to sorption behaviour. Materials with polar functional groups may exhibit electrostatic interactions with polar components of the oil, influencing sorption kinetics and oil retention [54]. Understanding and optimizing surface interactions is essential for developing sorbent materials with enhanced oil sorption capabilities. By tailoring the surface chemistry, texture, and topography of sorbent materials, researchers can improve their effectiveness in oil spill cleanup operations.

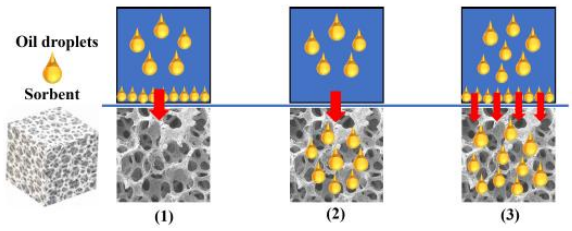

Figure 4. Schematic diagram of oil absorption process. (1) oil droplets accumulate on the surface of sorbents via weak interaction forces; (2) oil droplets penetrate the intermolecular of sorbents under the capillary forces; (3) both surface accumulation and intermolecular penetration exist [55]

Pore Structure: The pore structure of sorbent materials refers to the arrangement, size, and distribution of pores within the material. Materials with a high surface area and well-defined pore structure provide more sites for oil molecules to adhere or penetrate, thereby enhancing sorption performance [56]. The size of pores within the sorbent material affects the accessibility of oil molecules to the sorption sites. Materials with a range of pore sizes, including micro-, meso--, and macro-pores, can accommodate oil molecules of varying sizes, maximizing sorption capacity [54]. The distribution of pores within the sorbent material influences the diffusion of oil molecules into the material's structure. Materials with a homogeneous pore distribution facilitate uniform oil uptake and retention, ensuring efficient sorption throughout the material [57]. The interconnectedness of pores within the sorbent material is critical for facilitating the transport of oil molecules into the material's interior. Materials with interconnected pores allow for unhindered diffusion of oil molecules, enhancing sorption kinetics and overall efficiency [54]. Tailoring the pore structure of sorbent materials through methods such as templating, carbonization, or chemical modification enables the optimization of sorption performance for specific oil spill cleanup applications [58].

Chemical Composition: The chemical composition of sorbent materials plays a significant role in the sorption process for oil spill cleanup, influencing sorption behaviour, selectivity, and efficiency. Understanding the chemical composition mechanism is essential for designing sorbent materials with tailored properties to effectively mitigate the environmental impact of oil spills. The presence of functional groups on the surface of sorbent materials governs their interaction with oil molecules. Functional groups such as hydroxyl (-OH), carboxyl (-COOH), and amine ($-NH_2$) groups can form hydrogen bonds or undergo other chemical interactions with oil molecules, influencing sorption kinetics and selectivity [59]. The polarity of functional groups on the sorbent material's surface affects their affinity for polar or non-polar components of the oil. Materials with polar functional groups may exhibit stronger interactions with polar oil components, while materials with non-polar functional groups may preferentially adsorb non-polar oil molecules [60]. The abundance and distribution of functional groups on the sorbent material's surface influence sorption capacity and efficiency. Materials with a higher density of functional groups may offer more sites for oil molecule interaction, enhancing sorption performance [61]. Chemical modification of sorbent materials through processes such as grafting, impregnation, or surface coating allows for the incorporation of specific functional groups to tailor sorption properties. This enables the design of sorbent materials with enhanced affinity for target oil components and improved overall sorption performance [62]. The stability of chemical bonds between the sorbent material and oil molecules impacts sorption durability and reusability. Materials with strong, reversible bonds can undergo multiple sorption-desorption cycles without significant degradation, prolonging their effective lifespan for oil spill cleanup [60]. By understanding and manipulating the chemical composition of sorbent materials, researchers can develop tailored solutions for oil spill cleanup that effectively target specific oil components while minimizing environmental impact.

6.2 Isotherm for sorption process

Isotherms for sorption processes serve as fundamental tools in understanding the interaction between adsorbate molecules and solid surfaces. These isotherms depict the relationship between the amount of adsorbate molecules adsorbed onto a solid adsorbent and the concentration of the adsorbate in the gas or liquid phase, under conditions of constant temperature. One of the seminal works in this field is the Langmuir isotherm, proposed by Irving Langmuir in 1916. The Langmuir model assumes monolayer adsorption on a homogenous surface with no interaction between adsorbate molecules once a monolayer is formed. However, the Langmuir model has its limitations, particularly in situations where adsorption occurs in multiple layers or on heterogeneous surfaces. To address these shortcomings, alternative models have been developed. Among these is the Freundlich isotherm, introduced by Herbert Freundlich in 1906. The Freundlich model accounts for heterogeneous surface adsorption and permits multilayer adsorption, making it more suitable for describing a broader range of adsorption phenomena. Another significant advancement in isotherm modelling is the BET (Brunauer, Emmett, and Teller) theory, established in 1938 by Stephen Brunauer, Paul Hugh Emmett, and Edward Teller. The BET isotherm extends the Langmuir model by incorporating the formation of multilayer adsorption on a heterogeneous surface, considering different adsorption energies for each layer. The choice of the isotherm model depends on various factors, including the specific characteristics of the adsorbate and adsorbent, as well as the experimental conditions. Researchers often employ multiple isotherm models and compare their fits to experimental data to determine the most appropriate model for a particular adsorption system. In recent years, advancements in experimental techniques and computational methods have led to the development of more sophisticated isotherm models. These models aim to capture complex adsorption

phenomena, such as cooperative adsorption, surface heterogeneity, and non-ideal behaviour. Such advancements have enhanced our understanding of sorption processes in diverse applications, including environmental remediation, gas separation, and purification.

7. MATERIALS USED FOR OIL SORPTION

Materials for oil sorption in spill cleanup operations include a diverse array of substances, each suited to specific types and stages of spills. Sorbents, which absorb or adsorb oil from water, represent a primary category of materials. Polypropylene-based sorbents, such as pads and booms, are frequently employed due to their high oil sorption capacity and buoyancy, facilitating efficient recovery from water surfaces [63]. Biological agents like oleophilic bacteria and enzymes provide an eco-friendly alternative, accelerating oil degradation; research by Bharali et al. [64] underscores the role of microbial consortia in breaking down hydrocarbons, thereby enhancing bioremediation in oil-contaminated areas.

Chemical dispersants also play a key role, breaking oil slicks into smaller droplets that disperse more easily and biodegrade faster. However, the application of dispersants must be carefully evaluated for ecological impacts, as noted in studies by Merlin et al. [65]. Beyond traditional sorbents, innovative materials like graphene-based nanomaterials are being investigated for their superior oil sorption and reusability. For instance, Chowdhury et al. [66] demonstrated the high capacity and reuse potential of graphene-based aerogels, pointing to their promise in advanced oil spill technologies.

Natural sorbents like hay, straw, and peat moss have long been used for oil absorption, although they typically offer lower efficiency compared to synthetic options. Al-Jammal & Juzsakova [67] discuss the practicality of using natural sorbents in spill cleanup, emphasizing their biodegradability and ease of access. Meanwhile, magnetic nanoparticles present a novel approach, enabling targeted recovery of oil through magnetic separation. Research by Qiao et al. [68] highlights the effectiveness of magnetic nanocomposites in selectively removing oil, providing a sustainable and efficient cleanup option.

Sorbents are broadly categorized into seven classes: bio-sorbents, activated carbons, biochars, polymers and resins, clays and minerals, nanoparticles, and composites [32]. Among these, bio-sorbents are most commonly used for their availability and ease of preparation, whereas activated carbon, clays, and minerals see less frequent application. Typical examples of bio-sorbent materials include rice straw, wood fibre, sawdust, cotton, kapok, luffa, kenaf, coconut husk, and bagasse, among others [25]. Numerous studies have investigated the oil sorption potential of these materials, focusing on properties such as hydrophobicity or oleophilicity, high uptake capacity, buoyancy, durability, reusability, biodegradability, and oil recovery [8]. Since it may be difficult to find a single material with all these qualities, compromises are often necessary in selecting the most appropriate sorbent.

A comprehensive oil spill response considers the optimal use of these materials and technologies, carefully assessing factors like the type of oil spilled, spill size, and environmental conditions to maximize efficiency and minimize ecological impact. Sorbents are most often used to remove final traces of oil, or in areas that cannot be reached by skimmers. Once sorbents have been used to recover oil, they must be removed from the water and properly disposed of on land or cleaned for reuse. Any oil that is removed from sorbent materials must also be properly disposed of or recycled. Sorbent materials for oil spills present urgent environmental challenges, necessitating effective cleanup strategies. Sorbent materials play a crucial role in mitigating the impact of oil spills by adsorbing and removing oil from contaminated surfaces. A diverse range of sorbents, including natural, synthetic, and composite materials, have been investigated for their efficacy in oil spill cleanup applications [69].

Natural organic: Natural sorbents, such as peat moss, sawdust, and cotton, offer advantages in terms of biodegradability and cost-effectiveness [60]. They are relatively inexpensive and usually readily available. Organic sorbents can soak up from 3 to 15 times their weight in oil, but they do present some disadvantages. Some organic sorbents tend to soak up water as well as oil, causing them to sink. Many organic sorbents are loose Application of sorbents. Photo courtesy of US Coast Guard particles, such as sawdust, and are difficult to collect after they are spread on the water. Adding flotation devices, such as empty drums attached to sorbent bales of hay, can help to overcome the sinking problem, and wrapping loose particles in the mesh will aid in the collection. These materials have demonstrated promising performance in absorbing and retaining oil from aqueous environments, making them suitable candidates for oil spill remediation efforts [47].

Natural inorganic sorbents: Include clay, perlite, vermiculite, glass, wool, sand, and volcanic ash. They can absorb from 4 to 20 times their weight in oil. Inorganic substances, like organic substances, are inexpensive and readily available in large quantities.

Synthetic sorbents: Synthetic sorbents, such as polypropylene and polyurethane foam, possess high oil absorption capacities and can be engineered to target specific types of oil and environmental conditions [60]. Most synthetic sorbents can absorb as much as 70 times their weight in oil, and some types can be cleaned and reused several times. Synthetic sorbents that cannot be cleaned after they are used can present difficulties because they must be stored temporarily until they can be disposed of properly. However, concerns regarding the environmental impact and long-term persistence of synthetic sorbents have prompted researchers to explore alternative materials with reduced ecological footprint [70].

Composite sorbents: Combining natural and synthetic components, aims to harness the benefits of both material types while mitigating their respective drawbacks [71]. These hybrid sorbents offer improved oil absorption

capacities and environmental sustainability, making them attractive options for oil spill cleanup operations [36].

The following characteristics must be considered when choosing sorbents for cleaning up spills:

• **Rate of absorption**—The rate of absorption varies with the thickness of the oil. Light oils are soaked up more quickly than heavy ones.
• **Oil retention**—The weight of recovered oil can cause a sorbent structure to sag and deform. When it is lifted out of the water, it can release oil that is trapped in its pores. During the recovery of absorbent materials, lighter, less viscous oil is lost through the pores more easily than heavier, more viscous oil.
• **Ease of application**—Sorbents may be applied to spills manually or mechanically, using blowers or fans. Many natural organic sorbents that exist as loose materials, such as clay and vermiculite, are dusty, difficult to apply in windy conditions, and potentially hazardous if inhaled.

7.1 Factors affecting materials for sorption

The performance of materials used for remediation in hydrocarbon-contaminated environments is significantly influenced by their surface area, pore structure, and functional group chemistry. These factors play critical roles in enhancing the material's effectiveness in tasks such as adsorption, separation, and oil spill cleanup. Various studies have highlighted the importance of these characteristics.

In the context of petroleum hydrocarbon contamination, biochar has been demonstrated to possess a high surface area, which provides more active sites for the adsorption of pollutants. The extensive surface area of biochar-based materials allows them to adsorb larger quantities of hydrocarbons, thus improving their efficiency in soil and water remediation. Wei et al., [72] noted that the performance of biochar-based sorbents is closely related to their specific surface area and microporous structure, which enable greater interaction with petroleum contaminants. Similarly, the surface area of nanocellulose composites has been identified as a key factor for improving their oil sorption capabilities. In their review, Muhammad et al., [73] emphasized that enhancing the surface area of biomass-based aerogels can lead to better oil spill cleanup performance due to increased exposure to the contaminant molecules.

The pore structure of these materials is equally critical, as it dictates the accessibility and diffusion of hydrocarbons within the material. Pore size distribution and the volume of pores in biochar-based materials and cellulose-derived aerogels are crucial in determining their efficiency. Materials with a high proportion of mesopores and macropores provide better access for larger hydrocarbon molecules, while micropores are effective for smaller molecules. This structure facilitates a combination of adsorption and capillary action, which is essential for the removal of oils and other organic contaminants from affected water or soil. Studies by Soares et al., [74] highlighted that the pore structure of nanocellulose-based sorbent composites greatly impacts their sorption properties, with optimal pore sizes improving the rate of contaminant uptake. Likewise, the pore architecture in cellulose aerogels, as reviewed by Zhai et al., [75], allows for efficient separation of oil from water, with the ability to trap oil molecules while repelling water, showcasing the importance of tailoring pore size distribution in materials for oil spill remediation.

Functional group chemistry also plays a pivotal role in the performance of these materials. The presence of functional groups such as hydroxyl, carboxyl, and phenolic groups can significantly influence the adsorption of hydrophobic pollutants. These groups can enhance the interaction between the sorbent material and the oil molecules, increasing the overall efficiency of the cleanup process. Functionalization of biochar, for example, can introduce additional chemical sites that increase its affinity for hydrophobic substances, improving its performance in oil spill scenarios. In their study, Zamparas et al., [76] emphasized that natural-based modified materials, including biochar, with tailored functional groups, show promising results for oil spill cleanup by enhancing the hydrophobicity and adsorption capacity of the materials. Similarly, the modification of cellulose aerogels with functional groups like carboxyl and amine has been shown to increase their affinity for oil, as discussed by Chhajed et al., [77], further confirming the role of chemical modifications in improving performance.

7.2 Utilization used for sorbents

After the initial absorption of oil using biomass as a sorbent, exploring reutilization methods becomes crucial in tackling the problem of oil spills across various applications. One promising approach is the carbonization of the used sorbent material [78]. Wong *et al*., [79] have demonstrated the effectiveness of carbonization in transforming organic waste materials into activated carbon, which possesses enhanced adsorption properties. The carbonization process involves heating the used sorbent material to high temperatures in the absence of oxygen, resulting in the decomposition of organic components and the formation of a carbon-rich structure. This transformation enhances the surface area and porosity of the material, thereby increasing its capacity to adsorb oil and other hydrocarbons. Research by Shaer *et al*., [80] has shown that carbonized sorbents derived from natural fibres exhibit superior adsorption capacities compared to their non-carbonized counterparts. The carbonization process can help address concerns regarding the disposal of used sorbent materials. Instead of ending up in landfills or incinerators, which can contribute to environmental pollution, the carbonized sorbents can be repurposed for various applications. For instance, activated carbon derived from carbonized ginger fibre sorbents can be utilized in wastewater treatment, air purification, and even as a component in rechargeable batteries [81]. In addition to its environmental benefits, the reutilization of used sorbents through carbonization offers economic advantages by providing a cost-effective alternative to traditional disposal

methods. By transforming waste materials into valuable resources, this approach aligns with the principles of the circular economy, where resources are kept in use for as long as possible.

7.4 Different methods of conversion of used sorbents

Pyrolysis involves heating the sorbent material, such as ginger fibre, in the absence of oxygen to thermally decompose the absorbed oil. This process typically occurs at temperatures ranging from 300 to 800 ^{o}C [82]. During pyrolysis, the organic components of the absorbed oil break down into smaller molecules, producing gases, liquids, and char residues [83]. Vamvuka (2011) investigated the pyrolysis of oil-saturated sorbents, including plant-based materials, to recover energy and valuable products. Their study highlighted the potential of pyrolysis for oil recovery and sorbent regeneration.

Biomass includes the by-products and residues of farm products and agricultural processing industries, such as husks, cobs, leaves, straw, stalks, barks, grains, and weeds [85]. These materials have long remained the primary energy source for household usage in many underdeveloped and developing countries [86]. It is the only renewable energy source that can be utilized to make biofuel [87], and one of the techniques to achieve this in modern times is thermal conversion through retort carbonization. Carbonization is a slow pyrolysis process in which biomass is converted into a highly carbonaceous, charcoal-like material referred to as *biochar* [88]. Typically, it involves heating the biomass in the absence or insufficiency of oxygen, and reaction conditions can be tailored to maximize the production of the char. The characteristic feature that distinguishes carbonization from other, dry thermochemical conversion techniques is the heating time- it is significantly longer. However, this long duration results in a high yield of char with better porous properties. An overview of other characteristic features is highlighted in Table 3.

Table 3. Typical Reaction Conditions and Product Yields in wt% from Different Types of (Dry) Thermochemical Conversion Processes (Bridgwater, 2012; Nachenius et al., 2013)

Properties	**Thermochemical Conversion Process Type**			
	Fast Pyrolisis	**Carbonization**	**Gasification**	**Torrefaction**
Temperature	~500^{o}C	>400^{o}C	600-1800^{o}C	<300^{o}C
Heating rate	Fast, up to 100^{o}C	<80 ^{o}C/min	-	-
Reaction time	Few seconds	Hours ~days	-	<2h
Pressure	Atmospheric (and vacuum)	Atmospheric (or elevated up to 1MPa)	Oxygen-limited (air or steam/oxygen)	Oxygen-free
Medium	Oxygen-free	Oxygen-free or Oxygen-limited	Oxygen-limited (air or steam/oxygen)	Oxygen-free
Liquids (Bio-oil)	75%	30%	5%	5%
Noncondensable gases	13%	35%	85%	15%
Char/Solids	12%	35%	10%	80%

Gasification involves subjecting the sorbent material to high temperatures and controlled amounts of oxygen or steam to produce a combustible gas mixture known as syngas. This process occurs at temperatures above 700 ^{o}C [89]. Ali *et al*., [90] explored gasification as a method for treating oil-contaminated sorbents, demonstrating its potential for energy recovery and sorbent regeneration. Gasification offers a pathway for utilizing the energy content of the oil while simultaneously regenerating the sorbent material by converting the absorbed oil into syngas [91].

Hydrothermal treatment utilizes water at elevated temperatures and pressures to chemically decompose the absorbed oil and regenerate the sorbent material. This process typically occurs at temperatures above 200 ^{o}C and pressures above atmospheric pressure [92]. Zamparas *et al*., [69] Investigated the hydrothermal treatment of oil-contaminated sorbents, highlighting their effectiveness in removing oil and recovering the sorbent's adsorption capacity. Hydrothermal treatment offers a sustainable approach to sorbent regeneration by utilizing water as a medium for oil removal and sorbent recovery [93].

Catalytic Conversion: Catalytic conversion involves the use of catalysts to enhance thermochemical processes such as pyrolysis or gasification for more efficient oil recovery and sorbent regeneration [94]. Claydon, [95] explored the catalytic pyrolysis of oil-saturated sorbents, indicating improved oil recovery and sorbent reusability compared to non-catalytic methods. By facilitating the decomposition of absorbed oil at lower temperatures and promoting the

formation of valuable products, catalytic conversion enhances the overall efficiency of sorbent regeneration processes [7].

7.5 Biomass-based and synthetic sorbents

The synthesis and application of advanced materials for oil-water separation and spill cleanup have seen significant progress, offering solutions to critical environmental challenges. The reviewed studies present innovative approaches leveraging diverse mechanisms, material properties, and fabrication techniques to enhance oil absorption, separation efficiency, durability, and scalability, as well as address the viscosity challenges of crude oil. These advancements collectively contribute to the broader objectives of environmental sustainability and pollution control. Table 4 shows a list of both biomass-based and synthetic sorbents with their respective features.

In Lu et al., [96], the superhydrophilic Cu-HHTP@Cu foam and its superhydrophobic counterpart, PDMS@Cu-HHTP@Cu foam, demonstrated excellent oil/water separation efficiency and durability. Notably, the hierarchical structure and photothermal conversion properties of the modified foam enabled rapid reduction of crude oil viscosity under simulated sunlight, thereby facilitating effective cleanup. This multifunctionality addresses key challenges such as handling high-viscosity oils and achieving long-term performance. Additionally, the material's stability under acidic, alkaline, and saline conditions reinforces its practical applicability in diverse environmental settings, highlighting its potential for real-world implementation.

The work by Fu et al., [97] introduced SNC-g-P(MA-co-PMMA), a high-oil-absorbing resin prepared via grafting spherical nanocrystalline cellulose with methacrylic acid and methyl methacrylate. The porous structure and large specific surface area enhanced oil absorbency, while thermal stability allowed usage in high-temperature environments. These features, combined with the cost-effectiveness of cellulose as a raw material and the simplicity of the manufacturing process, make this resin a promising candidate for large-scale production and deployment in oil pollution mitigation.

Table 4. Comparison of Oil Absorption Capacities and Performance Metrics

Material	Type	Oil Absorption Capacity (g/g)	Key Features	Ref
Superhydrophobic Fe3O4/PAN/PBA Nanofibrous Aerogel (NFA)	Synthetic	54.4–97.1	Ultra-high absorption for oils and solvents; photothermal and magnetothermal effects for crude oil recovery (6.67 x 10^3 kg/m^3·h).	[101]
Recycled PET with PEG and HDIT	Synthetic	~22	Sustainable use of PET waste; effective oil-water separation with high flux (~726.7 L/m^2·h under gravity). >97% (oil-water emulsion)	[102]
Electrospun nanofibrous membranes based on fluorine-free polyimide.	Synthetic	35–60	Hydrophobic with water contact angle of 114° and oil contact angle of ~0°. Rapid sorption with equilibrium reached in minutes for crude oil. High flux (1991 L/m^2/h for dodecane, 1508 L/m^2/h for n-hexane, 206 L/m^2/h for crude oil).	[99]
Carbonized sponge (P-Fe_3O_4@CMS)	Synthetic	45.3–88.5	Superhydrophobic and magnetically responsive. Self-heating ability with high compressibility. Pump-assisted continuous oil recovery with a high flux of 785 kg/m^2/h.	[100]
PVA/CNC Membranes	Biomass-based	17.01–113.76	High absorption is influenced by oil viscosity, with exceptional reusability and separation efficiency (>99%).	[103]
SNC Resin	Biomass-based	8.5	High thermal stability, with effective network volume and surface area for enhanced absorption.	[97]
LPUF Foam	Biomass-based	13.2–53.0	High hydrophobicity (WCA = 151.3°) and mechanical performance, with flame retardancy for safe oil absorption.	[98]

Cui et al., [98] presented a lignin-based polyurethane foam modified with aluminium 12-hydroxy stearate (Al HSA) and expanded graphite (EG). The resulting composite demonstrated exceptional oil sorption capacity and hydrophobicity, alongside enhanced mechanical resilience and flame retardancy. The biomimetic

microstructure and the inclusion of organogelator components facilitated efficient oil retention and recyclability, even after repeated use. The combination of high porosity and robust physical properties suggests that this material is suitable for continuous oil/water separation and provides a sustainable approach to remediating oil spills and organic solvent pollution.

The electrospun fluorine-free polyimide nanofibrous membranes developed by Alharthi and Abdulhamid, [99] further contribute to advancements in oil spill cleanup technology. These membranes exhibited high adsorption capacities, rapid sorption kinetics, and impressive flux rates for various oils. Their hydrophobic nature and recyclability, coupled with stability at high temperatures, underline their effectiveness in real-world applications. The scalability of these membranes through industrial electrospinning also positions them as viable candidates for addressing large-scale oil and chemical spillages.

Liu et al., [100] tackled the challenge of high-viscosity crude oil by introducing a multifunctional, superhydrophobic, and magnetically responsive carbonized sponge. The sponge's electro-thermal and photo-thermal conversion capabilities enabled significant viscosity reduction, enhancing oil absorption speed and recovery efficiency. The pump-assisted continuous oil recovery system showcased the sponge's adaptability for energy-efficient, all-weather operation. Its straightforward fabrication process and 24/7 functionality underscore its practical value in addressing oil spill remediation challenges under varying environmental conditions.

While synthetic materials may excel in certain attributes, biomass-derived materials like PVA/CNC membranes with 113.76 g/g absorption capacity offer sustainable and competitive performance. Collectively, these studies underscore the transformative potential of engineered materials in oil spill cleanup and water-oil separation technologies. They highlight key innovations, including the integration of photothermal conversion for viscosity reduction, incorporation of cost-effective and biodegradable raw materials, enhancement of mechanical and thermal properties, and scalability for industrial applications. However, future research should address specific challenges, such as further optimizing material performance under extreme environmental conditions, reducing manufacturing costs for widespread adoption, and evaluating the long-term environmental impacts of these materials. By building on these advances, researchers can continue to refine and expand the applicability of these promising solutions to global environmental challenges.

4. CONCLUSION

Oil spill cleanup remains a critical environmental and ecological challenge with profound implications for marine ecosystems and coastal regions. This review has evaluated various oil spill remediation methods, including mechanical containment and recovery, chemical dispersion, in-situ burning, bioremediation, and sorption. Among these, sorption stands out as a particularly promising approach, especially when employing biomass-derived sorbent materials due to their sustainability, cost-effectiveness, and environmentally friendly properties.Biomass sorbents offer significant advantages over synthetic alternatives, such as biodegradability, renewability, and the potential for chemical modification to enhance sorption efficiency. Their adaptability enables the optimization of surface area, pore structure, and functional group composition, resulting in superior oil retention capacity, stability, and reusability. Despite these benefits, challenges related to their mechanical strength, stability under marine conditions, and scalability must be addressed to maximize their potential.

To advance the application of biomass sorbents for oil spill cleanup, future research should focus on:

- **Enhancing Material Performance**: Developing biomass sorbents with improved surface area, pore structure, and functional groups to boost sorption efficiency and oil affinity while maintaining hydrophobicity and water resistance.

- **Improving Mechanical Stability**: Investigating treatments or hybrid designs that integrate biomass with synthetic or inorganic materials to enhance mechanical strength and durability in harsh marine environments.

- **Assessing Environmental Impact**: Conducting studies on the long-term effects of biomass sorbents on marine ecosystems, including degradation byproducts and potential secondary contamination, while leveraging life cycle assessments to evaluate their environmental footprint.

- **Scalability and Cost Efficiency**: Exploring cost-effective, high-yield production methods to make biomass sorbents viable for large-scale applications, alongside assessing their economic feasibility compared to conventional methods.

- **Field Testing and Real-World Applications**: Performing field trials in diverse marine environments to validate laboratory findings, addressing variables such as wave action, temperature fluctuations, and oil composition to understand their practical performance.

ACKNOWLEDGEMENTS

We would like to thank the Faculty of Engineering and Technology University of Ilorin.

REFERENCES

[1] M. L. Bender, M. Frantzen, L. Camus, S. Le Floch, J. Palerud, and J. Nahrgang, (2018) 468–477.

[2] J. Short, (2003) 509–517.

[3] L. N. Dornberger, "Using Ecosystem-Based Modeling to Describe an Oil Spill and Assess the Long-Term Effects," University of South Florida, 2018.

[4] R. Al-Ruzouq, (2020) 3338. doi: 10.3390/rs12203338.

[5] A. Bejarano, E. Levine, and A. Mearns, (2013) 185. doi: 10.1007/s10661-013-3332-y.

[6] B. Laffon, E. Pásaro, and V. Valdiglesias, (2016) 105–128. doi: 10.1080/10937404.2016.1168730.

[7] S. Hammouda, Z. Chen, C. An, and K. Lee, (2021) 127630. doi: 10.1016/j.jclepro.2021.127630.

[8] N. A. binti Nordin, "Oil Spill Cleanup using Raw Kapok as the Sorbent Material," Universiti Teknologi PETRONAS, 2013.

[9] R. Gautam, A. Mudhoo, G. Lofrano, and M. Chattopadhyaya, (2013).

[10] H. Cheng, (2020) 101253. doi: 10.1016/j.progpolymsci.2020.101253.

[11] O. M. Lawal and N. C. Nwokem, (2017) 973–975.

[12] H. J. Perera, A. Goyal, S. M. Alhassan, and H. Banu, (2022) 5310. doi: 10.3390/polym14235310.

[13] Z. Raji, A. Karim, A. Karam, and S. Khalloufi, (2023) 74–91. doi: 10.1016/j.tifs.2023.05.004.

[14] Y. Wang, Z. Guo, and W. Liu, (2021) 4895–4928.

[15] S. M. Abegunde, K. S. Idowu, O. M. Adejuwon, and T. Adeyemi-Adejolu, (2020) 100001. doi: https://doi.org/10.1016/j.resenv.2020.100001.

[16] L. M. Macdonald, M. Williams, D. Oliver, and R. Kookana, (2015) 142–147.

[17] V. Singh, S. Jinka, K. Hake, S. Parameswaran, R. Kendall, and S. Ramkumar, (2014) 11954–11961. doi: 10.1021/ie5019436.

[18] S. E. Allan, B. W. Smith, and K. A. Anderson, (2012) 2033–2039. doi: 10.1021/es202942q.

[19] M. Husseien, A. Amer, A. El- Maghraby, and N. Taha, (2008).

[20] H. O. Nwabueze, P. N. Chiaha, B. C. Ezekannagha, and O. E. Okoani, (2016) 53–59.

[21] J. O. Nwadiogbu, V. I. E. Ajiwe, and P. A. C. Okoye, (2016) 56–63. doi: 10.1016/j.jtusci.2015.03.014.

[22] N. Duc, (2018) 201. doi: 10.15625/2525-2518/54/2A/11931.

[23] S. C. Pennings, B. D. McCall, and L. Hooper-Bui, (2014) 789–795. doi: 10.1093/biosci/biu118.

[24] N. K. Shah, Z. Li, and M. G. Ierapetritou, (2011) 1161–1170. doi: 10.1021/ie1010004.

[25] R. Asadpour, N. Sapari, and Z. Harith, (2013) 46–57.

[26] M. O. Mafiana, M. D. Bashiru, F. Erhunmwunsee, C. G. Dirisu, and S.-W. Li, (2021) 4073–4094. doi: 10.1007/s11356-020-11533-1.

[27] J. E. Johnston, E. Lim, and H. Roh, (2019) 187–199. doi: 10.1016/j.scitotenv.2018.11.483.

[28] R. Olawoyin, S. A. Oyewole, and R. L. Grayson, (2010) 120–130.

[29] A. D. Ogbu, W. Ozowe, and A. H. Ikevuje, (2024) 208–227. doi: 10.30574/gscarr.2024.20.1.0262.

[30] A. A. Al-Majed, A. R. Adebayo, and M. E. Hossain, (2012) 213–227.

[31] M. M. Nuhu, E. R. Rene, and A. Ishaq, (2017) 21793. doi: 10.1002/tqem.21793.

[32] E. C. Emenike, (2022) 103330. doi: 10.1016/j.jwpe.2022.103330.

[33] A. Dhaka and P. Chattopadhyay, (2021) 112428.

[34] J. Michel and M. Fingas, (2016) 159–201. doi: 10.1142/9789814699983_0007.

[35] M. Naseri, J. Barabady, T. Nowakowski, M. Młyńczak, A. Jodejko-Pietruczuk, and S. Werbińska-Wojciechowska, (2015) 6017–614.

[36] A. T. Hoang, X. P. Nguyen, X. Q. Duong, and T. T. Huynh, (2021) 28876–28910.

[37] M. A. Abdullah, A. U. Rahmah, and Z. Man, (2010) 683–691. doi: 10.1016/j.jhazmat.2009.12.085.

[38] P. Li, Q. Cai, W. Lin, B. Chen, and B. Zhang, (2016) 6–27.

[39] D. Dimitrakiev, Y. Dachev, and D. Milev, (2020) 710–712.

[40] Y. K. Adofo, E. Nyankson, and B. Agyei-Tuffour, (2022) e10153.

[41] M. Fingas, (2011) 737–903. doi: 10.1016/B978-1-85617-943-0.10023-1.

[42] B. Macaulay and D. Rees, (2014) 9–37.

[43] I. B. Ivshina, (2015) 1201–1219.

[44] C. Karan, R. Rengasamy, and D. Das, (2011).

[45] N. Bhardwaj and A. N. Bhaskarwar, (2018) 1758–1771. doi: 10.1016/j.envpol.2018.09.141.

[46] E. K. Sam, J. Liu, and X. Lv, (2021) 2353–2364.

[47] J. Ge, H. Zhao, H. Zhu, J. Huang, L. Shi, and S. Yu, (2016) 10459–10490.

[48] P. L. Yap, M. J. Nine, K. Hassan, T. T. Tung, D. N. H. Tran, and D. Losic, (2021) 2007356. doi: 10.1002/adfm.202007356.

[49] J. Zhang, G. Lu, and Z. You, (2020) 108340.

[50] L. Jiang and Z. Fan, (2014) 1922–1945. doi: 10.1039/C3NR04555B.

[51] Y. Lu, Y. Zhu, F. Yang, Z. Xu, and Q. Liu, (2021) 2004082.

[52] D. Angelova, I. Uzunov, S. Uzunova, A. Gigova, and L. Minchev, (2011) 306–311.

[53] A. T. Hoang, S. Nižetić, X. Q. Duong, L. Rowinski, and X. P. Nguyen, (2021) 130274.

[54] N. Babanejad, K. Mfoafo, E. Zhang, Y. Omidi, R. Razeghifard, and H. Omidian, (2022) 463546.

[55] D. Ouyang, X. Lei, and H. Zheng, (2023) 620.

[56] J. Dai and H. Zhang, (2021) 2005334. doi: 10.1002/smll.202005334.

[57] S. Dutta et al, (2017) 522–545.

[58] L. M. T. M. Oliveira, J. Saleem, A. Bazargan, J. L. D. S. Duarte, G. McKay, and L. Meili, (2020) 124842. doi: 10.1016/j.jhazmat.2020.124842.

[59] J. Li et al.,(2022) 118789.

[60] Q.-W. Zhang, L.-G. Lin, and W.-C. Ye, (2018) 20. doi: 10.1186/s13020-018-0177-x.
[61] F. Ding and M. Gao, (2021) 102377. doi: 10.1016/j.cis.2021.102377.
[62] A. Pintor, V. Vilar, C. Botelho, and R. Boaventura, (2016). doi: 10.1016/j.cej.2016.03.121.
[63] C. S. Quek, N. Ngadi, and M. A. Ahmad Zaini, (2020) 507–512.
[64] P. Bharali et al., (2022) 13, doi: 10.1007/s13205-021-03068-0.
[65] F. Merlin et al., (2021) 37. doi: 10.1186/s40068-021-00241-5.
[66] S. Chowdhury, S. Pan, R. Balasubramanian, and P. Das, (2019) 43–68. doi: 10.1007/978-3-319-75484-0_3.
[67] A. S. I. Al-Jammali, (2022) 47–63. doi: 10.52716/jprs.v12i2.657.
[68] K. Qiao et al., (2019) doi: 10.1016/j.jtice.2019.01.029.
[69] M. Zamparas, D. Tzivras, V. Dracopoulos, and T. Ioannides, (2020) 4522.
[70] H. Kim, G. Zhang, T. Chung, and C. Nam, (2021). doi: 10.1002/adsu.202100211.
[71] T.-C. Tang et al., (2020) 332–350. doi: 10.1038/s41578-020-00265-w.
[72] Z. Wei et al., (2024) 350–372. doi: 10.1016/j.jes.2023.04.008.
[73] S. Muhammad et al., (2024) 100249, doi: 10.1016/j.giant.2024.100249.
[74] A. P. S. Soares, Maria F. V. Marques, and M. G. Mothé, (2024) 4539–4553. doi: 10.1007/s13399-022-02660-5.
[75] Y. Zhai, X. Yuan, C. C. Weber, R. J. Varley, and L. C. Henderson, (2024) 113716. doi: 10.1016/j.jece.2024.113716.
[76] M. Zamparas, D. Tzivras, V. Dracopoulos, and T. Ioannides, (2020) 4522. doi: 10.3390/molecules25194522.
[77] M. Chhajed, C. Verma, and P. K. Maji, (2024) 116024. doi: 10.1016/j.marpolbul.2024.116024.
[78] A. I. Osman, A. M. Elgarahy, N. Mehta, A. H. Al-Muhtaseb, A. S. Al-Fatesh, and D. W. Rooney, (2022) 12433–12447.
[79] W. Syie Luing, N. Ngadi, I. Inuwa, and O. Hassan, (2018) 361–375.
[80] C. Shaer, L. Oppenheimer, A. Lin, and H. Ishida, (2021) 3775. doi: 10.3390/polym13213775.
[81] Z. Sun et al., (2021) 1–12. doi: 10.1007/s42114-021-00352-8.
[82] I. M. Maafa, (2021) 225.
[83] M. Sekar, V. K. Ponnusamy, A. Pugazhendhi, S. Nižetić, and T. Praveenkumar, (2022) 114046.
[84] D. Vamvuka, (2011) 835–862.
[85] A. Adeniyi et al., (2022). doi: 10.1007/s10098-022-02415-w.
[86] S. K. Sansaniwal, K. Pal, M. A. Rosen, and S. K. Tyagi, (2017) 363–384.
[87] Y.-K. Park et al., (2019) 1706–1718. doi: 10.1016/j.apenergy.2019.05.088.
[88] F. Ronsse, R. W. Nachenius, and W. Prins, (2015) 293–324. doi: 10.1016/B978-0-444-63289-0.00011-9.
[89] Y. A. Situmorang, Z. Zhao, A. Yoshida, A. Abudula, and G. Guan, (2020) 109486.
[90] I. Ali, M. Asim, and T. A. Khan, (2012) 170–183 doi:https://doi.org/10.1016/j.jenvman.2012.08.028
[91] B. Wang, R. Gupta, L. Bei, Q. Wan, and L. Sun, (2023) 26676–26706.
[92] T. R. Sarker, F. Pattnaik, S. Nanda, A. K. Dalai, V. Meda, and S. Naik, (2021) 131372.
[93] A. V. Baskar et al., (2022) 153555.
[94] Y. Wu et al., (2022) 462–481.
[95] R. Claydon, "Advanced assessment of in-situ thermal Enhanced Oil Recovery (EOR) to promote coproduction of both catalytically-upgraded oil and hydrogen gas," University of Birmingham, 2021.
[96] J. Lu, X. He, B. Li, S. Meng, and Z. Li, (2025) 128483. doi: 10.1016/j.seppur.2024.128483.
[97] E. Fu, L. He, J. Chao, and X. Dai, (2025) 140622, doi: 10.1016/j.molstruc.2024.140622.
[98] S. Cui et al., (2025) 130177. doi: 10.1016/j.seppur.2024.130177.
[99] S. N. Alharthi and M. A. Abdulhamid, (2025) 129189. doi: 10.1016/j.seppur.2024.129189.
[100] T. Liu et al., (2025) 128516. doi: 10.1016/j.seppur.2024.128516.
[101] X. Zeng et al., (2025) 128460. doi: 10.1016/j.seppur.2024.128460.
[102] Y. Gao, H. Xing, and Y. Zhang, (2025) 128721. doi: 10.1016/j.seppur.2024.128721.
[103] J. Bang et al., (2025) 129278. doi: 10.1016/j.seppur.2024.129278.

Malaysian Journal of Catalysis
http://mjcat.utm.my/
MJCat Research Article

Synthesis and Characterization of Fe_2O_3/g-C_3N_4 Photocatalyst from Waste Toner Powder

Asmawati @ Fatin Najihah Alias[1], Nur Hazirah Rozali Annuar[2*], Nurul Sahida Hassan[3], Sharifah Najiha Timmiati[4]

[1]*Faculty of Applied Sciences, Universiti Teknologi MARA, Cawangan Johor, Kampus Pasir Gudang, 81750 Masai, Johor, Malaysia.*
[2]*Advanced Biomaterials and Carbon Development, Universiti Teknologi MARA, 40450, Shah Alam, Selangor, Malaysia.*
[3]*Centre of Hydrogen Energy, Institute of Future Energy, Universiti Teknologi Malaysia, 81310 UTM Johor Bahru, Malaysia.*
[4]*Fuel Cell Institute, Universiti Kebangsaan Malaysia, 43600, Bangi, Selangor, Malaysia.*

**Corresponding Author: nurha8558@uitm.edu.my*

Article history:
Received 04 November 2024
Accepted 04 February 2025

ABSTRACT

Modern use of electrical and electronic equipment and the rapid development of technologies lead to the production of electronic waste. Electronic waste management is one of the key challenges for the green revolution without affecting the environment. One of the electronic wastes includes toner powder from the printer. Toner powder consists of polymer, carbon black, Fe_3O_4, additives and charge control agents. This paper focuses on the synthesis and characterization of Fe_2O_3/g-C_3N_4 photocatalyst. Initially, waste toner powder was calcined at 600 °C at air atmosphere to ensure the complete decomposition of organic residues. Then the obtained Fe_2O_3 was mixed with g-C_3N_4 by polycondensation method for fabrication of Fe_2O_3/g-C_3N_4 photocatalyst. The obtained Fe_2O_3, g-C_3N_4 and Fe_2O_3/g-C_3N_4 were characterized by FTIR, SEM, TGA and XRD. FTIR, SEM and XRD results confirm that Fe_2O_3 is successfully incorporated with g-C_3N_4 while TGA analysis demonstrates an excellent thermal stability for Fe_2O_3/g-C_3N_4 photocatalyst. The physicochemical properties of Fe_2O_3/g-C_3N_4 catalyst demonstrated its ability to be utilized in a variety of photocatalytic reactions. Therefore, the utilization of waste toner powder as an iron (Fe) precursor may offer a great opportunity for waste management and the fortification of the environment such as in wastewater treatment.

Keywords: *Electronic waste, Toner powder, Fe_2O_3/g-C_3N_4, Photocatalyst*

| eISSN 0128-2581 |

1. INTRODUCTION

The objectives of the Twelfth Malaysia Plan (12MP) 2021-2025 realigned with the vision of the Ekonomi MADANI relate to the effort for shared prosperity, which encompasses three dimensions: economic empowerment, environmental sustainability, and social re-engineering. Based on the environmental sustainability dimension, it comprises the blue economy, green technology, renewable energy, and climate change adaptation and mitigation [1].

In recent years, to address environmental challenges and promote economic efficiency, there has been a significant increase in interest in the use of waste-derived materials to synthesize advanced photocatalysts. Photocatalytic technology has gained a lot of attention as a potential solution to environmental issues. A photocatalyst is a substrate that absorbs light and acts as a catalyst for chemical reactions, essentially functioning as a semiconductor [2]. Waste-derived can be considered a potentially attractive option for photocatalytic reaction, either utilizing waste as a source of components for photocatalysts such as titanium, sulfur, carbon and Fe or reusing them as catalysts in a synthetic process. To date, electronic wastes such as spent batteries [3], waste printed circuit board [4], waste liquid crystal displays [5], electronic packaging [6], brick waste [7], biomass waste such as soybean [8], lotus seedpod [9], rice husk [10], coffee grounds [11], other agriculture, forestry and food waste have been exploited for the fabrication of photocatalytic materials, absorbent and electrolysis. The conversion of waste as photocatalyst materials is a fascinating option due to its environmentally beneficial, eco-friendly, sustainable technology and green approach [12].

Rapid development in modern technologies, particularly in electrical and electronics and information technology, contributes to producing electronic waste (e-waste). Global e-waste monitor data for 2019 show that only 17.4% of the approximately 53.6 Mt of generated e-waste

was collected and reused [13]. As reported by worldwide e-waste research only about 20% of total world's waste is appropriately handled. The effectiveness of recycling and e-waste disposal are expensive and time consuming compared to profits that might be generated from recycling the electronic waste [14]. To achieve the objective for the e-waste management, a financial system that serves society, procedures and consumers are required [15]. For example, in Asia Pacific countries are facing significance challenges due to lack of policies, infrastructure, and financial resources. Generally, the e-waste recycling step divide into three stages namely as 1) collection, 2) sorting and dismantling and 3) end processing. As for Asia Pacific countries, mostly all the steps are handled by informal recycling sector that shortages in skilled operation which might result in severe environment pollution. To overcome this problem, a strategy that focus on synergising the informal e-waste recycling sector with the formal sector mut be considered. This must include the financial, institutional, political, and social aspects of the country [16]. Besides, the recycling of e-waste also can offer an outstanding business opportunity by converting this e-waste into valuable sources.

Toner-based printing equipment, particularly toner cartridges, is mostly used in the office and printing industries. The quantity of waste toner powder in a used cartridge is about 8% or more depending on the type of printer [17]. The percentage of waste toner was recycled only about 20 – 30% globally and the remaining was disposed via landfilling. Due to its potential health hazard, waste toner was classified as a class 2B carcinogen by World Health Organization (WHO) [17]. The composition of waste toner powder consists of 55.0 wt % polystyrene, 35.0 wt % Fe_3O_4, 7.0 wt % polyacrylate and 3.0 wt % SiO_2, which 62.0 wt % toner waste comprises of organic components that may lead to disease [18]. In recent times, few research has been reported on the recycling of waste toner powder. Waste toner powder was successfully transformed and recycled into valuable materials such as carbon-coated ferric oxides for lithium-ion batteries [19], nano-Fe_3O_4 and nano-SiO_2 for removal of Cr(VI) [20]. Previously, researchers also reported on the reutilization of waste toner powder into 3D graphene oxide [21], TiO_2/Fe_2O_3@nanographite nanohybrid [22] for wastewater treatment and FeO-NC for styrene oxidation [23].

The utilization of waste toner powder as an iron (Fe) precursor can be considered a great opportunity for waste management and the fortification of the environment. Fe_2O_3 was considered as one of the best co-catalyst due to its abundance, stability and matched bond position for efficient charge separation and enhanced photocatalytic activity with TiO_2. Iron oxide can be found as crystal phases of hematite α-Fe_2O_3), maghemite (ν-Fe_2O_3), magnetite ($F_{e3}O_4$), and wustite (FeO). However, the most common iron oxides are Fe_2O_3 and Fe_3O_4. Ferromagnetic Fe_3O_4 was employed with various other compounds in water treatment due to its easy separation of the bulk NPs from aqueous solutions via external magnetic processes or materials. Meanwhile, Fe_2O_3 is widely used in numerous sectors due to its ability to be tailored to precise morphologies, dimension orientation, and structures to produce a chemically and thermodynamically stable oxide. It can also be a good photocatalyst due to its appropriate band gap energy of between 2.0 and 2.2 eV and has high stability in aqueous and simple synthesis and most importantly is the ability to be recycled [22]. According to Khasawneh and Palaniandy, the Fe_2O_3-TiO_3 showed remarkable performance for the removal of persistent organic po llutants (POPs) as well as successful recovery and reusability of the photocatalyst after the treatment process [25]. When hematite is combined with other semiconductors, the visible absorption of the other semiconductor will be increased.

Nowadays, graphitic carbon nitride (g-C_3N_4) catalyst is known as the efficient candidate used to degrade harmful and toxic compounds in the aqueous medium. Its extraordinary properties like high chemical stability, reducibility, low product cost, non-toxicity and tunable band gap (2.7 eV) make it a superior catalyst compared to the others. Nitrogen-rich precursors like thiourea, urea or melamine are thermally polymerized at high temperatures in regulated environments to produce g-C_3N_4. The precursors endure condensation reactions which result in the formation of polymeric structures that are high in carbon and nitrogen. Then, the polymers transformed into g-C_3N_4, a two-dimensional material consisting of hexagonally arranged carbon and nitrogen atoms, upon further annealing at even higher temperatures. The addition of Fe_2O_3 into g-C_3N_4 enhanced the photocatalytic performance under visible light due to the reduction of the recombination rate of photoinduced electron-hole pairs [26]. The presence of Fe_2O_3 allows for efficient charge separation and transfer, while the g-C_3N_4 component provides a high surface area and enhanced light absorption capabilities.

The mixture of carbon-based and other elements found in printer toner, which is typically thrown away after use, can be effectively repurposed to produce value-added products with major environmental benefits. The synthesis of Fe_2O_3/g-C_3N_4 photocatalyst from waste printer toner, on the other hand, may also offer a sustainable method of utilizing important resources for critical environmental applications. In addition, recycling toner powder as iron precursor nanocomposite can eliminate the environmental risks associated with the substantial toner powder waste, thereby fostering a sustainable environment and a circular economy. Therefore, this paper explores the Fe_2O_3/g-C_3N_4 photocatalyst including its preparation method using waste toner powder as an iron precursor via calcination and the synthesized Fe_2O_3/g-C_3N_4 by polycondensation method. Fe_2O_3/g-C_3N_4 photocatalyst was characterized using SEM, FTIR and TGA. Our study aims to understand the physicochemical properties of the photocatalysts and examine their potential uses.

2. EXPERIMENTS

2.1 Synthesis of Fe_2O_3 from Waste Toner Powder

Waste toner powder was obtained from the used toner powder cartridge from Hewlett-Packard printer. The waste toner powder was directly removed from the print cartridge and subsequently, was put into a container for storage purposes. The collected powder was calcined in a muffle furnace for 2 hours at 600 °C in an air atmosphere to obtain Fe_2O_3 and was cooled overnight [27]. The obtained crystalline orange-coloured powder was identified as Fe_2O_3.

2.2 Synthesis of g-C_3N_4 and Fe_2O_3/g-C_3N_4

A 10 g of thiourea purchased from Sigma Adrich was placed in a covered crucible and was heated at 450 °C in a muffle furnace for 2 hours. The calcined thiourea was cooled overnight and the obtained yellow colour product was then ground to a fine powder and designated as g-C_3N_4. For the synthesis of Fe_2O_3-/g-C_3N_4, about 0.25 g of Fe_2O_3 and 4.0 g of thiourea were grounded using a mortar for 15 minutes. The grounded samples then were heated for 2 hours at 450 ℃ in a muffle furnace. Next, the calcined sample was washed using distilled water and dried inside an oven at a temperature of 80 °C for 3 hours [28,29]. As reported by other researchers, thiourea was used as g-C_3N_4 precursor in this experiment due to its rough and porous surface. When the surface is exposed to the light it generates the carrier and as a result, the distance between the carrier and the surface becomes shorter. Then, the recombination process will reduce which promotes a favorable photocatalytic reaction [30].

A

2.3 Catalyst Characterization

The morphology and elements of catalyst materials were investigated using a Scanning Electron Microscope (SEM Jeol JSM, IT200) with a range of magnification for the sample between 1000 to 10000. The functional groups of materials were examined by Fourier transform infrared spectroscopy (Bruker, Vertex 70). Thermogravimetric analysis, TGA (Perkin Elmer, TGA8000) was executed at the temperature between 30 °C to 900 °C at a heating rate of 10 °C/min in the presence of nitrogen gas. The crystal phase of the synthesis catalyst was obtained by XRD (Siemens D5000 diffractometer) operated at 20 mA and 30 kV using Cu Kα radiation (λ = 0.15406 nm) at room temperature.

3. RESULTS AND DISCUSSION

The morphology of catalysts was examined by Scanning Electron Microscopy (SEM) with a magnification of 1000 and 5000 respectively. Figure 1 shows the morphology structure of a waste-derived Fe_2O_3. Based on Figure 1A, the surface structure of Fe_2O_3 shows a surface with a slight unevenness and a little rocky structure. Figure 1B confirms that the structure of the surface seems to be irregular surface with a small spherical shape covering the area [30].

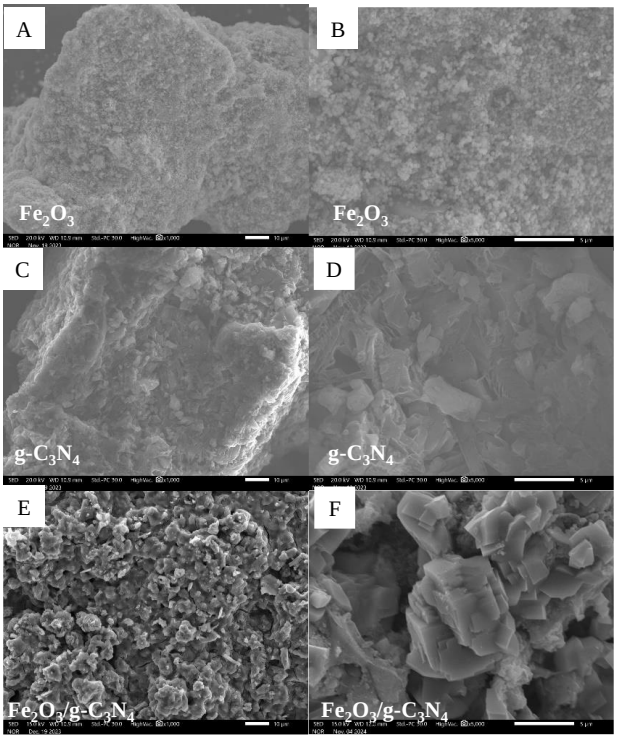

Figure 1. SEM images of Calcined Toner (Fe_2O_3) with a magnification of A) 1000, B) 5000, Calcined Thiourea (g-C_3N_4) with a magnification of D) 1000, E) 5000, and Fe_2O_3/g-C_3N_4 with a magnification of E) 1000, F) 5000

SEM images of g-C_3N_4 derived from thiourea as shown in Figure 1 (C, D) demonstrates the surface of a rocky structure with a large chunk all over the surface. Figure 1D displays the structure of g-C_3N_4 to be an aggregation of rocky particles with uneven size [30]. The microscopic morphology of Fe_2O_3/g-C_3N_4 is also obtained in this analysis. Based on Figure 1E, the surface consists of a rocky structure mixed with spherical-like particles. The surface also shows an unevenness with some areas seeming to be hollow. Figure 3C confirms the combination of Fe_2O_3 and g-C_3N_4 to form Fe_2O_3/g-C_3N_4 as it clearly shows the mixture of rocky and spherical structure shown in Figure 1 [31].

FTIR spectroscopy was utilised to identify the formation and functional groups present in the Fe_2O_3, g-C_3N_4 and Fe_2O_3/g-C_3N_4 as displayed in Figure 2. For Fe_2O_3 catalyst, peak identified at 689 cm^{-1} is attributed to vibration modes of Fe-O, while the peak at 869 cm^{-1} indicates the medium C=C bending [32,33]. An intense absorption peak at 1108 cm^{-1} is assigned to the stretching and bending of Fe-O of -Fe_2O_3 [27]. The bands between 1200 cm^{-1} to 1650 cm^{-1} for g-C_3N_4 and Fe_2O_3/g-C_3N_4 corresponds to the vibrations of C=C, C-N and C-H as reported by Wang et al. [34]. The broad bands ranging from 2900 cm^{-1} to 3400 cm^{-1} are associated to the N-H and O-H stretching vibration [34]. Besides, additional peak appeared at 2920 cm^{-1} can be assigned to Fe-N coordination bond representing an

interface interaction between Fe_2O_3 and g-C_3N_4, which may contribute to the advancement of photocatalytic activity [35]. The FTIR analysis confirms that Fe_2O_3 is successfully incorporated with g-C_3N_4 supported with SEM analysis.

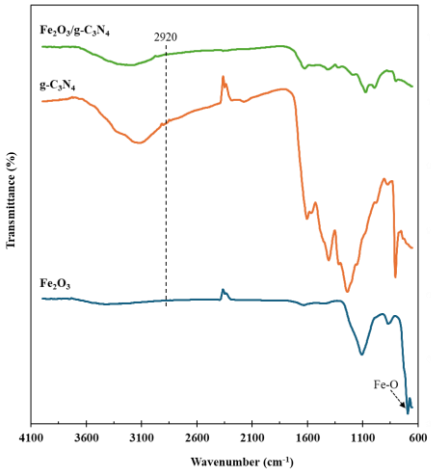

Figure 2. FTIR spectra for Fe_2O_3, g-C_3N_4 and Fe_2O_3/g-C_3N_4 photocatalysts

Thermogravimetric analysis (TGA) was performed to determine the thermal stability and content of organic components in the prepared catalyst. It was conducted under air conditions within the range of 0 to 800 °C. Figure 3A shows the inset of Fe_2O_3 photocatalyst where the weight loss of Fe_2O_3 derived from waste toner powder was slightly decreased to 98.8% due to a low percentage of organic components. The calcination process conducted prior to obtaining Fe_2O_3 removes most of the organic components. For figure 3B, it indicates that the significant weight loss for g-C_3N_4 starts at around 400 °C until the organic components completely decompose at around 700°C. The organic components in Fe_2O_3/g-C_3N_4 catalyst on the other hand starts to decompose around temperature 450°C. At temperature 600°C, maximum rate of decomposition is reached indicates that the catalyst undergoes rapid decomposition and oxidation of g-C_3N_4 and loses about 60% of their initial weight. Babar et al. explained that the decomposition of g-C_3N_4 could be ascribed to the weak van der Waals interactions between conjugated systems in g-C_3N_4 nanosheets caused by Fe_2O_3 particles [27]. At temperatures exceeding 600 °C, Fe_2O_3/g-C_3N_4 demonstrates only insignificant weight loss, implying excellent thermal stability. This divergence delivers valuable understandings into the thermal attributes of these catalysts and provide deeper conception of the role that Fe_2O_3 plays in shaping the behaviour of the photocatalyst.

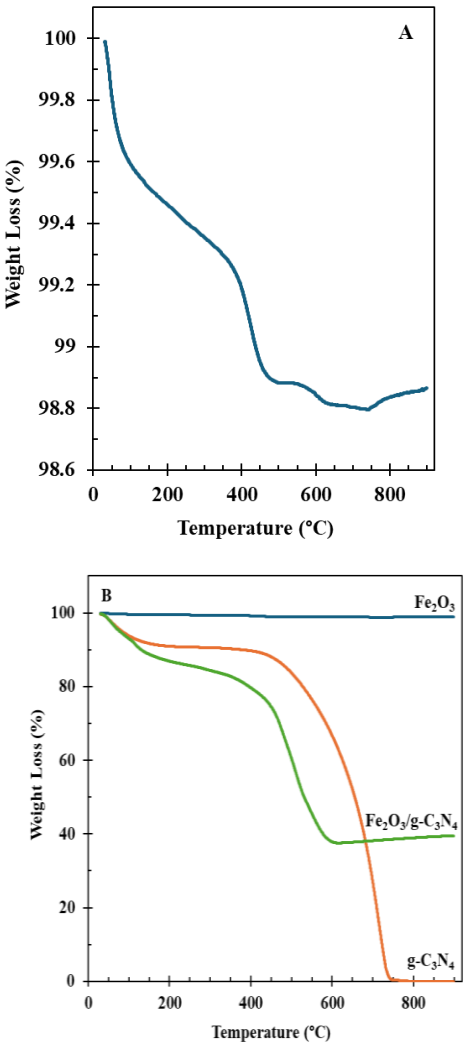

Figure 3. TGA curves of (A) inset of Fe_2O_3 and (B) Fe_2O_3, g-C_3N_4 and Fe_2O_3/g-C_3N_4 photocatalyst

The XRD analysis was carried out to investigate the crystalline structure of the fabricated photocatalyst. The peak of Fe_2O_3, g-C_3N_4 and Fe_2O_3/g-C_3N_4 are shown in Figure 4. The XRD pattern of g-C_3N_4 reveals the presence of hexagonal phase consistent with the standard (JCPDS 87-1526) for graphite-like structure of g-C_3N_4 with a distinct peak at 27.36º belongs to the (002) hkl reflection with a lattice spacing of 0.325 nm due to the interlayer stacking of conjugated aromatic systems [36]. Furthermore, Fe_2O_3 derived from waste toner powder reveals a series of characteristic peaks appeared at 26.36º, 30.43º, 35.79º, 43.54º, 54.09º, 57.42º and 63.09º which correspond to (012), (220), (110), (202), (116), (018) and (214) α-Fe_2O_3 Miller indices (JCPDS card N◦. 33–0664) [27]. The results show that the calcination of waste toner powder at 600 ºC is effective for the phase transformation of α-Fe_2O_3 from Fe_3O_4 and the decomposition of organic residues present in the toner powder [18]. As can be seen from the XRD pattern of Fe_2O_3/g-C_3N_4, adding α-Fe_2O_3 with g-C_3N_4 exhibits the same diffraction pattern as the g-C_3N_4 showing

that the crystal face of Fe_2O_3 successfully incorporates onto g-C_3N_4 with a slight shift of diffraction peak at 27.47° (002). This effect can be explained by the shrinking of the interplanar distance of g-C_3N_4 layers [37]. Meanwhile, the reduction of the intensity of the diffraction peak is due to the presence of Fe_2O_3 deterring the crystal growth of g-C_3N_4 [38]. The characteristics peak relative to α-Fe_2O_3 also can be observed in Fe_2O_3/g-C_3N_4 pattern. Notably, the diffraction peak pattern of Fe_2O_3 has well-resolved compared to Fe_2O_3/g-C_3N_4 with lesser noise. This indicates that the presence of g-C_3N_4 modifies the crystalline properties of α-Fe_2O_3 that might be due to polymeric chain of g-C_3N_4 intrinsic characteristics [39].

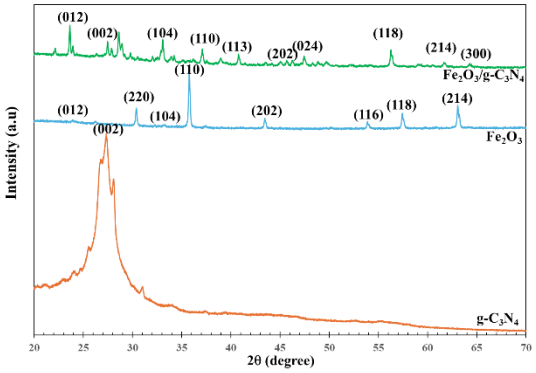

Figure 4. XRD patterns of Fe_2O_3, g-C_3N_4 and Fe_2O_3/g-C_3N_4 photocatalyst

The prepared Fe_2O_3/g-C_3N_4 photocatalyst can be used for the degradation of dye pollution such as methyl orange (MO), methylene blue (MB) and textile effluents (TE). Figure 5 shows the proposed mechanism of photocatalytic degradation using Fe_2O_3/g-C_3N_4 catalyst under sunlight radiation. Fe_2O_3 and g-C_3N_4 could generate electron and hole pairs under visible light irradiation owing to the narrow bandgap [31]. The generated Fe_2O_3 photo electrons migrated to g-C_3N_4 valence band, while the holes retained in conduction band of Fe_2O_3 attributed to the absorption of visible-light which enhanced the photocatalytic activity of the catalyst.

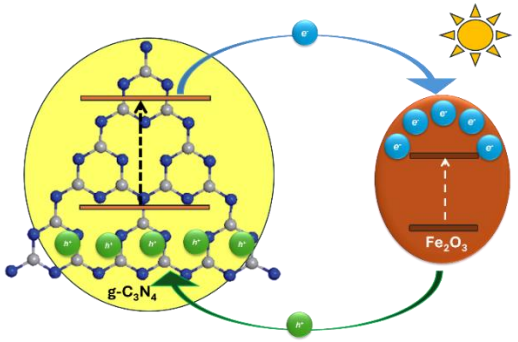

Figure 5. Proposed mechanism of Fe_2O_3/g-C_3N_4 photocatalyst under sunlight radiation

4. CONCLUSION

This study demonstrated a calcination method to transform waste toner powder into Fe_2O_3. The derived Fe_2O_3 was employed to synthesize Fe_2O_3/g-C_3N_4 photocatalyst using thiourea via polycondensation method. SEM, FTIR, TGA and XRD analysis were used to characterize the synthesized catalysts in which SEM images provide visual evidence of the formation of a strongly bonded composite between Fe_2O_3 and g-C_3N_4. Furthermore, the FTIR spectra and XRD analysis showed the existence of functional groups in the catalysts and confirmed a successful incorporation of Fe_2O_3 and g-C_3N_4. For TGA analysis, it depicted that Fe_2O_3/g-C_3N_4 photocatalyst has excellent thermal stability. Hence, Fe_2O_3/g-C_3N_4 photocatalyst derived from ink toner powder can be used as an initial reference for the photocatalytic reaction and industrial applications such as wastewater treatment. This method is cost-effective, safe and sustainable, making it environmentally friendly.

ACKNOWLEDGEMENTS

We would like to thank the School of Chemical Engineering, College of Engineering, Universiti Teknologi MARA, Johor Branch, Pasir Gudang Campus, Malaysia for the access to the instrumentations and facilities.

REFERENCES

[1] Economic Planning Unit (EPU) (2019). Twelfth Malaysia Plan, 2021-2025. Putrajaya.
[2] R. Ameta, M.S. Solanki, S. Benjamin, S.C. Ameta, Photocatalysis. Advanced oxidation processes for wastewater treatment. Academic Press, (2018) 135-175.
[3] W. Zou, X. Feng, W. Wei, Y. Zhou, R. Wang, R. Zheng, J.Li, S. Luo, H.Mi, H.Chen, (2021) 9496–9503.
[4] P. Hadi, J. Barford, G. McKay, (2013) 8248–8255.
[5] C.K. Tsai, R.-a. Doong, H.-Y. Hung, (2019) 337–346.
[6] T.-H. Liou, S.-M. Liu, (2022) 107283.
[7] U.A. Edet, A.O. Ifelebuegu, (2020) 665.
[8] A. Batool, S. Valiyaveettil, (2021) 104902.
[9] N. Liu, Y. Liu, G. Zeng, J. Gong, X. Tan, S. Liu, L. Jiang, Z. Yin, (2020) 10–23.
[10] Z. Wang, J. Yu, X. Zhang, N. Li, B.Liu, Y. Li, Y. Wang, W. Wang, Y. Li, L. Zhang, S. Dissanayake, (2016) 1434-1439.
[11] S. M. Unni., L. George, S.N. Bhange, R. N. Devi, S. Kurungot, (2016) 82103-82111.
[12] D. Rodríguez-Padrón, R. Luque, MJ. Batista. Wste-derived materials: opportunities in photocatalysis. Heterogeneous Photocatalysis: Recent Advances (2020)1-28
[13] V. Forti, C.P. Balde, R. Kuehr, G. Bel, The Global E-Waste Monitor 2020: Quantities, Flows and the

Circular Economy Potential, United Nations University/United Nations Institute for Training and Research, International Telecommunication Union, and International Solid Waste Association, Bonn, Germany; Geneva, Switzerland; Rotterdam, The Netherlands, 2020.
[14] Gregory, J. (2009). E-waste Take-back System Design and Policy Approaches. StEP Initiative, United Nations University.
[15] M. Jain, D. Kumar, J. Chaudhary, S. Kumar, S. Sharma, A. S. Verma, Waste Management Bulletin (2023).
[16] S. Herat, (2021) 45-53.
[16] M. Parthasarathy, (2021) 57.
[17] M. Kouser, B. Chowhan, N. Sharma, M. Gupta, (2022) 47619-47633.
[18] Y. Li, J. Mao, H. Xie, J. Li, (2018) 361–368.
[19] J. Ruan, L. Dong, J. Huang, Z. Huang, K. Huang, H. Dong, T. Zhang, R. Qiu, (2017) 4923–4929.
[20] Z. Tian, L. Sun, H. Tian, K. Cao, S. Bai, J. Li, Q. Zhu, (2021) 5275-5281.
[21] K. Mensah, H. Shokry, M. Elkady, M, H.B. Hawash, M.Samy, (2024) 226-235.
[22] D. Saini, R. Aggarwal, S. R. Anand, N. Satrawala, R. K. Joshi, S. K. Sonkar, (2020) 100256.
[23] C.N.C. Hitam, A. A. Jalil, (2020) 110050.
[24] Khasawneh, O.F.S, P. Puganeshwary,(2021) 101230.
[25] J. Theerthagiri, R. Senthil, A. Priya, J. Madhavan, R. Michael, M. Ashokkumar, (2014) 38222–38229.
[26] S. Babar, N. Gavade, H. Shinde, A. Gore, P. Mahajan, K.H. Lee, V. Bhuse, K. Garadkar, (2019) 103041.
[27] G. Zhang, J. Zhang, M. Zhang, X. Wang, (2012) 8083–8091.
[28] S. Babar, N. Gavade, H. Shinde, P. Mahajan, K.H. Lee, N. Mane, A. Deshmukh, K. Garadkar, V. Bhuse, (2018) 4682–4694.
[29] L.Cao, Y. Li, Z. Zheng, (2022) 1112-1123.
[30] T.J, Al-Musawi, R. Asgariyan, M.Yilmaz, N. Mengelizadeh, A. Asghari, D. Balarak, M. Darvishmotevall, (2022) 137.
[31] L. Wei, X. Zhang, J. Wang, J. Yang, X. Yang, (2024) 111890.
[32] R. Parvari, F. Ghorbani-Shahna, A. Bahrami, S. Azizian, M.J Assari, M. Farhadian, (2020) 112643.
[33] R. Jahanshahi, S. Sobhani, J.M. Sansano, (2020) 10114-10127.
[34] R. Wang, A. Dai, M. Vijayalakshmi, K.R. Reddy, H. Tang, B. Cheolho, J. Shim, C.V. Reddy, (2024) 176086.
[35] Q. Yu, J. Pan, X. Ren, Q. Wang, N. Shi, Y. Li, (2022) 106800.
[36] S. Hmamouchi, A. El Yacoubi, M. El Hezzat, B. Sallek, B. C. El Idrissi, (2024) 100577.
[37] Y. Li, S. Zhu, Y. Liang, Z. Li, S. Wu, C. Chang, Z. Cui, (2020) 109191.
[38] Y. Xu, S. Huang, M. Xie, Y. Li, H. Xu, L. Huang, Q. Zhang, (116) (2015) 95727-35.
[39] T.P. Vijayakumar, M. D. Benoy, J. Duraimurugan, G. S. Kumar, M. Shkir, P. Maadeswaran, R. Srinivasan, S. Prabhu, R. Ramesh, S. Haseena, (2022) 109021.

Malaysian Journal of Catalysis 9 (2025) 22-30

Malaysian Journal of Catalysis
http://mjcat.utm.my/

MJCat
Research Article

Enhancing Nickel-Based Catalysts for Hydrodeoxygenation: The Role of Sulfated and Phosphated Silica Supports

Fadli Rosyad[1,2], Sri Wahyuni[2], Egi Agustian[1], Adid Adep Dwiatmoko[1]*, Yati Maryati[1], Nino Rinaldi[1], Robert Ronal Widjaya[1], Anis Kristiani[1] and Avga Spica[1,3]

[1] *Research Center for Chemistry, National Research and Innovation Agency (BRIN), Tangerang Selatan, Indonesia.*
[2] *Department of Chemistry, Faculty of Mathematics and Natural Sciences, Universitas Negeri Semarang, Semarang, Indonesia.*
[3] *Department of Chemistry, Faculty of Mathematics and Natural Sciences, Universitas Indonesia, Depok, Indonesia.*

**Corresponding Author: adid001@brin.go.id*

Article history:
Received 20 November 2024
Accepted 21 January 2025

ABSTRACT

The development of efficient catalysts for hydrodeoxygenation (HDO) is crucial for producing sustainable hydrocarbons from biomass-derived feedstocks. In this investigation, silica (SiO_2) supports were modified through sulfation and phosphatization treatments to enhance the performance of nickel-based catalysts for HDO reactions. The modified silica supports, SiO_2-S (sulfated) and SiO_2-P (phosphated), were characterized using XRD, FTIR, N_2 physisorption, and FE-SEM techniques to assess their structural changes, surface area, and nickel dispersion. SiO_2-S exhibited the lowest surface acidity and pore volume; however, it showed superior nickel dispersion and smaller particle sizes. The catalytic performance was evaluated in HDO reactions, with Ni/SiO_2-S achieving the highest hydrocarbon selectivity (89.3%), particularly for C17 hydrocarbons, attributed to the replacement of hydroxyl group on the silica surface with sulfate groups. Ni/SiO_2-P also improved hydrocarbon production compared to untreated SiO_2, albeit with lower selectivity. This research elucidates the critical role of support modification in optimizing nickel-based catalysts for HDO reactions.

Keywords: *Oleic Acid, hydrodeoxygenation, Acid treatment, Silica, Ni/SiO_2*

| eISSN 0128-2581

1. INTRODUCTION

The global consumption of fuel oil has increased significantly owing to population growth and expansion of the market economy. Among various fuels, gasoline is the most widely used. It is derived from fossil materials, primarily formed from ancient plants and animals. However, fossil fuels are finite resources, and their continuous use could lead to depletion and disruption of the global fuel supply, especially for vehicles that rely heavily on them[1]. One potential solution to this problem is the development and use of biofuel fuels derived from plants. As biofuels are renewable and non-fossil fuels, they offer the potential to replace conventional fossil fuels[2].

Biofuels can be synthesized from fatty acids via several reactions including catalytic cracking, hydrocracking, hydrogenation, and hydrodeoxygenation (HDO)[3]. HDO is an industrial process used to remove oxygen from compounds by saturating double bonds. In these processes, catalysts play a key role by accelerating the reaction and breaking down long-chain molecules into shorter ones, which facilitates faster and more efficient biofuel production. Nickel (Ni) metals are frequently used as active components in these catalysts because of their effectiveness as transition metals[4–7]. However, Ni is prone to deactivation and sintering, which can lead to an increase in particle size and a reduction in catalyst quality[8]. To counteract these issues, a suitable support material is required to stabilize Ni particles, maintain their surface area, and prevent sintering[9].

Silica (SiO_2) derived from rice husk ash is an excellent candidate catalyst support. Rice husk ash, a byproduct of rice husk combustion, contains up to 96% SiO_2[10]. It has a high surface area and high thermal stability, making it an ideal support material for catalysts. Catalyst activity, which is a measure of catalyst performance, depends on several factors, including surface area and acidity.

Acid treatment of catalyst supports can further enhance their activity. For example, Sekewael et al. (2022) demonstrated that sulfated ZrO_2 catalysts achieved a conversion rate of 93% compared with 77% for untreated ZrO_2[11]. This improvement was attributed to the increase in the surface area and acidity resulting from sulfation treatment. Similarly, acid-treated SiO_2-supported Ni catalysts are expected to perform well for the production of

biofuels from oleic acid. Ni readily forms coordinate covalent bonds, facilitating the formation of intermediate compounds on the catalyst surface, which enhances the hydrodeoxygenation process.

Despite significant research on Ni-based catalysts and the benefits of acid-treated supports, there is limited understanding of the specific impact of different acid treatments on the structural and catalytic properties of rice-husk-ash-derived SiO_2-supported Ni catalysts. Additionally, there is a lack of comprehensive studies comparing the performance of these catalysts in the hydrodeoxygenation of oleic acid to that of other fatty acids.

This study aims to utilize the high SiO_2 content of rice husk ash as a catalyst support and synthesize Ni/SiO_2 catalysts to convert oleic acid into hydrocarbons suitable for biofuel production. Oleic acid, a fatty acid commonly found in vegetable oils, such as olive oil (55-80%), palm oil (38.4%)[12], sunflower oil (11.7%)[13], and grape seed oil (15%), is a promising feedstock for biofuel production. Thus, Ni catalysts can effectively convert oleic acid into hydrocarbon compounds, which can be used as biofuels. By enhancing the catalyst support through acid treatment, catalytic activity can be improved, leading to higher biofuel yields.

2. EXPERIMENTS

2.1 Isolation of SiO_2 from Rice Husk Ash

To isolate the SiO_2, 20 g of rice husk ash was dispersed in 100 mL of 2 M HCl and stirred for 6 h. The resulting mixture was vacuum filtered, and the solid residue was collected. The residue was then dried in an oven at 100 °C. The dried solid was then mixed with 100 mL of 2.5 M NaOH solution and stirred at 90 °C for 3 h to dissolve the silica. After filtration, the residue was washed with warm water. The resulting filtrate containing sodium silicate (Na_2SiO_3) was cooled to room temperature and left to stand overnight. To precipitate silica, the sodium silicate solution was titrated with 5 M H_2SO_4 under constant magnetic stirring. The titration was carefully controlled to induce the formation of white gelatinous silica gel. The gel was thoroughly washed with water until the pH of the washing solution reached neutrality. Finally, the silica gel was dried at 105 °C for 15 h to obtain the solid SiO_2.

2.2. Catalyst Preparation

2.2.1. Sulfated-SiO_2

In this step, 20 mL of acetone and 2 mL of H_2SO_4 were combined in an Erlenmeyer flask (Solution A). Separately, 12 g of SiO_2 derived from rice husk ash was immersed in 72 mL acetone. The immersed SiO_2 was then added to Solution A stirred for 4 h. The resulting solution was filtered, and the obtained solid was washed multiple times with distilled water to remove any excess acid. The washed solid was dried in an oven at 100 °C for 24 h to produce SiO_2 (SiO_2-S).

2.2.2. Phosphated-SiO_2

For phosphatizing, 20 mL of acetone and 2 mL H_3PO_4 were mixed in an Erlenmeyer flask (Solution B). Simultaneously, 18 g of SiO_2 from rice husk ash was added to 108 mL of acetone. The mixture was then added to Solution B and stirred for 4 h. The mixture was filtered and the solid was thoroughly washed with distilled water to remove excess acid. The washed solid was dried in an oven at 100 °C for 24 h to yield phosphated SiO_2 (SiO_2-P)

2.2.3. Ni/SiO_2 Catalyst

For the synthesis of the Ni/SiO_2 catalyst, 2.97 g of $Ni(NO_3)_2 \cdot 6H_2O$ was dissolved in 20 mL of distilled water in a 100 mL Erlenmeyer flask. To this solution, 5.4 g of SiO_2 was added to this solution and the mixture was refluxed on a hotplate with continuous stirring for 24 h. The mixture was dried at 90 °C and calcined at 450 °C for 2 h. Finally, the catalyst was reduced at 450 °C for 4 h to obtain Ni/SiO_2.

2.3. Catalyst characterizations

The crystal structure of the catalyst was analyzed using XRD with a PANalytical Empyrean instrument with monochromatic radiation CuKα (λ = 1.54056 Å). The XRD analysis was conducted within a scanning range of 5–90° at a rate of 10°/min with a step width of 0.02°. The morphologies and elemental analysis of the samples were characterized by scanning electron microscopy (SEM)-energy dispersive X-ray (EDX) using an SEM Hitachi SU3500. N_2-physisorption was obtained using a Micromeritics TriStar II 3020. The catalyst acidity was analyzed by the ammonia temperature-programmed desorption (NH_3-TPD) method using a Micromeritics Chemisorb 2750. All samples were pretreated in helium gas flow for 30 min at 350 °C and exposed to flowing diluted ammonia gas at 40 mL/min for 30 min at 100 °C. It was then purged with helium gas flow for 30 min at 100 °C to remove physically adsorbed ammonia. Subsequently, the sample was heated to 800 °C at a rate of 10 °C/min.

2.4. Catalytic reaction

The performance of Ni/SiO_2 as a catalyst was assessed by HDO using oleic acid in a batch reactor. The reaction setup involved placing 1 g of Ni/SiO_2 catalyst and 10 mL of oleic acid into the reactor, which was then securely positioned within a heating furnace. Before initiating the reaction, the system was subjected to a thorough leak check. Once leak-free, hydrogen gas (H_2) was introduced into the reactor at a pressure of 40 bar. The reactor temperature was

then increased to 350 °C and the reaction proceeded under these conditions for 2 h.

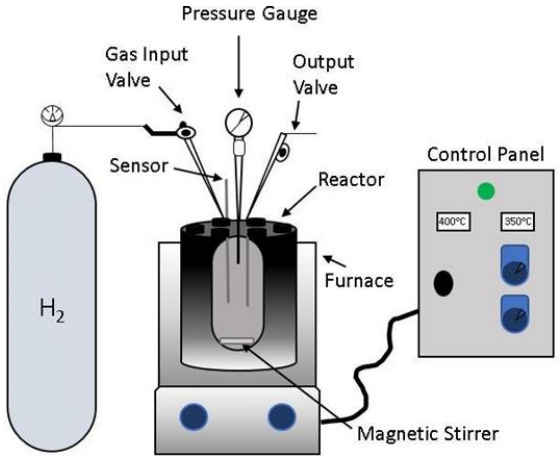

Schematic 1. Batch reactor setup for hydrodeoxygenation

3. RESULTS AND DISCUSSION

Sulfation and phosphatization treatments are commonly used to modify silica (SiO_2), making it more reactive and increasing its surface area. Sulfation involves the reaction of silica with sulfuric acid (H_2SO_4), which results in the protonation of silica and the release of hydroxyl ions (OH^-). The reaction can be represented as:

$$SiO_2 + H_2SO_4 \rightarrow Si\text{-}OH + HSO_4^-$$

In this process, the protonation of silica generates silanol groups (Si-OH), which are more reactive. Similarly, phosphatization involves the reaction of silica with phosphoric acid (H_3PO_4), producing reactive silanol groups via a comparable mechanism:

$$SiO_2 + H_3PO_4 \rightarrow Si\text{-}OH + H_2PO_4^-$$

Based on the XRD patterns presented in Figure 1A, the diffraction patterns of SiO_2-P, SiO_2-S, and SiO_2 reveal broad diffraction peaks at approximately $2\theta = 22°$, which is consistent with the characteristic amorphous silica pattern[14]. In contrast, the XRD patterns of Ni/SiO_2, Ni/SiO_2-P, and Ni/SiO_2-S in Figure 1b show sharp peaks at approximately $2\theta = 44.38°$, 51.73°, and 76.30°, respectively, which are indicative of the crystalline phases of metallic nickel (Ni). These peaks correspond to the (111), (200), and (220) planes of face-centered cubic (fcc) +Ni[15], indicating the presence of highly ordered crystalline Ni on the silica supports. The slight shifts in the 2θ values of the Ni/SiO_2, Ni/SiO_2-P, and Ni/SiO_2-S samples can be attributed to variations in the interaction between the Ni nanoparticles and different SiO_2 supports resulting from the acid treatments applied to the silica. These treatments, such as sulfation and phosphatization, appear to slightly affect the crystalline structure of the Ni phase, suggesting that the surface modification of silica influences the degree of crystallinity and the interaction between Ni particles and the SiO_2 surface, which may affect the catalytic performance of the materials[16].

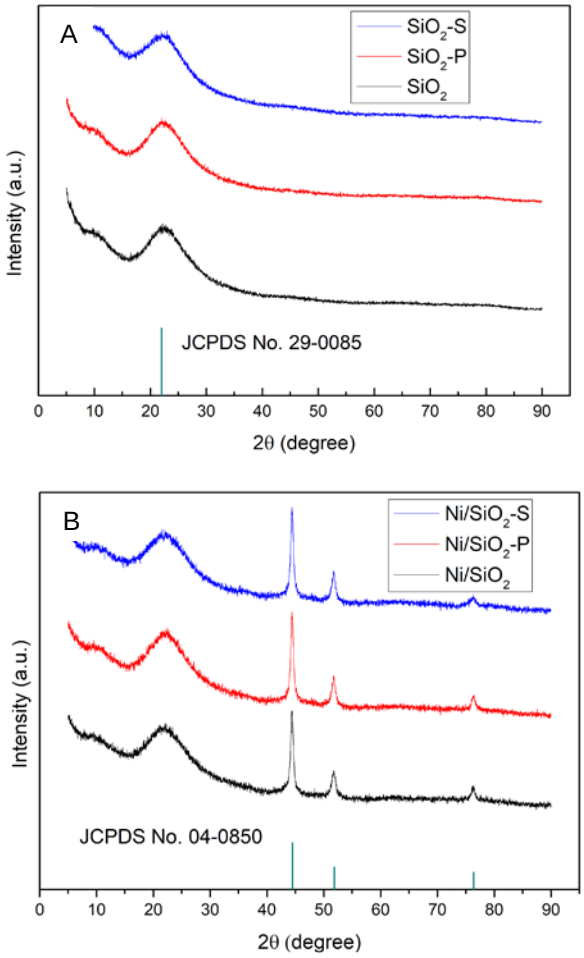

Figure 1. XRD pattern of the samples: (A) SiO_2 and (B) Ni/SiO_2

Figure 2 shows the FTIR spectra of the SiO_2 support. This provides important insights into the chemical composition of SiO_2. Several characteristic absorption bands corresponding to specific functional groups are observed, indicating the successful formation of SiO_2 and the presence of modifications in SiO_2-P and SiO_2-S. The absorption band around 3375 cm^{-1} is associated with the O-H stretching vibration, which is attributed to hydroxyl (-OH) groups, commonly referred to as silanol groups (Si-OH)[17]. This band is particularly significant because it indicates the presence of Brønsted acid sites, which contribute to the surface acidity of SiO_2[18,19]. Among the three samples, SiO_2-P showed the lowest transmittance at this wavenumber,

suggesting that phosphatization led to a reduction in hydroxyl groups, potentially owing to the formation of phosphate species on the surface. SiO_2-S shows a slightly higher transmittance than SiO_2-P, but is still lower than that of unmodified SiO2, indicating that sulfation also affects the concentration of hydroxyl groups on the surface. The strong band observed at approximately 1056 cm^{-1} corresponds to the asymmetric stretching vibration of the Si-O-Si bond, which is characteristic of siloxane groups[20]. This band was present in all the three samples, confirming the successful formation of the SiO_2 framework. This confirmed the presence of SiO_2 as the primary component in the samples. The transmittance values remained consistent across all the samples, suggesting that the siloxane network remained intact even after the phosphatization and sulfation treatments. The band at 1599 cm^{-1} corresponds to the bending vibration of Si-O bonds, which also contributes to the structural integrity of the siloxane (Si-O-Si) network[21]. The presence of this band in all samples indicates that the SiO_2 backbone was preserved across the different modifications. There were no significant shifts or changes in this band, indicating that the structural changes mainly involved surface functional groups.

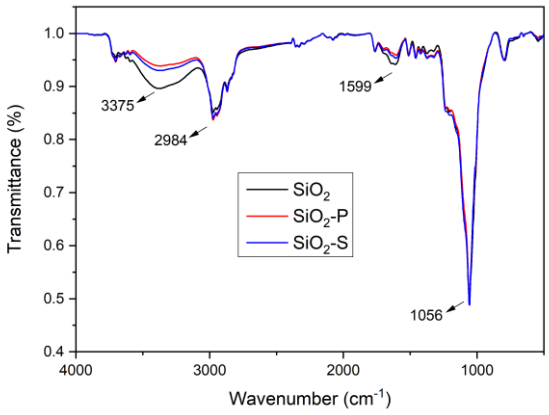

Figure 2. FTIR spectrum of SiO_2

The N_2 physisorption data of the SiO_2 samples, including untreated silica (SiO_2), phosphated silica (SiO_2-P), and sulfated silica (SiO_2-S), revealed significant differences in surface area, pore diameter, and pore volume owing to the varying chemical treatments and nickel impregnation. Table 1 shows that untreated silica (SiO_2) has a surface area of 194.7 m^2/g, a pore diameter of 10.37 nm, and a pore volume of 0.492 cm^3/g. After the phosphate (P) and sulfate (S) treatments, both SiO_2-P and SiO_2-S showed considerable changes. SiO_2-P exhibited the highest surface area of 263.5 m^2/g and a substantial increase in pore volume (0.945 cm^3/g). This suggests that phosphate treatment induces additional porosity and a greater mesoporous structure, likely owing to the formation of new pore channels or increased textural porosity[22], resulting in a higher surface area and pore volume[23], as observed from the slight increase in the pore diameter of SiO_2-P (13.75 nm) compared with that of untreated SiO_2. In contrast, SiO_2-S displays a lower surface area (135.1 m^2/g), pore volume (0.502 cm^3/g), and an increased pore diameter (13.24 nm), indicating that the sulfate treatment leads to pore expansion but reduces overall surface area, possibly due to the partial blockage of pores or restructuring caused by the acid treatment[24]. Sulfate treatment tends to block some pores owing to the strong interactions with sulfate groups, which can reduce the overall surface area while slightly expanding the remaining pores. Additionally, it may decrease the textural properties by altering the pore network structure. Thus, the chemical nature of these anions significantly influences the modification of SiO_2[25].

Table 1. Physical and chemical properties of prepared catalysts

Samples	Surface Area (m^2/g)	Pore diameter (nm)	Pore volume (cm3/g)	Total acidity (mmol/g)
SiO_2	194.7	10.37	0.492	1.079
SiO_2-S	135.1	13.24	0.502	0.091
SiO_2-P	263.5	13.75	0.945	0.975
Ni/SiO_2	106.3	14.35	0.740	-
Ni/SiO_2-S	90.2	15.26	1.013	-
Ni/SiO_2-P	127.8	15.71	0.760	-

The total acidity, as shown in Table 1, exhibited a notable trend: SiO_2 demonstrated the highest total acidity (1.079 mmol/g), which decreased substantially in SiO_2-S (0.091 mmol/g), indicating that sulfation significantly reduced the number of acidic sites, potentially due to the modification of acid sites during the sulfation process. In contrast, phosphate treatment resulted in a moderate acidity value of 0.975 mmol/g, suggesting that while phosphate treatment reduces acidity compared to pure SiO_2, it does not do so as extensively as sulfation. The reduction in acidity observed after sulfation and phosphate treatment can be attributed to alterations in the surface chemistry of SiO_2. In the case of sulfation, sulfate groups (SO_4^{2-}) are introduced onto the silica surface, which interact with surface hydroxyl groups (Si–OH), neutralizing some of the Brønsted acidic sites responsible for the material's acidity. This process modifies the surface structure and decreases the number of available acidic sites, as the sulfate groups are less acidic than the Si–OH groups, leading to a significant reduction in the total acidity. Similarly, phosphate treatment involves the introduction of phosphate groups (PO_4^{3-}) onto the silica surface, which can passivate the surface by interacting with hydroxyl groups and reducing the number of acidic sites. In both cases, modification of the surface and neutralization or replacement of acid sites with less acidic species resulted in a decrease in total acidity.

The pore size distribution graph in Figure 3A highlights these effects, with SiO_2-P demonstrating a higher

differential surface area across various pore widths, confirming the generation of additional mesopores or an enhancement in the connectivity of the porous network. SiO_2-S showed a more limited increase in mesopore volume, consistent with the moderate increase in pore diameter and relatively lower surface area. SiO_2-P exhibits a higher differential surface area across various pore widths than SiO_2-S owing to the formation of new mesopores and enhanced connectivity within the porous network. This increased accessibility allows for greater interaction with adsorbates, whereas sulfate treatment may block or partially occlude pores, limiting gas adsorption. Additionally, phosphate treatment stabilizes the pore structure of SiO_2, preventing collapse, whereas sulfate modification can inhibit pore accessibility, contributing to the observed differences in the surface area[26].

The nitrogen adsorption-desorption isotherms in Figure 3B further confirm these observations. The step increases in the adsorption curve at high relative pressures ($P/P_o > 0.8$) for SiO_2-P suggested the presence of larger mesopores or macropores, which correlated with the high pore volume and surface area. SiO_2-S, while showing similar trends, adsorbed less nitrogen overall, implying fewer available mesopores and a lower capacity for gas adsorption. Figure 3c shows the pore size distributions of the Ni/SiO_2 catalysts. The graph shows that Ni/SiO_2-S exhibits the highest pore distribution peak around the pore range of 20-40 nm, which is consistent with the table data, indicating an average pore diameter of 15.26 nm. This suggests a significant increase in differential surface area. Meanwhile, Ni/SiO_2-P displayed a broader pore distribution compared to the other variants, reflecting a higher surface area (127.8 m^2/g) and a substantial pore volume (0.760 cm^3/g). This enhancement implies that the phosphate treatment improved the structure and connectivity of the pores. Furthermore, Figure 3d presents the nitrogen adsorption-desorption isotherms for the Ni/SiO_2 catalysts. Ni/SiO_2-P showed a higher adsorption curve across the relative pressure range, particularly at high pressures ($P/Po > 0.8$), indicating the presence of larger mesopores or macropores. This is consistent with its high pore volume and large surface area. In contrast, Ni/SiO_2-S exhibited lower nitrogen adsorption, suggesting that sulfate treatment may restrict the pore accessibility. Although the pore volume is higher (1.013 cm^3/g), the lower surface area (90.2 m^2/g) implies that pore accessibility might be hindered by the sulfate treatment. Ni/SiO_2 demonstrated a more linear isotherm, indicating a more uniform mesopore distribution with a significant average pore size and volume. These differences underscore the substantial impact of chemical modifications on the pore structure and adsorption-desorption properties of the materials.

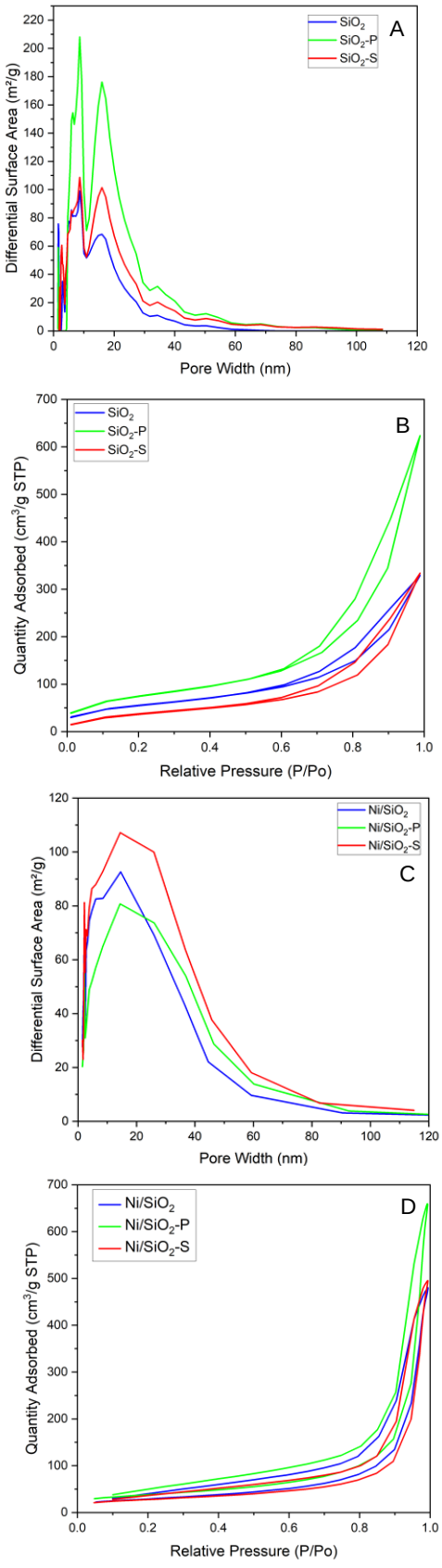

Figure 3. Pore size distribution and adsorption-desorption isotherm of SiO_2 (A, B) and Ni/SiO_2 (C, D)

Nickel impregnation significantly affected the surface properties of the Ni/SiO_2, Ni/SiO_2-S, and Ni/SiO_2-P samples. The surface areas of Ni-impregnated samples are consistently lower than their corresponding untreated counterparts, with Ni/SiO_2-P showing a surface area of 127.8 m^2/g compared to 263.5 m^2/g for SiO_2-P. This reduction is likely due to partial blockage of the pores by the nickel species. The pore diameters also increased slightly after Ni impregnation, suggesting that Ni deposition occurred primarily within the mesopores, expanding their size but reducing the surface area. The highest pore volume was observed for Ni/SiO_2-S (1.013 cm^3/g), reflecting enhanced mesoporosity, possibly due to changes in the silica structure induced by both sulfate and nickel.

Figure 4 displays the FESEM images and EDS analyses of Ni/SiO_2, Ni/SiO_2-S, and Ni/SiO_2-P, which provide valuable insights into the morphology, surface distribution, and nickel dispersion across the silica supports that have undergone acid treatment. These results reflect the impact of phosphate and sulfate acid treatments on the structural properties of silica and how these treatments influence the dispersion and particle size of Ni.

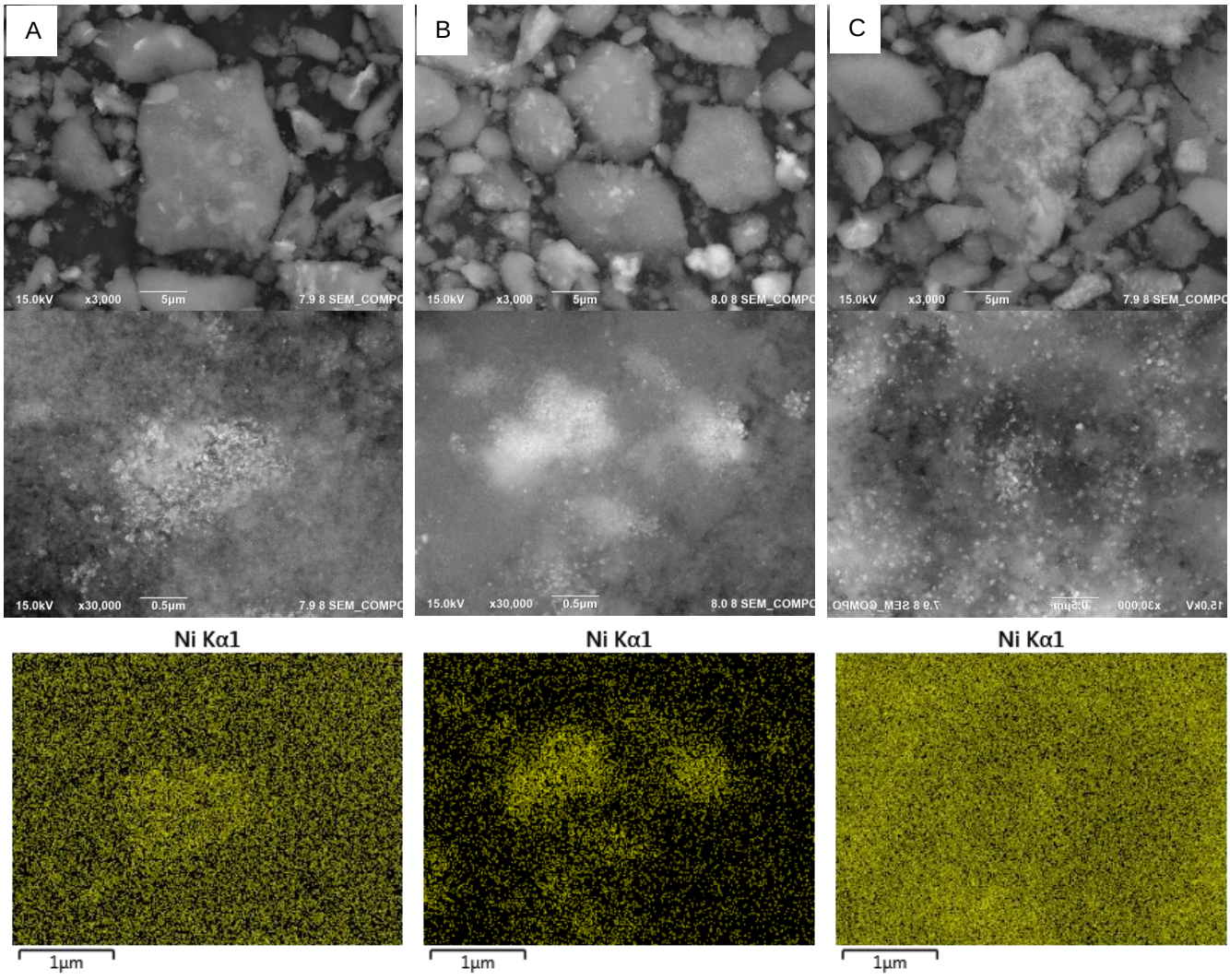

Figure 4. FESEM images and EDX analysis of Ni/SiO_2 (A), Ni/SiO_2-S (B) and Ni/SiO_2-P (C)

Significant differences in surface morphology were observed among the three samples. In the case of Ni/SiO_2 (Figure 4A), untreated silica exhibited relatively larger and more irregular particle aggregates. The surface presented a rough appearance with less uniformity in particle size. The EDS map of Ni Kα1 for Ni/SiO_2 revealed a reasonably even

distribution of nickel across the surface; however, the relatively lower magnification suggests that nickel particles may be present in larger clusters or agglomerates, potentially affecting the catalytic performance by reducing the active surface area and increasing the likelihood of sintering. In contrast, Ni/SiO_2-S (Figure 4B), where the silica support had undergone sulfate acid treatment, exhibited smaller, more defined particles, indicating restructuring of the silica surface due to the acid treatment. FE-SEM images at a higher magnification (30,000×) revealed finer Ni particles dispersed on the support. The EDS map demonstrated a highly homogeneous distribution of Ni, suggesting that sulfate treatment enhanced Ni dispersion. This enhancement was likely due to the sulfate groups anchoring the nickel species more effectively to the support, thus preventing the formation of larger nickel clusters[26]. The enhanced dispersion of Ni may also be attributed to the increased pore size observed in Ni/SiO_2-S, allowing better accessibility and uniform distribution of Ni throughout the mesopores. The phosphated silica (Figure 4C) support exhibited a morphology with small, well-distributed particles, similar to Ni/SiO_2-S, but with more significant textural differences. The FE-SEM image revealed more evenly dispersed smaller particles across the surface, and EDS mapping demonstrated a high concentration of nickel distributed evenly across the support. Phosphate treatment, similar to sulfate treatment, enhances Ni dispersion, albeit through a different mechanism. The phosphate groups may increase the surface acidity and facilitate a more favorable environment for the dispersion of nickel, potentially by forming stronger interactions between the nickel ions and phosphate-modified silica surface[23]. This results in a well-dispersed Ni phase, even at higher concentrations, preventing the agglomeration of large Ni particles.

The differences in Ni dispersion and particle size between these samples were strongly influenced by the acid treatments applied to the silica supports. Sulfate and phosphate treatments enhance nickel dispersion through different mechanisms. Sulfate treatment increases the pore size, providing better access for the uniform distribution of Ni ions, whereas phosphate treatment likely modifies the surface chemistry, enhancing the interaction between Ni and the support[25]. Additionally, the increase in the surface area and pore volume observed in the N_2 physisorption data for SiO_2-P supports the idea that phosphate treatment facilitates the uniform dispersion of nickel particles by providing a larger available surface and a more porous structure.

The GC-MS data presented in Figure 5 elucidate the influence of catalyst support modification on hydrocarbon selectivity during the hydrodeoxygenation reaction. Despite the fact that the majority of the product in our reaction is in the solid form, Figure 5A demonstrates that Ni/SiO_2-S exhibits the highest hydrocarbon selectivity (89.3%), followed by Ni/SiO_2-P (64.9%) and Ni/SiO_2 (56.5%). The sulfated silica catalyst demonstrated superior performance, indicating that the incorporation of sulfate groups significantly enhanced the production of hydrocarbons, while suppressing the formation of fatty acids, alcohols, and other oxygenated compounds. The high hydrocarbon selectivity of Ni/SiO_2-S can be attributed to the siloxane groups created by the sulfation process. These groups facilitate the hydrodeoxygenation pathway, leading to a more complete deoxygenation and higher selectivity towards hydrocarbons. Conversely, Ni/SiO_2-P, with moderate acidity from the phosphate groups, also performed well but did not reach the same level of hydrocarbon production as Ni/SiO_2-S. Untreated SiO_2, which lacks significant functional groups, displayed the lowest hydrocarbon selectivity and a higher presence of fatty acids and alcohols, suggesting less effective deoxygenation.

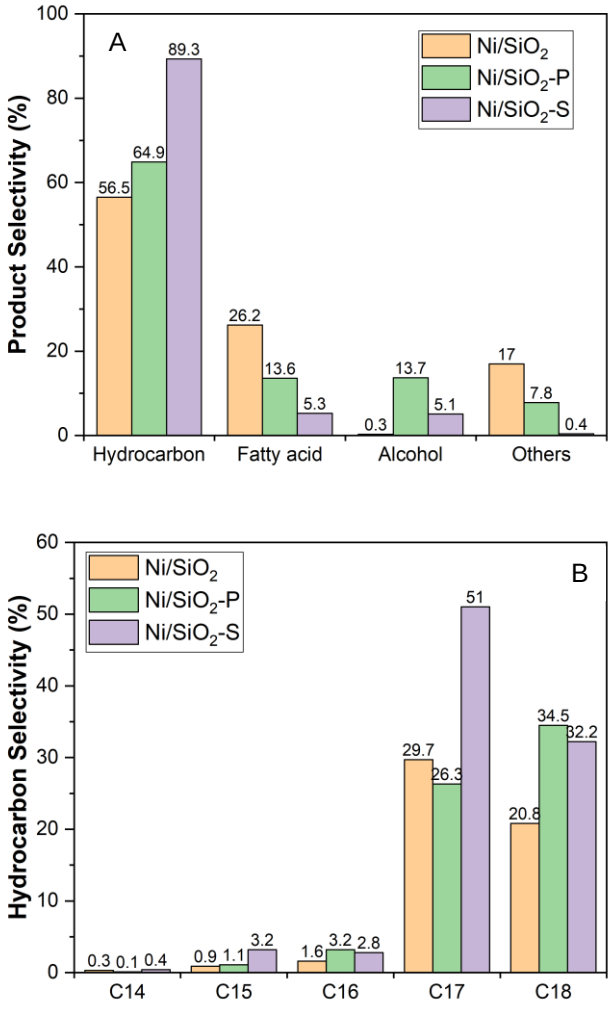

Figure 5. Product selectivity after the reaction

Figure 5B shows the detailed hydrocarbon selectivity by carbon chain length (C14–C18); further insights were gained into the distribution of products. Ni/SiO_2-S showed the highest selectivity for C17 hydrocarbons (51%), followed by Ni/SiO_2-P (26.3%), and Ni/SiO_2 (29.72%). For

C18 hydrocarbons, Ni/SiO_2-P displayed the highest selectivity (34.49%), followed closely by Ni/SiO_2-S (32.21%), and Ni/SiO_2 (20.78%). These results confirm that both Ni/SiO_2-S and Ni/SiO_2-P support the production of longer-chain hydrocarbons (C17 and C18), which are typically desirable for hydrodeoxygenation reactions, especially for producing diesel-range fuels.

The superior performance of Ni/SiO_2-S is believed to be linked to its enhanced siloxane functional groups, which promote catalytic cracking and hydrodeoxygenation, favoring the formation of longer-chain hydrocarbons[25]. Phosphated silica (Ni/SiO_2-P) also enhances catalytic activity compared to untreated SiO_2, but its lower acidity results in less efficient cracking and HDO compared to Ni/SiO_2-S. This also explains why Ni/SiO_2-P favors the formation of C18 hydrocarbons slightly more than C17, as the acidity may not be strong enough to break down the larger molecules into smaller fractions.

The Ni/SiO_2 catalyst, which lacks surface functional groups owing to the absence of sulfate or phosphate groups, shows a more balanced selectivity for C17 and C18, but generally lower hydrocarbon production. It is possible that poorer metal dispersion on the untreated SiO_2 support reduced the efficiency of the HDO process, leading to higher amounts of oxygenated compounds such as fatty acids and alcohols, as shown in the first figure. Nickel dispersion and particle size play crucial roles in the catalytic performance. The impregnation of nickel on sulfated and phosphated silica likely leads to better dispersion and smaller particle sizes, owing to the stronger interaction between the acidic support and nickel. This resulted in a higher number of active sites, which increased the catalytic efficiency and selectivity for hydrocarbons. In contrast, nickel on untreated silica may be less well dispersed, resulting in larger particles, fewer active sites, and therefore, lower catalytic activity.

The differences in hydrocarbon selectivity and product distribution across the Ni/SiO_2, Ni/SiO_2-S, and Ni/SiO_2-P catalysts can be explained by variations in surface acidity, nickel dispersion, and particle size. The strong acidity introduced by the sulfate groups in Ni/SiO_2-S dramatically improves hydrocarbon selectivity, particularly for C17 and C18 hydrocarbons, making it the most efficient catalyst in this study. Phosphated silica (Ni/SiO_2-P) also improves the catalytic performance compared to untreated silica, but to a lesser extent because of its moderate acidity. The untreated silica support (Ni/SiO_2) had lower hydrocarbon selectivity and higher oxygenated compound production, reflecting the lack of sufficient acidic sites and poor nickel dispersion.

4. CONCLUSION

The modification of silica with sulfate (SiO_2-S) and phosphate (SiO_2-P) significantly enhances the catalytic performance of Ni/SiO_2 catalysts in hydrodeoxygenation reactions, with Ni/SiO_2-S demonstrating the highest hydrocarbon selectivity (89.3%) owing to its chemical surface. The sulfation process improved nickel dispersion, pore structure, and acidity, resulting in superior selectivity for C17 hydrocarbons. Ni/SiO_2-P also increased the catalytic efficiency but exhibited lower hydrocarbon selectivity than Ni/SiO_2-S, which was attributed to its moderate acidity. Ni/SiO_2 displayed lower hydrocarbon production and higher oxygenated by-products, underscoring the critical role of support modification in enhancing the catalytic performance.

ACKNOWLEDGEMENTS

This work was supported by the Korea Institute of Science and Technology (KIST) through the KIST Alumni Project 2024, and the National Research and Innovation Agency (BRIN) through the RPORNM 2024 program.

REFERENCES

[1] A.N. Aini, M. Al-Muttaqii, A. Roesyadi, F. Kurniawansyah, (2021) 149–156.
[2] N. Rodiansono, H.P. Dewi, K. Mustikasari, M.D. Astuti, S. Husain, N. Sutomo, (2022) 13319–13329.
[3] A.A. Dwiatmoko, I. Kim, L. Zhou, J. Choi, D. Suh, J. Jae, J. Ha, (2017).
[4] I. Aziz, P. Sugita, N. Darmawan, A.A. Dwiatmoko, (2023).
[5] Y. Liu, L. Yao, H. Xin, G. Wang, D. Li, C. Hu, (2015) 504–514.
[6] F.I. Prihadiyono, W.W. Lestari, R. Putra, A.N.L. Aqna, I.S. Cahyani, G.T.M. Kadja, (2022) 931–931.
[7] R. Riyandi, N. Rinaldi, R.T. Yunarti, A.A. Dwiatmoko, F.S.H. Simanjuntak, (2024).
[8] P. Strucks, L. Failing, S. Kaluza, (2021) 1526–1536.
[9] X. Gao, Z. Ge, G. Zhu, Z. Wang, J. Ashok, S. Kawi, (2021) 1003.
[10] V.H. Le, C. Nhan, H. Thuc, H.H. Thuc, (2013) 1–10.
[11] S.J. Sekewael, R.A. Pratika, L. Hauli, A.K. Amin, M. Utami, K. Wijaya, (2022).
[12] M. Bahadi, N. Salih, J. Salimon, (2021) 175–186.
[13] S. Shabrina, R.TD.W. Broto, (2023) 1–4.
[14] H.F. Poulsen, J. Neuefeind, H.B. Neumann, J.R. Schneider, M.D. Zeidler, (1995) 63–74.
[15] I. Rossetti, A. Gallo, V. DalSanto, C.L. Bianchi, V. Nichele, M. Signoretto, E. Finocchio, G. Ramis, A. Di Michele, (2013) 294–306.
[16] K.D. Ghuge, A.N. Bhat, G.P. Babu, (1993) 183–204.
[17] I. Zuwanna, M. Riza, S. Aprilia, Y. Syamsuddin, R. Dewi, (2023) 337–343.
[18] M.L. Hair, (1975) 299–309.

[19] C. Carteret, (2009) 13300–13308.
[20] J.M. Zeigler, F.W.G. Fearon, eds., (1989).
[21] J. Lewandowska-Łańcucka, M. Staszewska, M. Szuwarzyński, S. Zapotoczny, M. Kepczynski, Z. Olejniczak, B. Sulikowski, M. Nowakowska, (2018) 57–68.
[22] L. Krösi, S. Papp, S. Beke, A. Oszkó, I. Dékány, (2010) 79–86.
[23] W. Huang, Y. Zhang, D. Li, (2017) 470–482.
[24] N. Asasian Kolur, S. Sharifian, T. Kaghazchi, (2019) 663–675.
[25] V. Hegde, P. Pandit, P. Rananaware, V.P. Brahmkhatri, (2022) 1198–1210.
[26] Y. Wei, W. Yang, Z. Yang, (2022) 9537–9565.

Malaysian Journal of Catalysis 9 (2025) 31-35

Malaysian Journal of Catalysis
http://mjcat.utm.my/

MJCat
Research Article

Preparation of Mesoporous Al-MCM-41 and Its Application for Hydrocracking *Cerbera manghas* Oil

Desy Anggraini[1], Lenny Marlinda[1], Rahmi[1], Sudibyo[2], Muhammad Amin[2], Erik Prasetyo[2], Sugeng Priyanto[3], Abdul Aziz[4], Reva Edra Nugraha[5], Sun Theo Constan Lotebulo Ndruru[6], Dicky Annas[6], Indri Yati[6], Muhammad Nur Khoiru Wihadi[6], Aishah Abdul Jalil[7,8], Muhammad Al Muttaqii[6]*

[1]*Department of Chemistry, Faculty of Science and Technology, Jambi University, Jambi*
[2]*Research Center for Mining Technology, National Research and Innovation Agency (BRIN-Indonesia), South Lampung 35361, Indonesia*
[3]*Department of Mechanical Engineering, State University of Jakarta, East Jakarta 13220, Indonesia*
[4]*Department of Chemistry, Faculty of Science and Data Analytics, Institut Teknologi Sepuluh Nopember, Keputih, Sukolilo, Surabaya 60111, Indonesia*
[5]*Department of Chemical Engineering, Faculty of Engineering, Universitas Pembangunan Nasional "Veteran" Jawa Timur, Surabaya, East Java, 60294, Indonesia*
[6]*Research Center for Chemistry, National Research and Innovation Agency (BRIN), South Tangerang 15310, Indonesia*
[7]*Centre of Hydrogen Energy, Institute of Future Energy, Johor Bahru, Johor 81310 UTM, Malaysia*
[8]*Faculty of Chemical and Energy Engineering, Universiti Teknologi Malaysia, Johor Bahru, Johor 81310 UTM, Malaysia*

**Corresponding Author: almuttaqiimuhammad@gmail.com; muhammad.al.muttaqii@brin.go.id*

Article history:
Received 8 January 2025
Accepted 28 February 2025

ABSTRACT

Mesoporous Al-MCM-41 was successfully prepared by hydrothermal method over CTABr template. The catalyst was varied of stirring time during the synthesis process, with 4 and 8 h. The results obtained showed that Al-MCM-41 with 4 h stirring had a surface area of 184.8508 m^2/g and an 8 h stirring of 655.4759 m^2/g. The Al-MCM-41 was used as a catalyst for hydrocracking *cerbera manghas* oil. Based on GC-MS analysis, the products contain 1-methyl-indan ($C_{10}H_{12}$), cyclotetracosane ($C_{24}H_{28}$) when using Al-MCM-41 4h. Meanwhile, when using Al-MCM-41 8h catalysts, the products contain 1,3 tetradecadiene ($C_{14}H_{26}$), and 1-tetracosene ($C_{24}H_{28}$). All products still contain high oxygenate compounds. The presence of carboxylic acids indicates that the hydrogenation reaction has required high temperature to convert them into biofuel. The results demonstrated that the synthesized Al-MCM-41 had potential applications as catalyst in the hydrocracking of non-edible oil to produce biofuel.

Keywords: mesoporous Al-MCM-41, hydrocracking, *cerbera manghas* oil

| eISSN 0128-2581 |

1. INTRODUCTION

As global energy demand increases, reliance on fossil fuels has led to an energy crisis and significant environmental impacts. The burning of fossil fuels contributes greatly to greenhouse gas emissions, which are a major cause of global warming and climate change. Therefore, there is an urgent need to find alternative energy sources that are cleaner and more sustainable [1]. One of the alternative energy sources is biofuel. Biofuel is an alternative renewable energy source that is environmentally friendly and sustainable. By using biofuels, dependence on petroleum and other fossil fuels can be reduced. one of the promising sources of biofuel is non-edible oil because it is not related to the food supply chain like edible oil. there are many examples of non-edible oil that have potential such as agricultural waste, plantations and other plants [2–4]. One of the sources of raw materials for biofuel production is *cerbera manghas* oil [5,6]. *Cerbera manghas* trees grow abundantly in Indonesia, especially on the islands of Java and Sumatra. *Cerbera manghas* seeds produce 46-64% oil after being pressed [7].

Biofuel production can be carried out through the hydrocracking process. Hydrocracking is a cracking process by reacting oil with a certain amount of hydrogen gas at a certain temperature and pressure. The product of the hydrocracking method will produce biofuels in the form of straight chain liquid alkanes from C-15 to C-18 [8]. The hydrocracking process uses acidic catalysts such as zeolite, Al_2O_3, SiO_2, alumina silica, Al-MCM-41 and is embedded with transition metals such as Co, Mo, Ni, Cr, Zn, Pt [9]. The use of metals to increase the active site and increase the acidity of the catalyst, so that the catalyst can be more active and selective [10].

Al-MCM-41 is one of the promising catalysts. This is because Al-MCM-41 has pores with a mesopore size range (2-50 nm). The presence of mesopores can reduce gas products and increase liquid products [11,12]. Al-MCM-41 catalyst can be synthesized using hydrothermal technique using sodium aluminate, tetraethyl orthosilicate and cetyltrimethylammonium bromide materials which are stirred until homogeneous using a magnetic stirrer at room temperature for 5 days, then heated at 110°C for 6 h to evaporate the solution. Furthermore, the solid was calcined at 550°C with nitrogen flow for 1 h and air for 6 h. The diffractogram of Al-MCM-41 synthesis catalyst using X-Ray Diffraction showed a peak at $2\theta = 26.3°$ with the results of biodiesel production from nyamplung oil to free acid methyl ester showed a conversion efficiency of 98.15% [13]. Hydrocracking reactions using Al-MCM-41 and Pd/Al-MCM-41 catalysts produce different product components in the hydrocracking of FAME. Hydrocarbon production will increase if alcohol production tends to decrease when there is palladium impregnation treatment on mesoporous aluminosilicate catalysts [13].

In addition, Chen et al. [14] have reported the synthesis of mesoporous silica material (Al-MCM-41) from natural pearlite mineral without the addition of silica or aluminum reagents. The stirring process was carried out for 2 h. The surface area of Al-MCM-41 produced was 1024 m^2/g. Gonzales et al., [15] also reported the synthesis of Al-MCM-41 using different Si/Al ratios. The stirring process was carried out for 1 hour and the AlM41S-25 sample produced a large surface area of 1126 m^2/g.

The purpose of this study is to synthesize Al-MCM-41 catalyst from rice husk waste material as a source of silica, stirring time of the synthesized catalysts, and can be used as a catalyst for hydrocracking of *cerbera manghas oil*.

2. EXPERIMENTS

2.1 Materials

The materials used were sodium hydroxide (NaOH, Merck, ≥99%), sulfuric acid (H_2SO_4, Merck, 95-97%), hexadecyltrimethylammonium bromide (CTABr, Merck, ≥99%), aluminum oxide (γ-Al_2O_3, Merck, surface area 120-190 m^2/g), SiO_2 source from rice husk waste from local market. *Cerbera manghas* seed oil collected and pressed in the area of Jambi University, Jambi.

2.2. Methods

The silica used was made from rice husk waste using a modified procedure carried out by Battegazzero et al. (2014) [16]. The stages are rice husk added with 200 ml of H_2O and 20 ml (1.828M) of H_2SO_4, then stirred using a magnetic stirrer for 5 h at 70°C, filtered and dried for 12 h at 50°C. Then, it was calcined with air for 5 h at 600°C. The results were analyzed by X-ray fluorescence (XRF) to investigate the chemical composition and the elements contained especially the SiO_2 content. Mesoporous aluminosilicate synthesis using a modified procedure carried out by Nugraha et al. (2021) [17]. The phases involve dissolving 0.025 mol Na_2O in 5 mol H_2O, adding 0.25 mol SiO_2, 0.005 mol γ-Al_2O_3, and a 0.05 mol CTABr template, and stirring for 4 h at 40°C. The mixture was aged overnight at room temperature, and the hydrothermal method was carried out at 160 °C for 48 h. The result was then washed with distilled water to pH=7, dried overnight at 120°C, and finally calcined with air for 5 h at 550°C. The same technique was used for the synthesis mixture, with an 8-h stirring duration. All Samples were noted as Al-MCM-41 4 h and Al-MCM-41 8 h.

2.3 Hydrocracking Process

The hydrocracking procedure was carried out in a batch reactor containing 0.5 g of catalyst and coated with a heating element. Then 50 mL of *cerbera manghas* oil was added to the batch reactor. Flow H_2 until the reactor pressure reaches 30 bar, then close the H_2 valve and heat the reactor from room temperature to the desired operating temperature of 330°C, maintaining it for 2 h. The product was collected and analyzed using a Gas Chromatography Mass Spectrophotometer (GCMS) with Agilent brand, type 19091S-433:93.92873 HP-5MS 5% Phenyl Methyl Silox to identify the compounds contained.

3. RESULTS AND DISCUSSION

The extracted silica was analyzed using XRF to determine the chemical composition. The XRF characterization results are shown in Table 1. Table 1 shows that the highest content contained in the extracted rice husk is SiO_2 with a percentage of 95.6527% and Al_2O_3 of 1.6143%. Based on several previous studies, it was stated that RHA contains >90% silica [18,19]. According to Ismail et al. (2015) [20], the crystal structure for amorphous SiO_2 will form with high temperature combustion above 600 °C, while the SiO_2 crystalline phase begins to form above 900 °C and at 1100 °C crystalline SiO_2 crystals are formed with high intensity so that the amount of silica obtained decreases.

Table 1. XRF Results of Rice Husk Extraction

Compounds	% wt
MgO	1.297
Al_2O_3	1.614
SiO_2	95.653
P_2O_5	0.588
SO_3	0.230
K_2O	0.115
CaO	0.132
TiO_2	0.007
MnO	0.021
Fe_2O_3	0.248

The XRD analysis was performed to identify the phase and crystallinity of the mesoporous aluminosilicate synthesis catalyst. The diffractogram patterns were observed at 2θ in the range of 10-80°. The diffractogram of Al-MCM-41 with 4 h and 8 h of stirring time synthesis is shown in Fig. 1. The diffractogram of the catalyst shows a broadened peak at 2θ = 22-23°. This peak suggested that Al-MCM-41 catalyst has an amorphous phase [21,22]. These results are in accordance with the previous study which also produced a broadened peak at 2θ = 22-23° [12].

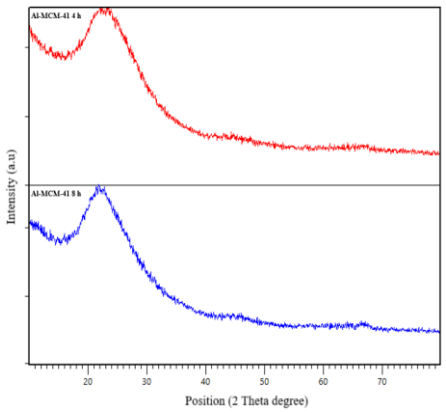

Fig. 1. The Diffractogram of Al-MCM-41 with 4 and 8 h of stirring time

The process of analyzing mesoporous materials can be known through Langmuir isotherm graphs based on the ratio of P/Po (mmHg) to the volume of N_2 per gram of sample (cm^3/g). The Langmuir isotherm graph shown in Fig. 2 illustrates a type IV graph which is a mesoporous material where there is a hysteresis loop in all different sample variations. A sharp gas change occurs at a relative pressure (P/Po) of about 0.1-0.3 which indicates the occurrence of mesoporous filling. All samples show the same pattern, in other words all samples indicate the presence of mesopores. This indication is reinforced by the occurrence of hysteresis or branching loops observed at relative pressure (P/Po) 0.3-0.9 in all samples [23]. In Fig. 2B, it can be seen that the pore diameter ranges from about 2-5 nm which is the pore size that can be used to access reactants. This indicates that the pore size distribution of all samples is in the mesoporous region (2-50 nm) [24].

Table 2 shows the physical properties of Al-MCM-41 stirred for 4 and 8 h. Al-MCM-41 with 8 h stirring time produces a larger surface area of 655.4759 m^2/g while Al-MCM-41 with 4 h stirring time produces a smaller surface area of 184.8508 m^2/g. This shows that the longer the stirring time process takes place, the greater the surface area produced. Table 2 shows that the surface area is influenced by pore volume and pore diameter, this is because the small pore diameter size will make the number of pores more and more so that the surface area will also be larger. In contrast to the pore volume, the larger the pore volume produced, the greater the surface area [25].

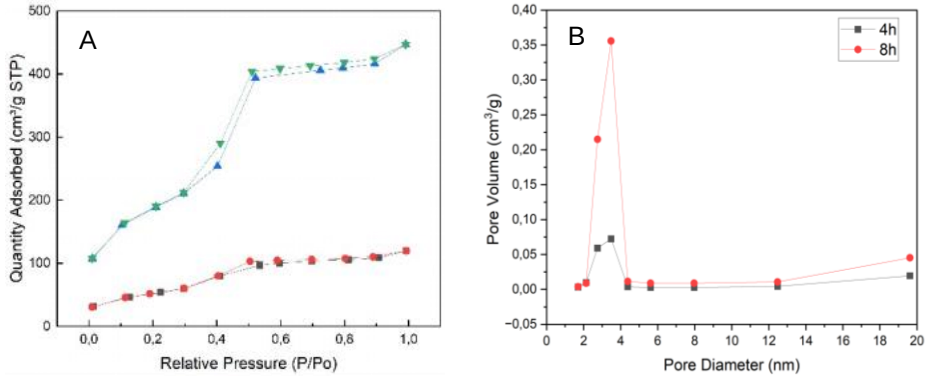

Fig. 2. (A) Comparison of Adsorption-Desorption of 4 h (red line) and 8 h Catalysts (green line), and (B) Pore Distribution Analysis of Catalyst by BJH Method

Table 2. Surface properties of Al-MCM-41

Samples	S_{area} (m^2/g)	S_{mikro} (m^2/g)	S_{meso} (m^2/g)	V_{tot} (cm^3/g)	V_{mikro} (cm^3/g)	V_{meso} (cm^3/g)
Al-MCM-41 4 h	184.851	2.764	182.086	0.186	0.001	0.185
Al-MCM-41 8 h	655.476	43.920	611.556	0.691	0.021	0.670

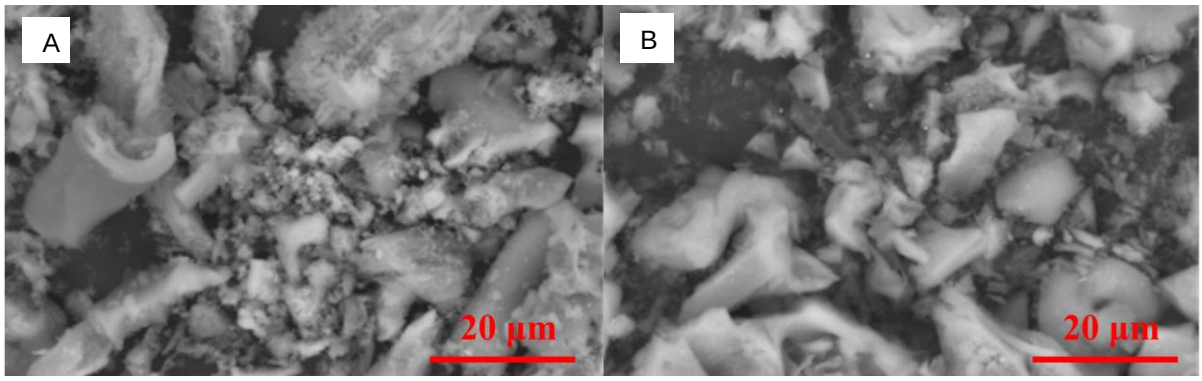

Fig. 3. 5000x SEM magnification (A) Al-MCM-41 4 h, and (B) Al-MCM-41 8 h

Fig. 3 shows the surface morphology of different catalysts using the SEM with magnification of 5000x. The non-uniformity of the visible particle size causes low crystallinity in the sample. This agglomeration and non-uniformity is supported by the research of Castro et al., (2021) [26], that the surface of Al-MCM-41 agglomerates in several particles with a non-uniform shape where some of them are round like a sleeve.

3.1 Catalytic Activity

The catalytic activity of Al-MCM-41 catalyst was tested in the hydrocracking process of *cerbera manghas* oil. The hydrocracking reaction was carried out for 2 h at temperature of 330 °C. The GC-MS analyzed was utilized to obtained the qualitative and quantitative product for the catalytic activity test. Table 3 shown the composition of hydrocarbon. Based on GCMS analysis, biofuel hydrocarbons contain hydrocarbons and oxygenate compounds [27]. Fig. 4 shown the Gas chromatography-mass spectrometry spectra of biofuel at temperature of 330 °C under pressure 30 bar in the batch reactor over (a) Al-MCM-41 4 h, and (b) Al-MCM-41 8 h catalyst with retention time of 22–24 min for different compounds of products. When using Al-MCM-41 4h catalyst, the products contain 1-methyl-indan ($C_{10}H_{12}$), cyclotetracosane ($C_{24}H_{28}$), and oxygenate compounds such as oleic acid, palmitic acid, and etc. Meanwhile, when using Al-MCM-41 8h catalysts, the products contain 1,3 tetradecadiene ($C_{14}H_{26}$), 1-tetracosene ($C_{24}H_{28}$), and still contain high oxygenate compounds. The presence of compounds that still contain a lot of oxygen such as carboxylic acids indicates that the hydrogenation reaction has not taken place properly at 330°C for 2 h to convert them into biofuel.

The oxygen removal process requires appropriate operating conditions of temperature, catalyst and reaction duration to optimize the decarboxylation/decarbonylation (HDC) and hydrodeoxygenation (HDO) reaction routes. The large amount of carboxylic acid shows that the hydrodeoxygenation reaction has not taken place well at 330°C with a reaction time of 2 h. An increase in temperature is needed to increase cracking activity and break large hydrocarbon chain molecules into small hydrocarbon chain molecules [28].

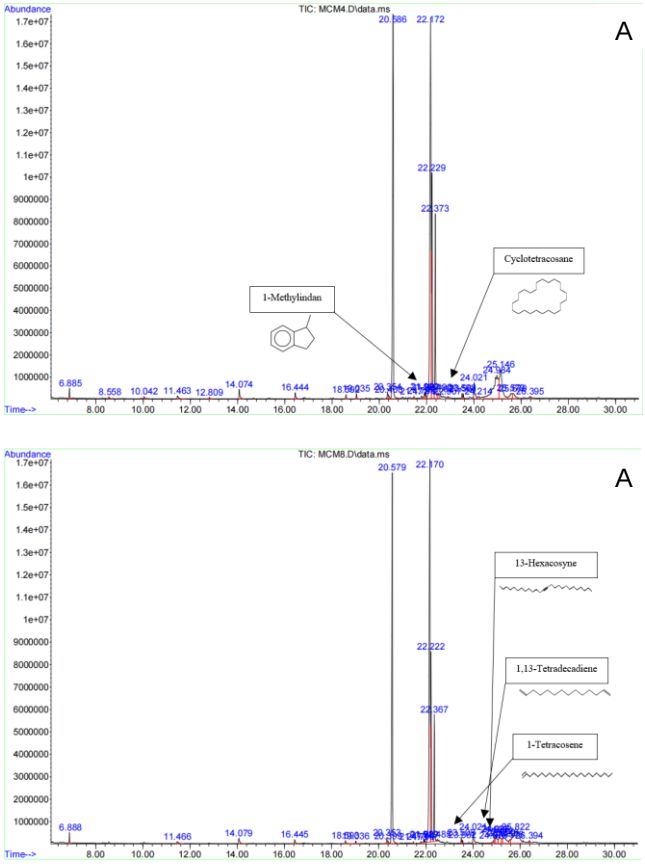

Fig. 4. Gas chromatography-mass spectrometry spectra of biofuel at temperature of 330 °C under pressure 30 bar in the batch reactor over (A) Al-MCM-41 4 h, and (B) Al-MCM-41 8 h catalyst

The difference in biofuel products produced from Al-MCM-41 8-h and 4-h catalysts is due to the catalyst's properties, such as pore structure, surface area, and pore diameter. Al-MCM-41 synthesized for 8 hours has a more regular mesoporous structure with a larger pore volume and surface

area than Al-MCM-41 synthesized for 4 hours. This can improve the accessibility of reactants and catalytic performance.

Table 3. The composition of hydrocarbon

Sample	Composition of hydrocarbon		
	C_{10}-C_{14}	C_{15}-C_{22}	>C_{22}
Al-MCM-41 4h	0.3	-	0.44
Al-MCM-41 8 h	0.8	-	1.48

4. CONCLUSION

Aluminosilicate synthesis catalyst has been successfully synthesized using materials made from rice husk waste with the addition of gamma alumina and CTABr template. The characteristics of aluminosilicate synthesis catalyst based on XRD analysis have amorphous phase at angle 2 theta = 22-23°. Based on GC-MS analysis, the product in the range fraction of biokerosene (C10-C14). The product of biofuel still contains high oxygenated compounds, it indicates that the hydrogenation reaction has not taken place properly at 330°C for 2 h to convert them into biofuel products.

ACKNOWLEDGEMENTS

This study was funded by the Research Organization for Nanotechnology and Materials – National Research and Innovation Agency (BRIN) research grant 2022 (No. 7/III/HK/2022). The authors would also like to thank Advanced Characterization Laboratories Serpong, National Research and Innovation Agency (BRIN) via E-Layanan Sains, Badan Riset dan Inovasi Nasional, for their facilities, scientific and technical support. MAM is the primary contributor to this manuscript.

REFERENCES

[1] M. Al-Muttaqii, F. Kurniawansyah, D.H. Prajitno, A. Roesyadi,(2019) 319–327.
[2] N.M.T. Al-Layla, L.A. Saleh, A.B. Fadhil, (2021).
[3] E. Emmanouilidou, A. Lazaridou, S. Mitkidou, N.C. Kokkinos, (2024) 137870.
[4] K. Musa, M. Munirat, J. Jacob, A. Rabiu, K. Dauda, A. Ali, I. Yahuza, (2025) 100201.
[5] L. Marlinda, D.H. Prajitno, A. Roesyadi, I. Gunardi, Y.W. Mirzayanti, M. Al Muttaqii, A. Budianto, (2022) 17–39.
[6] L. Marlinda, M. Al-Muttaqii, I. Gunardi, A. Roesyadi, D.H. Prajitno, (2017) 167–184.
[7] M. Al, D. Annas, I. Yati, H. Hendarsyah, S. Theo, C. Lotebulo, S. Priyanto, A. Aziz, D. Prasetyoko, R. Edra, L. Marlinda,Inorg. (2025) 113855.
[8] A.P.P. Nugroho, 6422-20491-1-Pb, (2014) 2337–3539.
[9] R.- Rasyid, R. Aditya S. W, D. Dian.L, M. Mahfud, A. Roesyadi, (2015) 268–273.
[10] F. Cheng, Z. Wang, X. Cui, L. Li, Z. Shi, S. Liu, S. Yu, J (2023).
[11] R. Ganesan, S. Subramaniam, R. Paramasivam, J.S.M. Sabir, J.S. Femilda Josephin, K. Brindhadevi, A. Pugazhendhi, (2021) 143781. https://doi.org/10.1016/j.scitotenv.2020.143781.
[12] F. Wang, F. Yu, Y. Wei, A. Li, S. Xu, X. Lu, J. https://doi.org/10.1016/j.jaap.2021.105146.
[13] H. Juwono, T. Triyono, S. Sutarno, E.T. Wahyuni, H. Harmami, I. Ulfin, F. Kurniawan, (2017) 337–342. .
[14] H. Chen, S. Fu, L. Fu, H. Yang, D. Chen, (2019) 1–11.
[15] F. González, C. Pesquera, A. Perdigón, C. Blanco, (2009) 7825–7830.
[16] D. Battegazzore, S. Bocchini, J. Alongi, A. Frache, (2014) 54703–54712.
[17] R.E. Nugraha, D. Prasetyoko, N. Asikin-Mijan, H. Bahruji, S. Suprapto, Y.H. Taufiq-Yap, A.A. Jalil, (2021) 110917.
[18] S. Steven, E. Restiawaty, P. Pasymi, Y. Bindar, (2021) 51–57. .
[19] J. Bin Haider, M.I. Haque, M. Hoque, M.M. Hossen, M. Mottakin, M.A. Khaleque, M.A.H. Johir, J.L. Zhou, M.B. Ahmed, M. Zargar, (2022) 135121.
[20] N.A.A. Ismail, M.A. Azmi, S. Ahmad, H. Taib, (2015) 470–474.
[21] R.E. Nugraha, (2023) 31–36.
[22] F. Guo, J. Li, W. Li, X. Chen, H. Qi, X. Wang, Y. Yu, Russ.(2017) 2055–2063.
[23] A. Aziz, B.G. Andini Putri, D. Prasetyoko, R.E. Nugraha, H. Holilah, H. Bahruji, A.A. Jalil, (2023) 32648–32659.
[24] R.E. Nugraha, D. Prasetyoko, N.A. Nareswari, A. Aziz, H. Holilah, H. Bahruji, M.R. Yusop, N. Asikin-Mijan, S. Suprapto, Y.H. Taufiq-Yap, A.A. Jalil, S.W. Purnami, H. Hartati, (2024) 100877.
[25] R.E. Nugraha, D. Prasetyoko, H. Bahruji, S. Suprapto, N. Asikin-Mijan, T.P. Oetami, A.A. Jalil, D.V.N. Vo, Y.H. Taufiq-Yap, (2021) 21885–21896.
[26] K. de Sousa Castro, L. Fernando de Medeiros Costa, V.J. Fernandes, R. de Oliveira Lima, A. Mabel de Morais Araújo, M.C. Sousa de Sant'Anna, N. Albuquerque dos Santos, A.D. Gondim, (2020) 555–564.
[27] H. Hasanudin, W.R. Asri, A. Mara, M. Al Muttaqii, R. Maryana, N. Rinaldi, S. Sagadevan, Q. Zhang, Z. Fanani, F. Hadiah, (2023) 20858–20868.
[28] M. Al Muttaqii, M.P. Marbun, S. Sudibyo, A. Aunillah, D. Pranowo, H. Hasanudin, N. Rinaldi, T.B. Bardant, (2024) 141–148.

Malaysian Journal of Catalysis
http://mjcat.utm.my/
MJCat Research Article

Removal of Heavy Metals from Wastewater Using Albizia Lebbeck Seed-Based Activated Carbon

Peter Bolutife Ogundokun[1], Amani David Haruna[2*], Baba Saje Muhammad[3*], Abdulkareem Mika'il Alhaji[2], Issah Babatunde Alabi[1]

[1]*Department of Chemical Engineering, Faculty of Engineering and Technology, University of Ilorin, P.M.B. 1515, Ilorin, Nigeria.*
[2]*Department of Chemical Engineering, Federal University Wukari, Taraba State, Nigeria.*
[3]*Department of Chemistry, Nile University of Nigeria, Abuja.*

**Corresponding Author: davidamani60@gmail.com, baba.saje@nileuniversity.edu.ng*

Article history:
Received 25 January 2025
Accepted 05 March 2025

ABSTRACT

Water, a vital resource for sustaining life, is increasingly threatened by pollution caused by industrialization, population growth, and modernization. This study evaluates the potential of Albizia lebbeck seed-based activated carbon for the removal of Chromium VI [Cr (VI)] ions from aqueous solutions. The Albizia lebbeck seed was chemically modified using phosphoric acid into activated carbon and its performance was tested based on contact time, adsorbent dosage, temperature, concentration, and pH of the wastewater. The efficiency of the preparation was evaluated using batch adsorption isotherm, Fourier Transform Infrared spectroscopy (FTIR), Scanning Electron Microscopy (SEM), Brunauer-Emmett-Teller (BET), and Energy Dispersive X-ray Spectroscopy (EDS). Batch adsorption results revealed that the removal of Cr (VI) ions from its aqueous solution on the studied adsorbents was influenced by the investigated parameters in varying degrees. The adsorption process was found to be endothermic and best described by the Freundlich as determined from isotherm modelling. The FTIR analysis also show the presence of more surface functional groups and sharper peaks in the activated adsorbent than the original form. The SEM micrograph revealed the morphology of the prepared activated adsorbent and the activated adsorbent exhibited higher BET surface area (336.436 m2/g), pore volume (0.305 cc/g), and pore size (6.602 nm), enhancing its mesoporous nature compared to the unmodified adsorbent (236.617 m^2/g), (0.215 cc/g) and (6.214 nm) which likely improved its performance. The results confirm that activated Albizia lebbeck seeds are effective adsorbents for removing chromium (VI) ions from aqueous solutions, particularly when treated with inorganic acid. This highlights their potential for removing heavy metal contaminants from industrial wastewater.

Keywords: *Activated Carbon, Albizia Lebbeck Seed, Wastewater, Heavy Metals*

| eISSN 0128-2581 |

1. INTRODUCTION

The rapid industrialization and urbanization of modern society have led to a significant increase in the generation of wastewater contaminants with heavy metals [1]. Heavy metals such as lead Pb), Cadmium (Cd), and Nickel (Ni) are highly toxic and can cause severe environmental and health problems, even at low concentrations. The removal of heavy metals from wastewater is therefore a critical environmental concern. Water is the most important and essential resource on Earth for maintaining life's basic processes, but regrettably, economic expansion, population growth, modernization, and other physical and biological changes are all causing its quality to continue declining, which has a negative effect on both human health and the environment as a whole [2-3]. Advancements in human procedures since the days of the Industrial Revolution have charted the course of industrial processes towards utilizing the full potential of water, especially as a process utility. Unfortunately, this has also rendered water bodies vulnerable to untreated or partially treated wastewater that are end products of industrial processes. These wastewaters are laden with heavy metals like Chromium which when taken up by living things in water bodies even at very low concentrations, can result into irremediable consequences in them [6-7]. The bio-

accumulation tendencies of heavy metals enable them to be transferred to the apex of the food and this makes them highly risky to ingest. In addition to industrial and consumer waste, acid rain can also release heavy metals into streams, lakes, rivers, and groundwater [8]. Due to the rapid expansion of sectors, heavy metal wastewater is rapidly being discharged into the environment, particularly in developing nations, through facilities such as metal plating, mining, fertilizer production, textile making, battery production, paper production, and pesticides [9].

As such, the world continues to struggle with the environmental challenge of effective waste disposal even as it urgently seeks to surpass previous advancements and meet endless human needs on an industrial scale. As a result, special legal and social attention is placed on industries on a global scale to ensure that the possible disaster that may result from large concentrations of heavy metals in water bodies is averted [10-11]. In many developed countries, stringent penalties are meted out to industries that release these heavy metals into water bodies, ensuring that pollution of the water bodies is kept to the minimum. Unfortunately, similar policies and measures are not widely implemented in most developing countries, leaving the poor people who depend solely on water from polluted water bodies vulnerable to diseases and infection that result from the deposit and synthesis of heavy metals into living organisms [12]. Hence, researchers need to elaborate on economically sustainable means of solving wastewater problems to carry developing nations along as they rapidly industrialize to bridge the gap with developed countries [13-14].

Many methods have been explored for the removal of heavy metals from wastewater but adsorption in particular stands out as the most economical and effective method in removing a wide variety of harmful heavy metal substances from industrial wastewater [15]. Several materials have been evaluated as suitable adsorbents such as biomass because they are good sources of carbon: animal wastes, fruit wastes (fruit peels and seeds), aquatic plants, wood-based materials (sawdust, wood shavings, the bark of trees) and agricultural wastes. The availability, cost of acquisition, porosity and presence of certain functional groups on the biomass surfaces make them excellent materials for adsorption processes [16-17]. In addition, the surface area, chemical stability and regenerability of carbon-based substances are major factors that ensure adsorption occurs on their surfaces thereby making them favourable as choices of adsorbents [18].

Several studies have been conducted on the potential of Albizia Lebbeck as an adsorbent for purifying industrial wastewater. Activated biochar obtained from the pods, leaves and seeds of the Albizia lebbeck plants have shown potential in adsorption, especially in removing heavy metals from industrial wastewater [19]. The plant is grown widely and exists both through natural propagation and through plantations by humans. Its ability to thrive in various climatic conditions makes it a favourable choice as a source of adsorbent. The relative availability of the trees makes it an excellent source of adsorbent material however, most previous studies have been focused on adsorbents derived from the pods of the plant thus there is a need to evaluate the potential of other parts of the plant such as the seeds and leaves [20].

Thus, this research aimed at synthesizing, characterizing, and applying Albizia lebbeck seeds-derived adsorbent for the removal of chromium VI ions from its aqueous solution; Sourcing and preparation of seeds obtained from Albizia lebbeck trees, carbonization, and activation of the seeds, characterization of both activated and raw adsorbents using BET, FTIR and SEM-EDS techniques, application of the activated adsorbent in adsorption experiment for the removal of chromium (VI) ions from simulated solution and determination of best adsorption isotherm model for the description of the adsorption process. This study was limited to the preparation, characterization, and activation of Albizia lebbeck seeds-derived adsorbent and testing its effectiveness in removing chromium from its aqueous solution.

2. EXPERIMENTS

The activated carbon was prepared from Albizia Lebbeck seed through chemical activation with phosphoric acid. Stock solution of Pb(II), Cd(II) and Ni(II) were prepared using their respective nitrate salts. Wastewater samples were collected from local industrial effluent treatment plant and all these reagents used were of analytical grade.

2.1 Sample Collection and Preparation of the seeds

Albizia lebbeck pods were collected from the University of Ilorin premises. The seeds were thoroughly washed with tap water, followed by distilled water. They were then purified by soaking in a 0.1 M HCl solution for 24 hours, rinsed with deionized water until a neutral pH was achieved, air-dried at room temperature for three days, and stored in glassware for further analysis.

2.2 Preparation of Un-modified Albizia Lebbeck seed adsorbent

The dried seeds were placed in the muffle furnace for 2 hours 30 minutes at 300°C. The biochar obtained was then crushed to powder using mortar and pestle and sieved with a 53 µm sieve respectively. The sieved powder was washed repeatedly with deionised water until a colourless filtrate was obtained to remove any traces of absorbed salt. Subsequently, the residue was dried in an oven at 105°C for 10h after which it was cooled, stored, and labelled in a sterile sample container as un-modified Albizia lebbeck seed (ALS).

2.3 Preparation of Modified Albizia Lebbeck seed adsorbent

Some parts of ALS were carbonized for 2:30 h in a muffle furnace at 300°C before chemical activation with 1 M Phosphoric acid (H_3PO_4) for 72 hours. After activation, the sample was washed with deionised water to remove any unreacted material and oven dried at 105°C after which it was stored as Chemically activated Albizia Lebbeck Seed (CMALS).

2.4 Catalyst Characterization

Fourier Transform Infrared (FT-IR) spectroscopy was used to analyse the functional groups on the adsorbents while the surface area, pore volume, pore diameter, and pore size distribution were determined using Brunauer-Ennett-Teller (BET) analysis. The surface structures and compositions were determined by Scanning Electron Microscope (SEM) coupled with energy-dispersive X-ray Spectroscopy (EDS) Analysis.

Proximate analysis is a laboratory technique used to determine the approximate composition of material, typically biomass or coal. The analysis has to do with the determination of the material's ash content, moisture content, volatile matter and carbon content.

For moisture content, a pre-weighed crucible was filled with 1 g of the adsorbent, which was then sealed with a covering. The sample's complete mass, including the container itself and cover, was measured. After being loaded with samples, the container was placed in an oven without its cover. The oven was heated to 110°C for three hours to ensure that the sample weights were consistent. The process was repeated three times, and the moisture percentage was determined using equation 1 [22].

$$\text{Moisture content (\%)} = \frac{(B-F)}{(B-G)} \times 100 \quad (1)$$

B is the mass of container with lid + original sampling.
F is mass of container with lid + dried sampling
G is the mass of container with a lid.

To check for the ash content in the sample, an open crucible was filled with 5g of the material, and the resulting mass was measured. The sample was heated to 900°C for 3 hours. The material was measured after being cooled to room temperature. The process was repeated three times. The ash content was determined using equation 2:

$$\text{Ash content (\%)} = \frac{(A-C)}{(K-C)} \times 100 \quad (2)$$

C is the mass of empty crucible in g
K is the mass of crucible + original sample
A is the mass of crucible + ash sample in gram

2.5 Adsorption Experiments

Batch experiments were conducted to determine the adsorption isotherms of synthetic wastewater onto the adsorbents in a glass flask. The experiments were conducted at room temperature to be indicative of climatic conditions and the impacts of interaction duration, temperature, as well as adsorbent dosage on the decline in heavy metal concentration were examined [23]. A certain volume of the synthetic wastewater sample was measured into series of graduated flasks. The kinetics of the adsorption was studied at different time intervals (5-90minutes) using a certain mass of adsorbent added into solutions in the flasks. The effect of temperature was investigated at different temperatures. The effect of pH was also studied within the range of 2 – 12 by making adjustments where necessary with NaOH or HCl. The mixtures were filtered, and the residual concentrations of the heavy metal were determined.

2.5.1 Effect of Contact Time

Contact time refers to the duration for which the contaminated water is in contact with activated carbon. Initially the rate of adsorption is rapid as the available active sites on the carbon surface are occupied by heavy metal ions. As time progresses, the rate of adsorption decreases and eventually reaches an equilibrium point where no significant changes in metal concentration occur. Determining the optimal contact time is crucial for maximizing the removal efficiency. Studies have shown that the longer contact times generally leads to higher removal rates, but at some point, the increase in removal efficiency diminishes. At 120 minutes equilibrium is attained. Therefore, it is essential to identify the equilibrium time to optimize the process and reduce costs.

2.5.2 Effect of pH

The pH of solution significantly influences the adsorption capacity of activated carbon for heavy metals. Different metals exhibit varying solubility and ionization states at different pH levels. For instance, at low pH, the concentration of H^+ ions is high, which can compete with metals for ions adsorption sites on activated carbon, potentially reducing removal efficiency. The method of adsorption was performed at multiple pH levels (2, 4, 6, 7, 8, 10 and 12) for the starting concentration, constant adsorbent dosage, and constant contact time were observed in order to investigate the impact of the pH on the adsorption of heavy metals from synthetic wastewater. The Optimal pH range was neutral to slightly alkaline pH (around 6 – 8) is favourable for the adsorption of many of the heavy metals. However, the pH can vary depending on the specific heavy metals being targeted.

2.5.3 Effect of Temperature

Temperature plays a dual role in the adsorption process. An increase in temperature can enhance the kinetic energy of the molecules leading to increased diffusion rate and potentially higher adsorption capacities. However high

temperatures may also disrupt the adsorption process by desorbing metal ions from the activated carbon surface. The optimal temperature for heavy metal removal using Albezia lebbeck seed-based activated carbon falls within the range of ambient to moderately elevated temperatures (20 – 50 °C). beyond this range, the benefit of increased kinetic energy may be outweighed by the desorption effect.

2.5.4 Effect of Concentration

The initial concentration of heavy metals in the solution directly impacts the adsorption capacity of activated carbon. Higher concentrations of metal ions can lead to increased driving force for adsorption, resulting in higher removal efficiencies. However, once the active sits on the carbon are saturated, the removal efficiency will be low. Optimal concentration is essential to determine the saturation point of the activated carbon. The six concentrations were; 120 ppm, 80 ppm, 60 ppm, 50ppm, 40 ppm and 20 ppm. It was observed that the percentage removal of chromium increased with the potassium dichromate solution

2.6 Adsorption Kinetics

Adsorption Kinetics is a process by which solute molecules attach to the surface of an adsorbent. Adsorption kinetics is a line or curve that explains the rate of retention or release of a solute from an aqueous to solid-phase boundary at a specified adsorbent dose, temperature, flow rate and pH.

2.6.1 Pseudo-First Order Kinetics Model

Pseudo first order kinetics model describes solute adsorption unto adsorbent following the first order mechanism, the following formulars represents the pseudo first order reaction kinetics

$$\frac{de}{dt} = k1\ (qe - qt) \quad (3)$$

This equation could further be expressed as

$$Log\ (qe - qt) = log\ log\ qe\ - \frac{k1}{2.303xt} \quad (4)$$

Where;

$qe = amount\ of\ adsorbate\ at\ equiliruim$ (mg/g)
$qt = amount\ of\ adsorbate\ adsorbed\ at\ time\ t$ (mg/g)
$k1 =$
$rate\ constant\ of\ pseudo\ first\ order\ per\ minutes$
(min^{-1})

2.6.2 Pseudo – Second Order Adsorption

According to the pseudo-second order kinetics model, the concentration of metallic ions inside any fluid in question and the number of open adsorption sites on the adsorbent's outermost layer are both important factors in the adsorption process. The sole disparity between the pseudo-second-order kinetic model and the pseudo-first-order kinetic model is the speed of the model. This is proven by the pseudo-second order kinetics rate equation may be express equation 5 and 6.

$$\frac{de}{dt} = k1\ (qe - q)^2 \quad (5)$$

$$\frac{t}{qt} = \frac{1}{k2qe^2} + \frac{1}{k2qe} + \frac{t}{qe} \quad (6)$$

Where $k2 = the\ rate\ constant$ pseudo- second order sorption (mg/min)

2.6.3 Elovich Kinetics model

According to the Elovich equation, neither desorption nor the interactions among the species that are absorbed could substantially alter the rates of adsorption at minimal coverage because the solid surface is assumed to be inherently heterogeneous. The Elovich kinetics model suggests that the adsorption of the heavy metal ions onto the activated carbon is a complex process involving multiple mechanisms, such as surface adsorption and pore diffusion. The model parameters (α and β) provides valuable insights into the adsorption kinetics and capacity.The following represents the Elovich dynamics model mathematically as:

$$\frac{dq}{dt} = \frac{1}{\beta in(\alpha\beta)} - \frac{1}{\beta in(t)} \quad (7)$$

where:

$\frac{dq}{dt}$ is the rate of adsorption
α is the initial sorption rate ($mgg^{-1}min^{-1}$)
β is the desorption constant ($g.mg^{-1}$).
q is the amount of adsorbate adsorbed at time t.

2.7 Adsorption Thermodynamics

Thermodynamic factors are crucial for determining whether the adsorption process is feasible and spontaneous. The thermodynamics parameters generally give an understanding into the minimum kinetic energy required for the adsorbate to become bound to the adsorption site. Usually, the nature of the adsorption process which are the main factors that control viability and spontaneity are thermodynamic parameters, specifically heat of enthalpy (H), Gibbs free energy (G), and entropy (S). The Langmuir isothermal constant ($C_{ad,e}$), the solvent coefficient distribution (K_d), and the equilibrium content (C_e), which varies with temperature, are all provided in the equations below were used to determine the thermodynamic parameters in this research.

$$In\ K_d = \frac{\Delta S}{R} + \frac{\Delta H}{RT} \quad (8)$$

$$\Delta G = \Delta H - T\Delta S \quad (9)$$

For the Langmuir constant

$$InK_c = \frac{C_{ad,e}}{C_e} \quad (10)$$

$$\Delta G = -RTInK_c \quad (11)$$

ΔS can also be obtained by Gibbs- Helmholtz equation:

$$\Delta S = \frac{\Delta H - \Delta G}{T} \quad (12)$$

3. RESULTS AND DISCUSSION

3.1 Characterization

The Modified Albizia lebbeck seeds (MALS) and the unmodified calcined Albizia lebbeck (ALS) were analyzed for their surface area, pore volume and pore size of all the absorbent were analyzed using BET under N_2 adsorption-desorption study and the results are presented in Table 1. The results showed that the modified adsorbent has higher surface area which serves as an indicator that they may have higher adsorption capacity. It was also observed that the modified Albizia lebbeck seed (MALS) adsorbent has a higher surface area compared to the unmodified [24].

Table 1. BET Analysis of Modified and Unmodified Adsorbents.

Sample	Surface Area (m^2/g)	Pore Volume (cc/g)	Pore Size (nm)
ALS	236.617	0.215	6.214
MALS	336.436	0.305	6.602

The enhanced surface area of MALS may be attributed to incorporation of the phosphoric acid as a synthesizing agent, which may have improved the MALS because the pore size of this adsorbent was about 6.602 nm which indicated that they are more mesoporous in nature compared with the unmodified adsorbent (ALS) with pore size 6.214 nm. It follows that adding acid to the adsorbent during synthesis can change its surface characteristics, resulting in an increase in porosity and surface area. It is expected that due to such desirable properties adsorption capacity and reactivity is enhanced, making it more effective for capturing ions from a solution [1]. BET test is significant because it provides valuable insights into the surface properties and porosity of materials, which are critical for understanding their behaviour in various applications.

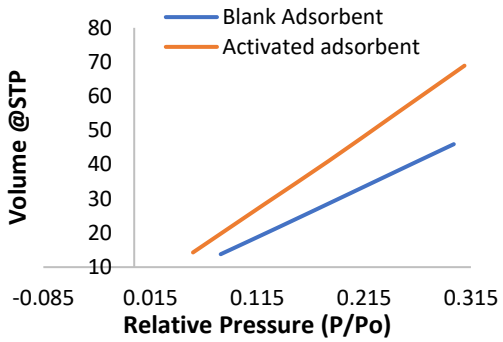

Figure 1. Relative Pressure vs Volume at STP for Blank and Activated Adsorbents.

The SEM analysis shows the nature of the Albizia lebbeck seeds activated adsorbent, and it elaborates on the clarity of the development of pores which are pivotal to adsorb the chromium heavy metal unto the Albizia lebbeck seed adsorbent. The SEM figure below show the analysis images for the modified Albizia lebbeck seed adsorbent after synthesis with phosphoric acid, by Scanning Electron Microscopy (SEM). The images show the SEM analysis at 500, 1000 and 1500 magnification. The images depict how the particles in the adsorbent are in aggregated form instead of in separated forms, which can be attributed to the large surface area of the adsorbent. The SEM images show a highly irregular and rough appearance on the surface which may be due to synthesis with the auto phosphoric acid (Figure 2A). The irregular and rough appearance when observed after SEM analysis is valid indicator of a good adsorbent [25-26].

Pores were evident on the surface of the modified Albizia lebbeck seeds (MALS) after the SEM analysis, which can be attributed to the presence of an elementary pore network [24][27]. The evident elementary pores can be most observed on the Figure 3a below which is a 1500X view of the surface of the adsorbent. The Figure 2B best depicts the extent of the coarseness and roughness of the adsorbent with SEM analysis. Figure 2C draws into perspective the active pores in addition to the roughness of the adsorbent.

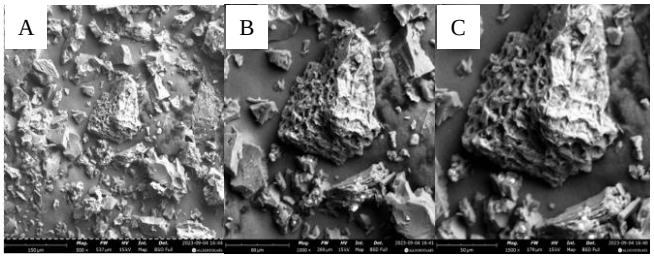

Figure 2. Micrographs of Modified *Albizia lebbeck* Seed Adsorbent at (A)500x, (B) 1000x, and (C) 1500x magnification

The Energy Dispersive X-ray Spectroscopy (EDS) Analysis technique used to determine the elemental

composition of the modified albizia lebbeck seeds sample. The peaks observed in the spectrum show the composition of the elements present in the MALS adsorbent. It can be seen from the spectrum plotted below that C, O and Si are present on the surface of the MALS adsorbent. As it can be observed from the Figure 4a, the carbon composition in the adsorbent is far greater than for the rest of the other elemental compositions. From background studies on adsorption, the higher the carbon content the more desirable the adsorbent is. The large amount of carbon is synonymous with the high carbon composition that can be seen from literature studies [28].

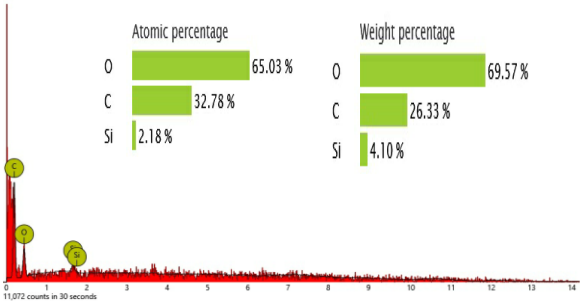

Figure 3. EDX Spectra, atomic percentage and weight percentage of Modified *Albizia lebbeck* Seed Adsorbent

Accuracy of EDS can be affected by a variety of factors. These factors might affect the chemical composition or nature of the albizia lebbeck seeds adsorbent. One of the major factors that might show inconsistency is the fact that the analysis is focused on a particular section of the adsorbent, which might not pick up elemental compositions present only in other parts of the adsorbent. The presence of negligible silicon (as shown in Figure 3) on the adsorbent surface maybe attributed to partial contamination during the course of preparation of the adsorbent. Silicon is generally chemically stable and inert, which means it is less likely to react with adsorbates.

The FTIR technique is a pivotal means in order to unravel the intricacies of functional groups present in the adsorbent and to predict the interaction with the adsorbate as a result of the functional groups present [29]. These groups are specific arrangements of atoms within the adsorbent's structure that can interact with adsorbate molecules, influencing adsorption capacity, selectivity, and other adsorption-related properties. The spectra were collected in the range from 400 cm^{-1} to 4000 cm^{-1} (Figure 4). It was observed that the while that unmodified spectrum has about 10 peaks, the modified adsorbent (MALS) possessed more than 20 peaks within its spectrum. The presence of more peaks in the modified adsorbent's spectrum can be said to be function of the synthesis of the MALS with an acidic agent. A higher number of peaks in the FTIR spectrum of the modified adsorbent suggests greater chemical complexity and diversity within the sample. Diversity and complexity depicted in the spectrum of the modified adsorbent reflect heavily on the expected broader selectivity affinity of the modified adsorbent to target contaminants [30].

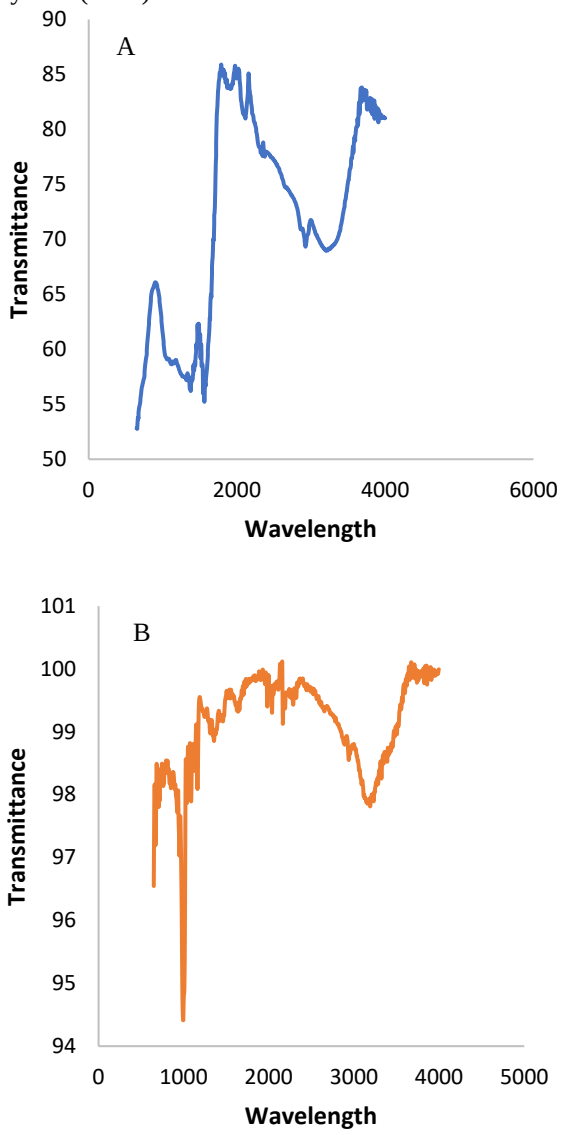

Figure 4. FTIR Spectra of (A) Blank and (B) Modified *Albizia lebbeck* Seed Adsorbents

The important peaks represented are the C-H bond which is stretching vibration, indicating the presence of alkyl groups, the O-H bond which indicates the presence of hydroxyl groups, the C=C bond and C-O bonds indicates the presence of carbon and carboxyl groups [7]. The Figure 4A and the Figure 5B show the plots of the activated and blank adsorbent. The high range of values for transmittance on the FTIR plot for the activated adsorbent can be attributed to several factors related to the changes in the adsorbent's structure, composition, and surface properties during the activation process. The activation process generated more active sites with functional groups. This increased availability of functional groups contributed to higher transmittance values due to enhanced adsorption [31].

It is clear that for the unmodified Albizia seed adsorbent the absorption peaks observed at about $3201cm^{-1}$ indicate the presence of the O-H group due to alcohol or phenol [32]. The peaks observed at about $1118cm^{-1}$

indicates the presence of C-O bond within the unmodified Albizia seed adsorbent. The peak observed at the range of 13700 to 1400 for the unmodified adsorbent indicates the presence of C-H bond within the adsorbent. The peak number between 3000cm^{-1} and 3980 indicate a high density of various functional groups in the fingerprint section of the spectra. The peaks observed between 3200cm^{-1} and 3260 cm^{-1} indicate the presence of the O-H bond in the modified adsorbent. The observable peaks seen between 2850cm^{-1} and 2960cm^{-1} indicated the presence of C-H functional group in the adsorbent compound. The observable peaks between 1650cm^{-1} and 1800cm^{-1} indicate the presence of C=O functional group in the adsorbent between 1400cm^{-1} and 1600cm^{-1}, the observable peaks detected signify the presence of C-C bond within the adsorbent spectra. Observable peaks around 2300cm^{-1} were attributed to the presence of C≡C bonds in that range of the spectra. Peaks observed between 1100cm^{-1} and 1300cm^{-1} could also serve as an indication of the presence of phosphates (P=O) as a result of synthesis of the adsorbent with autophosphoric acid. The greater number of peaks seen in the modified Albizia seed adsorbent as compared to the unmodified Albizia seed adsorbent elaborates on the effect of the synthesizing agent that has been added to the Albizia lebbeck seed adsorbent to increase its adsorption efficiency. Hence, the modified adsorbent contains more functional groups than the unmodified adsorbent ensuring greater adsorption efficiency during the experiment.

3.2 Physiochemical Study of Albizia lebbeck Seeds Adsorbent Biomass

The physiochemical study of Albizia Lebbek seed adsorbent biomass reveals its potential as low-cost, eco-friendly adsorbent for removing various pollutant from waste water. After a preliminary carbonization process to check for the optimum duration and temperature for carbonization, the ideal carbonization conditions were set at 300°C and 2.5 hours instead of the initial 400°C for 1.5 h.

Table 2. The summary of the carbonization process

Temperature	300 °C
Time	2.5 hours
Initial weight (g)	112.32
Final weight (g)	46.13

The Bulk density is a measure of the mass of the Albizia lebbeck seeds adsorbent per unit volume. The Bulk density measures how tightly the adsorbent particles are packed together. Adsorbents with higher bulk densities generally have more tightly packed particles. Proper packing ensures uniform flow distribution of the fluid (gas or liquid) through the adsorbent bed, reducing channelling and improving the adsorption efficiency. As it can be seen, the bulk density of the Albizia seed adsorbent is 0.865 meaning the biomass has undergone carbonization at high temperature and it can be deduced that it has high packing quantity of solid and can hold much adsorbate [33].

The Ash content in the Albizia seed adsorbent refers to the non-combustible residue left behind after the adsorbent material has been subjected to high temperatures. This residue typically consists of minerals, inorganic impurities, and other non-volatile substances. Impurities in the ash may interfere with the adsorption process by occupying active sites on the adsorbent surface, reducing the available surface area for adsorption, and affecting the selectivity of the adsorbent. An ash content of about 0.97% as shown in Table 3 is satisfactory as it shows that there is a very low amount of ash and possible impurity accompanied with it [34].

Moisture content can affect the adsorption capacity of the Albizia seeds adsorbent. When an adsorbent contains moisture, some of its surface area and pore space may be occupied by water molecules. This can reduce the available sites for adsorption of the target substances. In some cases, moisture itself can be the target of adsorption. A moisture content of about 6% as shown in Table 3 is fairly satisfactory. As opposed to Moisture Content, the Percentage Dryness of about 94% as shown in Table 3 is a strong indicator that the adsorbent is fairly satisfactory for storage and adsorption process.

Table 3. The physiochemical analysis of the Albizia lebbeck seeds derived adsorbent

Parameters	**Value**
Bulk density	0.86
Ash content (%)	0.97
Moisture content (%)	6.00
Dryness content (%)	93.9

3.3 Batch Experiment Studies

The batch adsorption studies were undergone with five predominant factors in consideration: pH, time, adsorbent dosage, temperature and initial concentration. Figure 5 below depicts the calibration curve which is a graphical representation of the relationship between absorbance and concentration of a sample before adsorption takes place. By understanding the graph of absorbance against concentration, you can accurately determine the concentration of a substance and identify potential issues with the measurement.

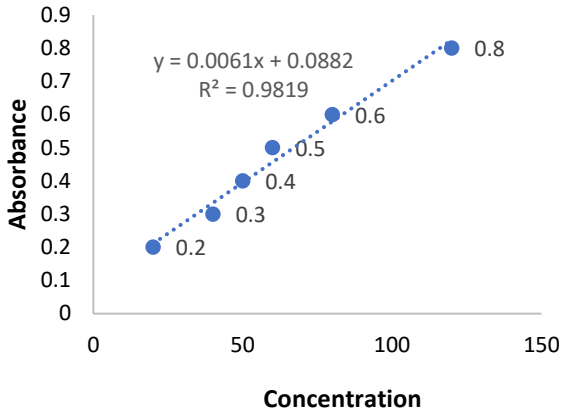

Figure 5. The calibration curve from the result for the initial AAS test before adsorption

The effect of pH on heavy metals removal is a critical aspect of environmental remediation and waste water treatment. Figure 6 dipicts the effect of adsorption with respect to the varying pH values.

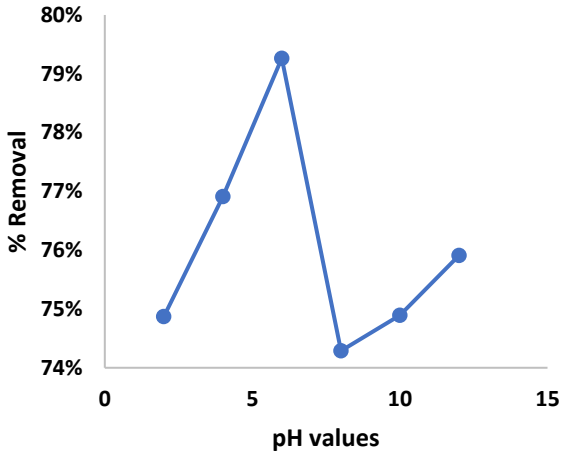

Figure 6. The effect of pH on percentage removal of heavy metals

The effect of pH was investigated for the adsorption of chromium from a solution of potassium dichromate solution of 50 ppm. The pH parameters were varied between the values of 2 and 12 over a wide range of acidic and basic pH regions, with a pH interval of 2(i.e., 2,4,6,8,10,12). A uniform volume of 20mL of 50ppm potassium dichromate solution was measured and added to 0.02g of modified Albizia lebbeck seeds derived activated adsorbent (MALS). The six conical flasks of varying pH values were left inside a water bath at a constant temperature of 25°C and were agitated for 120 minutes. Hence, while all other factors were kept constant the pH values were varied. It was observed that the optimum pH for adsorption was a pH value of 6. This could be attributed due to several factors, including the adsorbate and the surface charge of the adsorbent. The maximum level of percentage removal observed around a pH of 6 is due to charges that attract or facilitate binding of the adsorbate atop the surface of the adsorbent, enhancing the adsorption efficiency.

As the pH increases gradually from 6 and into the basic range, the surface charge of the adsorbent may change. Electrostatic repulsion between the adsorbate and the adsorbent could be a significant factor that accounts for the sharp decline in the percentage removal as it progresses into the basic region. The increase in percentage removal of chromium as the pH value increases from 8 to 12 is as a result of the surface charge of the adsorbent becoming positively charged, reaching a point where it can favourably interact with the adsorbate. As a result of possible changes, the adsorbate could undergo changes in ionization state, leading to improved adsorption efficiency due to more favorable interactions between with the positively charged adsorbent surface.

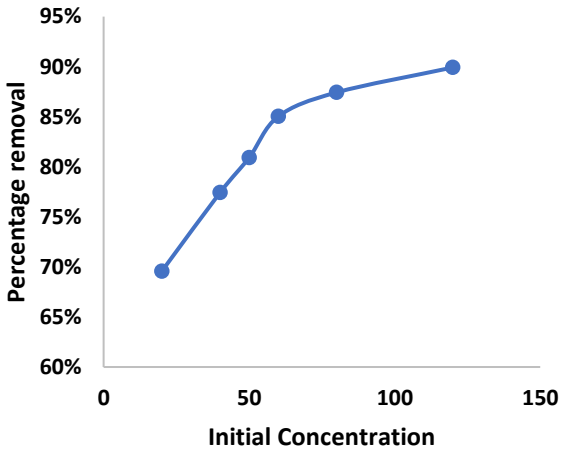

Figure 7. The effect of Initial concentration against percentage removal

The Figure 7 shows the plot that depicts the relationship between the percentage removal and the initial concentration of the solution.Six standard solutions of varying concentrations were prepared using a stock solution of potassium dichromate with concentration of 1000 ppm. The six concentrations were; 120 ppm, 80 ppm, 60 ppm, 50ppm, 40 ppm and 20 ppm. It was observed that the percentage removal of chromium increased with the potassium dichromate solution. It was further observed that equilibrium was approached as the plot progressed towards 120ppm against percentage removal. It has been ascertained from research that adsorption processes generally follow equilibrium kinetics. When the system reaches equilibrium, the percentage removal stabilizes. It can be seen from the plot of initial concentration against percent removal that the percent removal begins to stabilize at around 120ppm. At lower concentrations, it may take longer for the system to reach equilibrium, which can result in a lower percentage removal when compared to higher concentrations where equilibrium is reached more quickly [35]. Another reason for

the trend may be attributed to the fact that at lower concentrations, the adsorption sites may not be fully utilized, resulting in a lower percentage removal. As the concentration increases, the adsorption sites become saturated, and the percentage removal approaches a maximum value.

The effect of adsorbent dosage on the percentage removal of chromium from the solution is also a critical parameter in the adsorption processes, as it directly impacts the efficiency of the pollutant. The general increase in the percentage removal as the dosage of the adsorbent increased as shown in Figure 8 can be attributed to the available surface area for adsorption. Adsorption occurs at the surface of the adsorbent, so a greater surface area provides more sites for the target substance to adsorb to. This leads to higher adsorption capacity and, therefore, greater percentage removal [19].

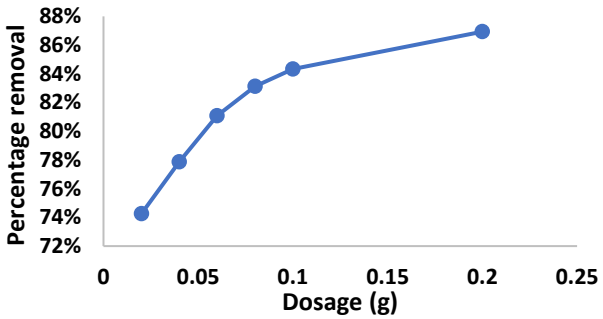

Figure 8. The effect of Absorbent dosage

It is evident that as the dosage increases, more sites become available for adsorption, resulting in increased percentage removal. At lower dosages, some adsorption sites are apparently unoccupied, which may be the resulting factor for limit in the percentage removal. Hence, the maximum adsorption as seen in Figure 8 occurred at an adsorbent dosage of 0.2g.

Effect of time on the removal of heavy metals is also another crucial aspect of adsorption processes. Longer time can lead to higher removal efficiency, as more heavy metal ions are adsorbed. The time required to reach equilibrium varies depending on the adsorbent, initial metal concentration and environmental condition. Figure 9 shows the plot of the removal of chromium from the solution with respect to contact time.The graph result presented showed the removal efficiency of MALS adsorbents increased with an increase in contact time. Equilibrium started to be attained as it approached towards 120 minutes. The increase in the percentage removal may be due to the presence of functional group for long periods being in contact with the adsorbate.

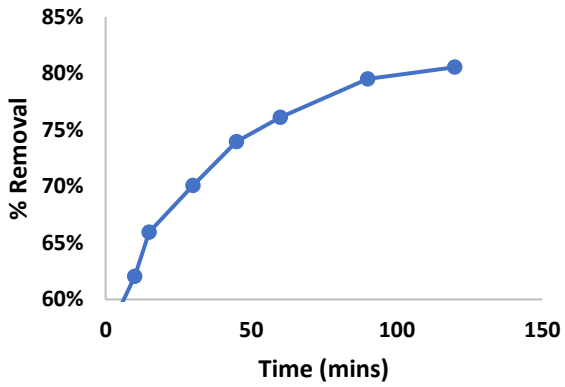

Figure 9. The effect of contact time in the % removal of heavy metals

The effect of temperature on the removal of heavy metals is also of importance in adsorption processes. The factors influencing temperature-dependent removals includes adsorbent type, heavy metal type and the pH and ionic strength. Figure 10 shows the effect og temperature on the adsorption of chromium from the solution.Temperature has strong effect on the intermolecular force between the adsorbate and the adsorbent particles. Effect of temperature on the adsorption process was investigated and the result is as presented in Figure 11. An increase in the temperature causes an increase in the efficiency of MALS removal. This fairly proportional relationship indicated that the adsorption process is an endothermic reaction.

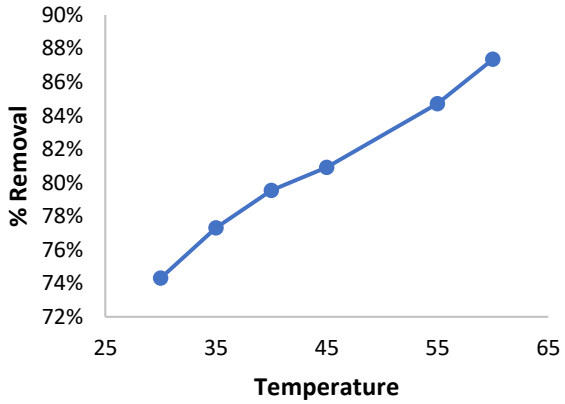

Figure 10. The effects of Temperature in the removal of heavy metals

Mechanism of adsorption refers to the physical and chemical processes that occur when a substance (adsorbate) accumulates on the surface of another substance (adsorbent). When the Potassium dichromate solution came into contact with the activated Albizia adsorbent, it initiated the adsorption process. There were lots of active sites for the chromium ions to interact with the activated adsorbent because of the large surface area [36]. Similar findings have

been reported by authors concerning the similar studies on other heavy metals [37].

Physical adsorption, commonly referred to as Van der Waals forces, could be responsible the main initial contact between the chromium ions and the Albizia adsorbent. The attraction interactions between the positively charged chromium ions and the negatively charged adsorbent surface could have caused this weak contact. These chemical reactions depended critically on the existence of oxygen-containing functional groups, such as carboxyl (-COOH), and hydroxyl (-OH), on the Albizia adsorbent surface [38]. Observed a dominant OH species in his biomass which led to high adsorption of X pollutant. This can be referred back to the FTIR studies of the adsorbent which highlighted the presence of these functional groups in the adsorbent [39].

Chemical adsorption was deduced to have been initiated during the course of the experiment when the solution and Albizia adsorbent had more contact time. Compared to physical adsorption, this contact is said to be more focused. Chemical linkages between chromium ions and functional groups that exist on the Albizia surface are possible. For instance, hydroxyl groups and chromium ions can combine to create stable complexes like Cr-OH or Cr-O-Cr given ample time of reaction. The adsorption process is deduced to have reached equilibrium when the rate of adsorption equals the rate of desorption. Adsorption kinetics studies can help determine the rate at which chromium is removed and how long it takes to reach equilibrium [40].

The Adsorption mechanism can be said to be a complex process involving physical and chemical interactions, ion exchange, and electrostatic attraction. Understanding and optimization of these mechanisms was crucial for effective chromium removal during the experiment, which can be attributes to the distinct qualities found in the adsorbent as also found in adsorption studies that involve the removal of heavy metals [32]. The functional groups present, the active sites atop the adsorbent, and the available volume in the various pores are all believed to have played a crucial role in initiating the adsorption process in the removal of chromium from the solution [36].

3.4 Adsorption Isotherms Study

The plots (Figure 11) below illustrate the isotherm studies of the adsorption experiment using the Langmiur and Freundlich isotherms.The experimental model was more suited to the Freundlich model. Experimental data of the chromium removal by activated Albizia seeds adsorbent were successfully fitted using Langmuir and Freundlich isotherms. Table 4 below presents the summary of the data obtained from the isotherms and kinetic studies. The correlation co-efficient (R^2) value for Langmuir was found to be greater than 0.8, but lesser than that of Freundlich with $R^2 > 0.9$ thus, indicating that although both the models can be used to describe the adsorption process the Freundlich model was more suited for the experiment. The 1/n value for Freundlich model was positive, ranging between 0 and 1 implies that the adsorption of chromium onto activated Albizia lebbeck seeds adsorbent was favorable at the studied conditions. The adsorption being more suited to the Freundlich model suggests the formation of heterogeneous multilayers adsorption process is more heterogenous and does not conform to ideal monolayer adsorption assumed by Langmuir model.

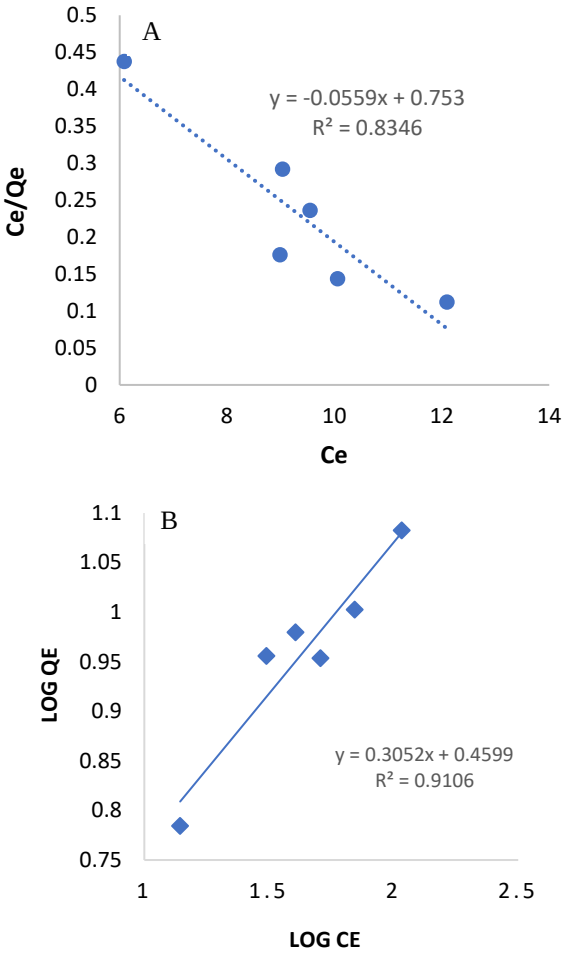

Figure 11. Plot of (A) Langmuir and (B) Freundlich Isotherm model

3.5 Adsorption Kinetic

Figures 12 show the plots of the Pseudo-first and Pseudo-second order. It was observed that the Pseudo-second order kinetics was more suitable for the experimental model [41].The experiment was suitable to both first and second order kinetics, with second order kinetics taking precedence. The kinetics of the adsorption experiment was studied by pseudo-first order and pseudo-second order kinetic models. Data presented in Figure 13b as well as Table 5 showed that the linear correlation coefficient of the pseudo-second-order model (R^2 = 0.991) was minutely higher than the correlation coefficient (R^2) of the pseudo-first-order for (R^2 = 0.986) and. Besides, the calculated Qe (14.718 mg/g) according to the pseudo-second-order model was closer to the experimental Qe (18.344 mg/g), suggesting

that the pseudo-second-order kinetic model could better interpret the adsorption behavior. Pseudo-first-order model was also well correlated with predicted in the sense that the R^2 value is also very close to 1, but it has a Qe value that is farther away from the experimentally determined Qe value. As previously known, the pseudo-second-order model suggested that the adsorption process would be the rate-limiting stage in a chemisorption process that involved covalent forces and ion exchange [42]. It also established that the pseudo-second-order kinetic model could more clearly explain the adsorption behaviour, which was consistent with other studies [43].

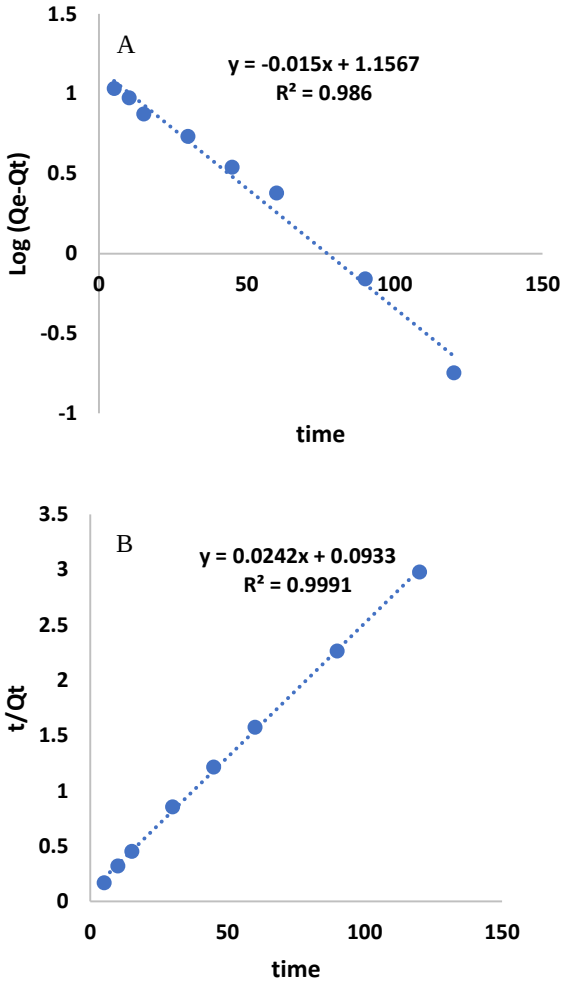

Figure 12. Plot of (A) First Order and (B) Second Oder Adsorption Kinetics

Table 4. The summary of the Isotherm models

Adsorption Models		Chromium removal
Langmuir		
	K_L (L/mg)	-13.47
	Q_{max} (mg/g)	17.889
	R^2	0.8346
	Regression Equation	y = -0.0559x + 0.753
Freundlich		
	K_f (mg/g)	2.8834
	1/n	0.3052
	R^2	0.9106
	Regression Equation	y = 0.3052x + 0.4599

Table 5. Kinetic Model Parameters for removal of chromium

Kinetic Models	Chromium removal
Q_e experimental (mg/g)	18.344
Pseudo-first-order	
K_1 (min^{-1})	0.015
Q_e (mg/g)	10.435
R^2	0.986
Regression Equation	y = -0.015x + 1.1567
Pseudo-Second-order	
K_2 (g mg^{-1} min^{-1})	0.0933
Q_e (mg/g)	14.718
R^2	0.991
Regression Equation	y= 0.0242x + 0.0933

3.6 Adsorption Thermodynamics Study

Using the principles of thermodynamics characteristics such change in enthalpy (ΔH°), change in entropy (ΔS°) and change in free energy (ΔG°), the variation in the amount of adsorption with regard to temperature is explained through the relationship obtained from the plot of ln K_d against T^{-1}. The Kd values calculated for the adsorption of chromium is given in Table 6. It was observed that, the Kd values increased with increase in temperature which resulted a shift of equilibrium to the right i.e., it signifies that the adsorption process is favoured, and more molecules are adsorbed onto the solid surface than desorbed from it at the given conditions. The negative values of ΔG° decreased with the rise in temperature; a more negative ΔG indicates that the adsorption process is increasingly favourable at higher temperatures. This implies that the adsorbate molecules have a stronger tendency to be adsorbed onto the solid adsorbent surface as the temperature increases [44].

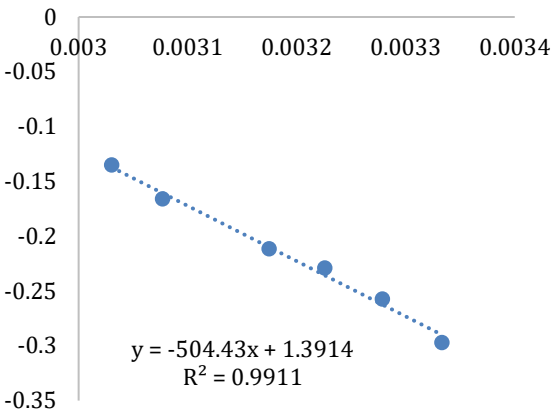

Figure 13. The Thermodynamic study plot of the Adsorption experiment

The negative value of enthalpy (ΔH) as seen in Table 6 typically indicates that the adsorption process is highly exothermic. The ΔH value suggests that the adsorbate molecules are strongly attracted to the adsorbent surface, typically through chemical bonding or strong physical interactions. The strong negative ΔH value is often associated with chemisorption. Chemisorption typically leads to highly stable adsorption, as the adsorbate molecules are bound tightly to the surface [45]. The ΔS (entropy change) value is positive in this adsorption thermodynamics; it suggests that the adsorption process leads to an increase in disorder or randomness in the system as chromium molecules transition from the solution phase to the Albizia adsorbent surface [19].

Table 6. Thermodynamics parameters for adsorption of Chromium

Temperature (°C)	**ΔG° (kJmol^{-1})**	**ΔS° (J K^{-1} mol^{-1})**	**ΔH° (kJ mol^{-1})**	**K_d**
30	-7664.26	11.5681	-4193.831	0.74306
35	-7722.10	11.5681	-4193.831	0.7731
40	-7779.94	11.5681	-4193.831	0.79534
45	-7837.78	11.5681	-4193.831	0.80924
55	-7953.46	11.5681	-4193.831	0.84712
60	-8011.30	11.5681	-4193.831	0.87356

4. CONCLUSION

The removal of heavy metals was achieved from this research, characterization studies which include Scanning Electronic Microscopy (SEM), reveals the irregular surface morphology with pore, similarly the Fourier Transform Infrared Spectroscopy (FTIR), identified all the functional groups (hydroxy, carboxyl and amino) while the Brunauer-Emmett-Teller (BET) analysis determine the surface area to volume ratio of the pour space (1023m^2/g and 0.57cm^3/g respectively). Furthermore, the adsorption studies of the Albizia lebbeck seed based investigated the best pH, contact time, and the initial metal concentration, dosage and temperature at pH 6, 120ppm, 0.2g and 60oC respectively. In the same way the physiochemical properties such as bulk density, ash content, and moisture content were obtained with a good performance as compared to other literatures.

The removal of heavy metals from wastewater is a critical environmental concern, and the development of effective sustainable adsorbents is essential. This study demonstrated the potential of Albizia lebbek seed based activated carbon as a low, eco-friendly adsorbent for the removal of heavy metals from wastewater. The results showed that the Albizia Lebbek seed based activated carbon exhibited high adsorption capacities for Cr. Pb (II), Cd (II), and Ni (II) ions with maximum adsorption capacities. The adsorption process was found to be pH- dependent, with optimal removal efficiencies achieved at pH 6.0. The kinetic and equilibrium data were well described by the pseudo first and second order and Langmuir models, respectively. The thermodynamic analysis revealed that the adsorption process was spontaneous and exothermic with **Δ**G ranging from -7664.2609 to 8011.30388 and **Δ**H-4193.831 similarly, 17.718 mg/g and 18.344mg/g for both pseudo first and second order models with Linear correlation of R^2 found to be 0.986 and 0.991 for pseudo first order and pseudo second order respectively. Overall, this study highlights the potential of Albizia Lebbek seed-based activated carbon as a sustainable, effective adsorbent for heavy metals removal from wastewater. Further research needed to scale up to explore its application in real world wastewater treatment scenarios.

ACKNOWLEDGEMENTS

We would like to thank the Faculty of Engineering and Technology, University of Ilorin.

REFERENCES

[1] I. Pet, M.N.Sanad, M. Farouz, M.M. Elfaham, A. El-Hussein, M.S. Abdel-sadek, R.A. Althobiti, A. Loanid, (2024) 62.
[2] A.B. Rashid and A.K. Kausik, (2024) 100277.
[3] P. Li and J. Wu, (2019) 73-79.
[4] L.D. Jathar, K. Nikam, U.V. Awasarmol, R. Gurav, J.D. Patil, K. Shahapurkar, U. Ağbulut, (2024).
[5] J. Willet, K. Wetser, J. Vreeburg, & H.H. Rijnaarts, (2019) 100110.
[6] A. Singh, S.S. Shah, C. Sharma, V. Gupta, A.K. Sundramoorthy, P. Kumar, & S. Arya, (2024).
[7] M. Ullah, N. Ruqia, M. Khan, W. Khan, M. Shah, S.G. Afridi, and A. Zada, (2020) 30-37.
[8] K. Hikimat, H. Aziz, R. Kareem, (2023) 100495.
[9] A.H. Jagaba, I.M. Lawal, A.H. Birniwa, A.C. Affam, A.K. Usman, U.B. Soja, N.S.A. Yaro, (pp. 3-27). (2024) CRC Press.
[10] Q. Zhang, J. Lv, Y. Ge, C. Guo, Q. Wang, M. Hao, Z. Liu, (2024) 108-114.

[11] S.R. Qasim, and C. E. Parker, (1993) 45-52.
[12] E.A. Ekong and A.P. Oniwopomayo, (2023) 50-56
[13] M. Agarwal, and K. Singh, (2017) 387-419.
[14] V.C. Renge, S.V. Khedkar, S.V. Pande, (2012) 580-584.
[15] A.E. Burakov, E.V. Galunin, I.V. Burakova, A.E. Kucherova, S. Agarwal, A.G. Tkachev, V.K. Gupta, (2018) 702-712.
[16] N.H. Solangi, J. Kumar, S.A. Mazari, S. Ahmed, N. Fatima, N.M. Mubarak, (2021) 125848.
[17] W. Liao, X. Zhang, S. Ke, J. Shao, H. Yang, S. Zhang, H. Chen, (2022) 115238.
[18] M. Ghorbani, O. Seyedin, & M. Aghamohammadhassan, (2020) 109814.
[19] S. Mustapha, D.T. Shuaib, M.M. Ndamitso, M.B. Etsuyankpa, A. Sumaila, U.M. Mohammed, M.B. Nasirudeen, (2019) 1-11.
[20] M.J. Ahmed, and S. K. Theydan, (2012) 200-207.
[21] W.S. Chai, J.Y. Cheun, P.S. Kumar, M. Mubashir, Z. Majeed, F. Banat, P.L. Show, (2021) 126589.
[22] T.E. Oladimeji, B.O. Odunoye, F.B. Elehinafe, R.O. Oyinlola, A.O. Olayemi, (2021).
[23] T.C. Umeh, J.K. Nduka, K.G. Akpomie, (2021) 65.
[24] A.D. Haruna, H. U.Hambali, A. I.Hayes, L.Ayinla, F. E.Macaulay, O. S.Onyekwere, O. P. Oyelade-Akinsola, (2024) 82-92.
[25] M. Sultana, M.H. Rownok, M. Sabrin, M. H. Rahaman, S.N. Alam, (2022) 100382.
[26] D.J. Stokes, (2003) 2771-2787.
[27] K. Vos, N. Vandenberghe, J. Elsen, (2014) 93-104.
[28] H. Heryanto, D, Tahir, B. Abdullah, M, Kavgaci, A. Rinovian, R. Masrour, H.I. Sayyed, (2024) 100758.
[29] K. Elmaadawy, M.R. Hamed, H. Al-Hazmi, G.K. Hassan, (2024) 40.
[30] S. Hanchang, (2009) 191.
[31] S. Yurdakal, C. Garlisi, L. Özcan, M. Bellardita, G. Palmisano, G. (2019). In Heterogeneous photocatalysis (pp. 87-152). Elsevier.
[32] M.R. Mahananda, S.K. Behera, S. Mishra, B. Prava, (2022).
[33] J. Gua, Y. Fan, Y. Li, Y. Bi, S. Wang, Y. Hu, L. Zhang and W. Song, (2024) 9670. https// dio.org/10.3390/su16229670.
[34] V. Kumar, A. Kumar, P. Baredar, (2018) 4510-4522
[35] K.S. Padmavathy, G. Madhu, P.V. Haseena, (2016) 585-594.
[36] E.A. Gendy, J. Ifthikar, J. Ali, D.T. Oyekunle, Z. Elkhlifia, I.I. Shahib, Z. Chen, (2021), 105687.
[37] D. Sameer, N.K. Al-Ani, H.A. Jasim, (2016) 1175-1184.
[38] R. Shahrokhi-Shahraki, C. Benally, M.G. El-Din, J. Park, (2021) 128455.
[39] A. Kuroki, M. Hiroto, Y. Urushihara, T. Horikawa, K.I. Sotowa, J.R. Alcántara Avila, (2019) 1251-1258.
[40] M. Mariana, A.K. Hps, E.M. Mistar, E.B. Yahya, T. Alfatah, M. Danish, M. Amayreh, (2021) 102221.
[41] J. Wang, X. Guo, (2020) 122156.
[42] S. Gupta, S. Saksena, O.F. Baris, (2019) 313-327.
[43] A. Anandan, T. Janakiram, (2022).
[44] H.N. Tran, E.C. Lima, R.S. Juang, J.C. Bollinger, H.P. Chao, (2021) 106674.
[45] J. Zhao, C. Wang, S. Wang, Y. Zhou, (2020) 111-122.